

https://dspace.org/

Gamma ray fluorescence for in situ evaluation of ore in Witwatersrand gold mines

Rolle, Rainer

2015
http://hdl.handle.net/10539/19229

Downloaded from a DSpace repository. https://dspace.org/

GAMMA RAY FLUORESCENCE FOR IN SITU EVALUATION OF ORE IN WITWATERSRAND GOLD MINES

R. ROLLE

GAMMA RAY FLUORESCENCE FOR IN SITU EVALUATION OF ORE IN WITWATERSRAND GOLD MINES

Rainer Rolle

A Thesis Submitted to the Faculty of Science
University of the Witwatersrand, Johannesburg
for the Degree of Doctor of Philosophy

Johannesburg 1979

ABSTRACT

A system for quantitative in situ evaluation of ore in Witwatersrand gold mines was researched and subsequently developed.

The principle of measurement is based on the excitation of gold K X-rays in rock face samples by the 88 keV gamma radiation from a Cadmium-109 radioisotope source. The X-rays and scattered radiation from the rock matrix are detected by a hyperpure germanium detector cooled by liquid nitrogen in a portable probe. In the fluorescence spectrum the intensity ratio of the gold $K\beta$ peaks to their immediate scattered background is evaluated and quantitatively converted in the portable analyser to area concentration units.

All aspects of the physical and instrumental measurement had to be investigated to arrive at a system capable of quantitative evaluation of trace concentrations in stope face ore samples. The parameters of efficiency of excitation of the gold K X-rays, and the energy distribution after scattering from the rock matrix at different angles were investigated from basic principles to determine an optimum source-sample-detector geometry which would allow quantitative evaluation of homogeneous ore concentrations. For edged-on measurement of rough-surfaced thin layer deposits a method of controlling the measurement geometry through ratemeter feedback was developed to allow conversion of mass concentration values to units of area concentration.

The parameters of spectrum evaluation were investigated from fundamental principles to allow qualitative assessment of different methods of peak evaluation for optimization of the method as a whole. The basic concepts of random signal processing times were developed together with new concepts of pileup parameters to allow a quantitative description of the data acquisition rate of a complete analog pulse processing system.

With this foundation a practical measuring geometry and optimum values for signal processing time parameters, for detector size and for discriminator positions for spectrum evaluation could be determined.

Parallel with the derivation of optimum measurement parameters went the development of instruments, their field testing and appraisal of the method. The underground results obtained with prototype versions of the gamma ray fluorescence analyser were in all instances found to have a highly significant correlation with those obtained from the same locations by conventional chip or bulk sampling and fire assay.

The development of the gamma ray fluorescence method has shown the potential of the method to serve as an ore valuation tool and to assist in the geological identificaion of strata in Witwatersrand gold mines.

To NELMA

DECLARATION

The work presented in this thesis is my own and has not previously been submitted for a degree at any university.

R. Rolle

R. ROLLE

FEBRUARY 1979

ACKNOWLEDGEMENTS

This research was undertaken at the Metallurgy Laboratory of the Chamber of Mines Research Organisation, which is an extended campus of the University of the Witwatersrand, Johannesburg. The facilities made available by this laboratory are gratefully acknowledged.

The author wishes to express his sincere thanks to the following people:

Dr. P.J.D. Lloyd, the director of the Chamber of Mines Metallurgy Laboratory for the encouragement and understanding for this work through often difficult times.

Prof. J.P.F. Sellschop for his guidance, encouragement and understanding.

Prof. J.T. Moelwyn-Hughes for encouragement to continue the work.

Mr. T.A. Davies for his pleasant co-operation in looking after the instrumentation and the gathering of underground data.

Dr. P.J.D. Lloyd for permission to use the laboratory's HP9825 calculator for production of the manuscript.

Finally I wish to thank my wife Nelma, for her understanding and encouragement to complete this work, and for the final help in duplicating the manuscript.

CONTENTS

ABSTRACT ii

DEDICATION iv

DECLARATION v

ACKNOWLEDGEMENT vi

CONTENTS viii

LIST OF TABLES xi

LIST OF FIGURES xii

1 INTRODUCTION 1

1.1 Nature of the Witwatersrand gold deposits 1

1.2 Ore valuation 3

1.3 Alternative methods of evaluation of ores 8

1.4 Discussion 11

2 OUTLINE OF THE DEVELOPMENT OF THE FLUORESCENCE METHOD 14

2.1 Rock penetration for an instrumental method 14

2.2 Description of the fluorescence system 16

3 EXCITATION OF FLUORESCENT X-RAYS 20

3.1 Particle induced X-ray emission 21

3.2 Photon excitation 21

3.2.1 Bremsstrahlung sources 22

3.2.2 X-ray sources 22

3.2.3 Low energy gamma sources 23

3.3 Comparison of X-ray tubes and radioisotope sources 24

3.4 Radioisotope sources for excitation of gold K X-rays 24

3.4.1 Primary emission of potential radioisotopes 25

3.4.2 Secondary emissions from sources 25

3.4.3 The excitation spectrum in thick samples 27

3.4.4 Excitation of other heavy elements 31

4 THE BACKGROUND SPECTRUM 33

4.1 Photon scattering 34

4.2 Scattering spectrum from thick samples 38

4.3 Source - sample - detector geometry 40

5 DETECTION OF FLUORESCENT SPECTRA 46

5.1 Geometrical detection efficiency 46

5.1.1 Detector thickness 47

5.2 Energy resolution 48

5.2.1 Resolution of germanium detectors 50

6 FUNDAMENTALS IN SPECTRUM EVALUATION 54

6.1 Gaussian peak on a constant background 55

6.2 Generalized evaluation 56

6.3 Variance of the peak to background ratio 59

6.4 Comparison of multichannel and few channel methods 69

7 EVALUATION OF SPECTRA FOR GOLD ANALYSIS 73

7.1 Comparison of different peaks and backgrounds 73

7.2 Comparison of spectra from Co-109, Co-57 and Te-123m 75

7.3 Measurement of the Cd-109 gold Kα spectrum 79

8 FUNDAMENTALS IN SIGNAL PROCESSING 82

8.1 Extending and non-extending processing times 83

8.2 Processing overlap parameters 84

8.3 Effective processing times and efficiency 86

8.4 Relative importance of various processing parameters 88

8.5 Pileup rejection 90

8.6 Appendix: Derivation of equations 91

9 ANALOG SIGNAL PROCESSING IN THE GOLD ANALYSER 95

9.1 The gold Kβ′ peaks 96

9.2 Maximum available background region 99

9.3 Two- and pseudo-two-channel analysis 99

9.4 The peak to background ratio detection limit 101

9.5 System time constant and detector size 104

9.6 The gold detection limit 106

9.7 Discussion 107

10 QUANTITATIVE MEASUREMENT OF ROUGH ORE SAMPLES 111

10.1 Homogeneous concentrations 111

10.2 Thin layered sedimentary concentrations 113

10.3 Shape of the fluorescence sample 117

11 INSTRUMENTATION FOR THE GOLD ANALYSER 119

11.1 Instrumental requirements 119

11.2 Evolution of instrument 121

11.3 Components (block diagram) 123

12 CADMIUM-109 SOURCE AND COLLIMATOR 129

12.1 Production of Cd-109 129

12.2 Source and collimator design 134

12.2.1 Source window 137

12.2.2 Collimator shield 138

13 SAFETY ASPECTS 143

13.1 Liquid nitrogen 143

13.2 Intrinsic safety for fiery mines 146

13.3 Radiation safety 147

14 RESULTS OF THE FLUORESCENCE METHOD 153

14.1 Measurements at Leslie Gold Mine Ltd. 153

14.1.1 Equipment 153

14.1.2 Test site 154

14.1.3 Experimental 154

14.1.4 Details of the fluorescence measurements 155

14.1.5 Details of chip sampling and analysis 156

14.1.6 Comparison of XRF and chip sample values 158

14.1.7 Discussion 162

14.2 First prototype results from Marievale Gold Mine 165

14.2.1 Minimum length of stope face for quantitative estimation of the gold content at Marievale 170

14.3 Results obtained with the first prototype at Blyvooruitzicht Gold Mine 171

14.3.1 Results using the second prototype at Blyvooruitzicht Gold Mine 179

14.3.2 Minimum lenght of stope face at Blyvooruitzicht Mine for quantitative estimation of the gold value 184

15 CONCLUSIONS 186

REFERENCES 189

LIST OF TABLES

3.1 Potential radioisotopes for gold determination 26

7.1 Energy and relative intensity of the K X-rays of gold and lead 78

8.1 Effective non-extending processing times 87

9.1 Individual K X-ray lines of gold and lead 96

9.2 Spectral region and variances in gold ore analysis at various system resolutions 100

9.3 Data acquisition parameters in gold ore analysis for a typical 200mm^2 Ge detector at r=50kHz 103

12.1 Isotopes in the production of Cd-109 130

12.2 Absorption properties of shielding metals 139

14.1 Comparison of means of XRF and chip samples 158

14.2 Correlation between XRF and chip samples 160

14.3 Fluorescence measurements with the first prototype on 30 stope face samples at Marievale 166

14.4 Calculation of variances in the determination of gold concentrations at Marievale 168

14.5 Batch measurements at Blyvooruitzicht 173

14.6 Prototype 1 fluorescence and chip values and their correlation at Blyvooruitzicht 178

14.7 Prototype 2 fluorescence and chip values 180

14.8 Prototype 2 fluorescence measurements on 19 samples at Blyvooruitzicht 182

LIST OF FIGURES

3.1 Spectra of sources for gold K X-ray fluorescence 26

3.2 Angle required in incoherent scatterin to reduce energy of primary photon to 81 keV 30

4.1 Co-109 backscatter spectrum from blank 'rock' 33

4.2 Photon interaction data for 'rock' 35

4.3 Shape of differential cross sections per unit solid angle for scattering of 88 kev photons from iron 36

4.4 Backscatter spectra from iron samples 39

4.5 Backscatter spectra from large sample of standard ore for different measuring geometries 43

4.6 Increase in backscatter intensity at 88 kev from peripheral sources relative to that from a central source 44

5.1 Linear detection efficiencies and their ratio vs. Ge detector thickness 48

5.2 Energy resolution of a 200mm^2 x 7mm Ge detector 52

6.1 Normalized Gaussian peak and background 57

6.2 General peak and background measurement 57

6.3 Single channel schemes for peak evaluation 60

6.4 Standardized background variances of R; background region unlimited 62

6.5 Standardized multichannel variances $^{m}V_{t_{max}}$ relative to $^{m}V_{\infty}$ 63

6.6a Minimum two channel variance in R 66

6.6b Discriminator positions in two channel analysis for minimum variance in R 66

6.7a Minimum pseudo two channel variance in R 67

6.7b Discriminator positions in pseudo two channel analysis for minimum variance in R 67

6.8a Minimum three channel variance in R 68

6.8b Discriminator positions in three channel analysis for minimum variance in R 68

7.1 Fluorescence spectra of standard gold ore sample 76

7.2 Fluorescence spectra of pure gold and lead 78

8.1 Analog pulse processing times 84

9.1 Discriminator positions for two channel evaluation of gold $K\beta$ peaks 100

9.2 Measurement times for specified ratio detection limit vs. TC for various detector sizes 105

9.3 Minimum measurement times @ 250n2/mm² vs. detector size 105

10.1 Edge-on fluorescence measurements of a 'sandwich' ore sample 115

10.2 Total count rate (>50keV) vs. probe to sample distance 116

11.1 First modular analyzer for in situ gold analysis 124

11.2 First prototype portable analyzer in use underground 124

11.3 Third prototype portable gold analyzer 125

11.4 Electronic block diagram of the third prototype gold analyzer 126

12.1 Cyclotron production yields of Cd-109 133

12.2 Source detector arrangement in the third prototype gold analyzer 136

14.1 Fluorescence and corresponding chip sample values from Leslie Gold Mine 159

14.2 Group means of fluorescence and chip values 160

14.3 Prototype 1 measurement error $(\sigma_c^2 + \sigma_q^2)^{0.5}$ 169

14.4 Length of face to be scanned at Marievale using prototype 1, to achieve a given precision in the given time 172

14.5 Comparison of batch and X-ray fluorescence estimates at Blyvooruitzicht 175

14.6 Bulk values of 152 batches at Blyvooruitzicht 176

14.7 Variogram of 152 consecutive batch values at Blyvooruitzicht 177

14.8 Length of face to be scanned at Blyvooruitzicht using prototype 2 to achieve the given precision in the given time 185

1 INTRODUCTION

The Witwatersrand geological system contains the world's largest known deposits of gold and it thus plays a major role in the economy of the Republic of South Africa. By the end of 1975 gold had accounted for approximately 66 percent of the total value of mineral products of the country from its earliest mining activities (Coetsee, 1976).

The depletion of ore reserves and ever increasing production costs have focussed attention upon the profitability of all aspects of gold mining. One of these, ore valuation, plays an important role in this. The great magnitude and the exceptional continuity of the Witwatersrand ore body make *in situ* evaluation of underground ore deposits feasible; at the low concentrations generally encountered evaluation from without the deep ore deposits would not allow anywhere near as high a precision of ore valuation.

The average mining depth is approximately 1,6 km below surface, approximately 75 Mt of ore are treated annually and the average grade of the ore treated is approximately 10g/t (10 parts per million).

1.1 Nature of the Witwatersrand gold deposit

The Witwatersrand gold ores were stratigraphically deposited in Precambrian times in successive cycles of sedimentation, with each cycle constituted by a varying

number of pulses of different intensity and character.

At present geological times, the planes of these tabular deposits are often almost horizontal, though they may be inclined at any angle up to the vertical and they have varying degrees of undulation and faulting. About sixty per cent of all gold ore is mined by explosive methods at a stoping (tabular excavation) width of less than one metre and the important heavy metal bearing conglomerate in these has a layer thickness or reef width of less than 200mm.

The gold bearing reefs are composed of a variety of quartz pebbles in a matrix consisting predominantly of quartz of sand size, with varying amounts of pyrite and other sulphides and some heavy minerals. The ore density averages 2,76t/m^3. Carbon is notable in some of the conglomerates. The gold occurs in the form of highly irregular particles ranging from 0,005 - 0,5m. across. The silver content of the metallic particles varies greatly - from less than 4 per cent to more than 32 per cent. (Coetzee, 1976).

The concentration of gold is at trace levels, the gold is thus seldom visible to the naked eye and other geological features commonly have to be relied upon for identification. The most prominent indicator is usually a reef band of pebble conglomerate; sometimes a carbon band or the separation of two geological layers, e.g. quartz and shale, serve as visual identification. These features are often not distinct and it is important to realize that although they are correlated with the gold concentration,

the correlation is poor. Discontinuities in the features and geological faulting and undulation augment the *in situ* problem of following the gold containing layer, and it is not uncommon that some mining is carried out on completely the wrong horizons, mistakes which can be rather costly particularly since the payable horizons missed may have become unmineable through this operation.

Uranium is often associated with the gold ores and the radiation from its decay products is sometimes used as a measurable indicator of the gold content, but the correlation is only medium to poor and uranium or radioactivity cannot be relied upon as primary indicator for gold without continued verification of the correlation.

1.2 Ore valuation

Ore valuation entails sampling of the ore body, determination of the mineral content of the samples, these two processes being referred to as evaluation of the ore, and assessment of the results to allow mining decisions to be made. In the valuation of three dimensional deposits only the position, mass and mass concentration of samples is required. Evaluation of samples of thin tabular deposits, however, entails the determination of mass of mineral per unit area. The dimensions of each sample thus need to be known so that the mass concentrations determined in the assay may be converted to the area concentration.

The conventional method of sampling (Storrar, 1977) in the gold mining industry has been chip sampling. At regular intervals of 3 to 10 metres in stopes, and at shorter intervals in development ends, delineating blocks, the rock

face (wall) is washed and dressed, i.e. cleared of loose pieces of rock and large steps, and the outline of the sample to be chipped is measured and marked off with crayon. A groove nominally 25mm or so deep and about 70 to 100mm or 150mm broad is chipped with hammer and chisel across the mineralized zone. For narrow reefs only a single sample of specified width (height) 80mm, 100mm or 150mm normal to the reef plane is cut if non-mineralized rock can be included in the upper and lower parts of the sample, otherwise the groove is lengthened to provide several samples. Between 0,5 to 2 kg of chippings are caught in a pan below the sample being taken. A rubber guard or a piece of cloth wound around the chisel near its point reduces the number of rock chips flying off.

Groove samples across tabular deposits, as far as possible should be of even depth, and rectangular in shape with solid square corners to allow simple conversion of mass- to area concentrations. The quartzites generally encountered in the Witwatersrand gold mines make this rather difficult in manual sampling and uneven friability across the mineralized zone can readily introduce sampling bias. Mechanical sampling with diamond wheel cutters offers only slight improvement at higher cost and inconvenience and, therefore, has limited application.

The highly erratic deposition of gold and the overall low values call for the area sampling ratio, i.e. the total projected area of the samples to that of the ore body, to be as large as possible, and for the samples to be representatively distributed throughout the ore body. The area sampling ratio and the distribution of

gold values determine the precision with which the value of a standard size ore body thathas been mined, or of one that is to be mined, may be assessed. In stope and development end chip sampling usually an area ratio of less than 0,0001 of the area mined is representatively sampled. A standard size ore body has not yet been stipulated and the required precision of valuation for this standard size for mining decisions frequently encountered still have to evolve; the precision of valuation can then be related to any size of ore body.

The main use of ore valuation from chip sampling has been for control of the grade of ore mined and to provide estimation of future ore reserves. Many mining decisions at present made on an arbitrary basis could benefit greatly from on improved precision in ore valuation. The maximun benefit (of ore valuation) is obtained from low grade areas as they become payable and the mining of areas is terminated as soon as possible after they become unpayable (Johnston, 1973). The impending introduction of mechanisation into the gold mines will require much more concentrated mining for efficient use of the costly equipment. This will require a higher precision of valuation of ore bodies of the smallest sizes amenable to select. - mining. A higher precision can be attained through better sampling continuity and a higher area sampling ratio usually at increased cost.

Other methods of underground sampling have been employed under particular situations to reduce valuation costs with varying degrees of success. Grab sampling of

broken ore is used in some mines, often in conjunction with chip sampling, for control of the grade of ore mined. For ore valuation the average stoping width of the area covered by a broken ore sample collection point needs to be known to allow conversion of mass- to area concentration. For narrow reefs a broken ore sample of 10 kg represents an area of the ore body similar to that of a chip sample of the order of 1 kg. It appears that even if the area sampling ratio of the ore body sampled is less than in chip sampling, the higher continuity feasible in broken ore sampling through reduced acquisition costs allows better representation of the parent ore body and thus improvement in valuation precision in some mining areas (Chelius, 1973). A limitation of broken ore sampling is that the smallest size of ore body that may be valued for selective mining is of the order of the total area covered by a sample collection point, i.e. usually one or more stopes.

Special bulk sampling, where 100% of the ore of a small area of an ore body is extracted and put through a sampling plant, has been used to obtain information for comparison with routine sampling results (Wallbauer, 1977), but this method precludes good sampling continuity for extended ore bodies.

The ore samples from underground are fed to a small jaw crusher and reduced to a certain size. The sample is then divided to reduce the amount and fed to a pulverizer where it is reduced to 100% -74μm. Fifteen to sixty grams of sample is placed in a fire-clay crucible and 80-90g of flux (Litharge 30%, Sodium carbonate 45%, Borax 25%, Maize meal

2g) is added. The crucible is placed in a reverberatory furnace at 1100°C, where the gold collects in a lead bead. The contents are then poured into a mould and cooled. The lead bead is removed and hammered into a cube and placed in a cupel in a muffle furnace. After about half an hour the lead has been absorbed and evaporated and the cupel is removed. The Au/Ag bead is weighed and the mass recorded. An average correction is normally applied for the silver content, the average being checked periodically. Although losses in the furnaces and during cupellation can cause errors (Wall et al., 1973), these errors are not serious in the evaluation of ores as sampling errors are dominant; they can, however, be important in the assaying of much lower concentration samples such as from tailings.

Usually the sample results are combined to obtain averages for valuation of stretches of ore for grade control and ore reserve calculations.

Improved geostatistical methods of valuation, dating from the 1950's (reviewed by Krige, 1964), have more recently been applied at a number of gold mines to control the quality of routine sampling and assaying and to provide realistic confidence limits in the ore valuation of any size of ore body.

The geostatistical methods are continuously being improved and it may be expected that the area sampling ratio, instead of being a stipulated value for a large section of a mine, will be able to be determined on a precise cost benefit basis according to the uses of the valuation and to the gold distributions encountered.

1.3 Alternative methods of evaluation of ores

The disadvantages of the conventional method of evaluation, where samples collected underground are assayed on surface, are the difficulty of unbiased chipping of samples from the narrow stope faces, the transportation of the samples to surface and the delay from the time of chipping until the results are available. Once in the laboratory the concentration of the samples can easily be determined by fire assay to high accuracy and precision.

Alternative laboratory methods of measuring the gold content, such as conventional X-ray fluorescence analysis, radioisotopic X-ray fluorescence analysis (Burkhalter et al., 1970), instrumental neutron activation analysis (Uken et al., 1966) and acid leaching, solvent extraction with atomic absorption spectrometry (Groenewald, 1969) have been investigated and were found to offer some advantages over fire assaying. However, to reduce the sampling problem in situ methods of evaluation of ore were considered.

Of the chemical methods chromatographic paint (Hallbauer, 1973) was shown to be useful in some qualitative investigations and while in situ chemical leaching or cyanidation (Lloyd et al., 1969) also has some potential, it is probably too time consuming for this application.

Instrumental methods for quantitative measurement of the gold content directly on unprepared stope faces were investigated. Although dispensing with arduous sample extraction and with preparation of the sample may seem very attractive, these methods face the problem of direct

physical measurement of trace concentrations of gold without any form of preconcentration with sophisticated equipment that needs to be carried through and operated in stopes. Furthermore even though an instrumental method may be used in rapid scanning of the whole stope face, thereby improving continuity of sampling over conventional periodic distance sampling, the depth of measurement into the rock face needs to be high enough so that also the area sampling ratio of the area of the ore body mined may be improved. For example chip sampling of sections 20mm deep and 100mm broad on a square grid pattern of 5m has an area sampling ratio of $20 \times 100mm^2/25m^2 = 0,00008$ whereas an instrumental method of scanning the whole stope face after similar 5m advances to a depth of only 0,1mm would have a poorer ratio of only 0,00002.

Measurement of gold values in narrow reefs directly on the stope face has the advantage over measuring gold values in broken rock in that the conglomerate is not diluted with waste rock and that there is no complicating factor of segregated broken sizes. The times to measure the same mass of rock to the same percentage precision are disproportionately longer for the lower average concentrations in the broken rock. Also, the surface of the rock to be measurred is somewhat less rough on the stope face than on the broken ore and the problem of controlling or correcting for a variable measuring geometry in quantitative sample evaluation is thus slightly reduced.

In considering the physical properties of gold which could be usefully applied in the design of a stope face

gold analyser, the entire electromagnetic spectrum had been reviewed. In the radio and microwave regions there appeared to be no properties of use; in the infra-red region the high reflectivity of metallic gold was noted; in the X-ray and gamma ray regions fluorescence and Mössbauer effects seemed potentially useful with electron excitation of X-rays a poor alternate; while in the heavy particle field, neutron activation showed some promise. Consideration of the thermal, electrical and magnetic properties did not reveal anything of interest.

Thus four physical, non-destructive methods appeared to be potentially useful.

Infrared reflectivity measurement with a 'vidicon' tube gave encouraging results (Hinde, 1971). This method, however, had three shortcomings: Optical resolution for the very fine gold particles was insufficient, only the surface of gold particles and not their mass could be directly assessed and the penetration into the rock is insufficient for the requirement of sampling a high ratio of the area of the ore body.

A closer assessment of the Mossbauer effect suggested that any method based on this effect would probably be impractical. It appeared that it would be neccessary to cool the rock to obtain the effect and that the rate of data acquisition would probably be too slow.

Gold K level X-ray fluorescence did, however, appear practicable and its development will be outlined in the next chapter.

The high cross section for resonance neutrons, the high

sensitivity of instrumental neutron activation analysis and the high penetration of neutron and gamma rays through rock had focussed much attention on this method. Laboratory investigations had been carried out at the National Institute for Metallurgy (Uken et al., 1966), and indications were that adequate sensitivity and rapidity could possibly be attained with gold ores. However, a high flux neutron source of californium-252 would be required and the difficulties of safe handling of such a source in a portable instrument in stopes seemed too great.

1.4 Discussion

To meet ever increasing mining costs definite improvements in the precision of ore valuation will be required. The conventional method of chip sampling offers little potential for improved evaluation of ores. Improvements in the laboratory analysis of samples can only have a minor effect on the evaluation because the main problems lie on the sampling side.

Bulk sampling of broken ore appears to alleviate the sampling situation in some mines under present mining conditions, but the area selectivity and degree of improvement will be insufficient for future demands.

It was realized that only by rapid scanning of exposed stops faces to a depth of more than a millimetre could the continuity and area sampling ratio be improved sufficiently for selective mining to a scale smaller than the size of present day stopes. The important criterion was that as much rock as possible should be measured per unit time to an acceptable measurement precision.

The underground environment where ores have to be evaluated is fairly harsh for a sophisticated instrument that is usually operated in an air conditioned laboratory. The industry average wet bulb temperature in working stopes is about 29°C and average wet Kata readings are about 11,5. Working height is often restricted to less than one metre because of broken rock lying in working places, and instruments may have to be dragged across this highly abrasive quartzite. Air velocity averages 1m/s and the air may be dusty. Illumination is by caplamp. Ore evaluation is sometimes required in non-working places and in these places conditions may be considerably poorer.

A number of potential instrumental methods were considered for direct quantitative measurement of the gold content in the rock without having to remove a sample from the stope face. Careful preparation of the sample surface also was to be avoided as this would defeat the object of not having to take a sample. Only penetrating radiation has the potential of increasing the area sampling ratio. Of the instrumental methods only radioisotope excited K level X-ray fluorescence of gold and detection of the radiation with a high resolution solid state detector appeared to be within reach of present day technology for this application.

The term gamma ray fluorescence is used in this work to distinguish the method from conventional X-ray fluorescence analysis. The energy region used for excitation and measurement falls above the energy region conventionally used in X-ray fluorescence analysis and at the lower end of conventional gamma ray specrometry: Gamma radiation is used

for excitation and the high energy gold K X-rays are detected. A 'low energy' photon detector suitable for this intermediate or transitional energy region is employed. Both the disciplines of gamma ray spectrometry and of X-ray spectrometry are merged in this application.

To achieve an acceptable rate of rock analysis all the parameters of excitation, detection and data processing had to be optimised for a portable instrument to be used in the hostile stope environment. In the following chapters, after an outline of the method, the various parameters critical to the method are discussed and developed from fundamental principles as the empirical approximations most commonly employed in both disciplines were not amenable to the rigorous treatment and would not have permitted an indication of the maximum improvement possible on a given combination of parameters. Some early underground sample evaluations taken with prototype instruments are presented to illustrate the introduction of gamma ray fluorescence analysis into ore valuation of the Witwatersrand gold deposits.

2 OUTLINE OF THE DEVELOPMENT OF THE FLUORESCENCE METHOD

The *in situ* instrumental evaluation of gold ores is a sophisticated task involving a large number of aspects. These may be considered as a chain of parameters that need to be optimised as a whole. Some of the parameters may be considered almost independently of each other while the dependence on others calls for a compromise, yet weakness of any one parameter results in poor overall performance while excessive strength in another may simply be wasteful.

The aspects that needed consideration were the nature of the ore deposit on both a large scale and a microscopic scale, the requirements for ore valuation, the environment for the evaluation, the human aspects of *in situ* instrumental operation and operational procedure, operational safety, a series of measurement and instrumental parameters, measurement interferences and the presentation and utilization of measurement data.

It was mentioned in the opening chapter that most of the gold occurs in very narrow deposits and in a wide range of particle sizes, and that the ratio of the area sampled to the area mined needs to be higher than the area ratio hitherto employed with chip sampling if the precision of ore valuation is to be improved.

2.1 Rock penetration for an instrumental method

The effective depth of measurement in rock of a potential

instrumental method would have to be an improvement on the maximum effective depth of current chip sampling. This is nominally a 20mm deep cut of 100mm length made every 5 metres of an exposed stope face; if this projected area were spread out evenly along the stope face from one cut to the next, the effective depth of sampling would be 20mmx100mm/5m=0,2mm. The sizes of gold particles found in the reef require that also the measurement depth in gold be sufficient to penetrate the larger gold particles. If only a thin surface layer of the larger gold particles could be penetrated then the projected area of the particles, rather than their mass would be reflected in the measurement values.

The narrowness of most of the gold bearing ore layers needs to be taken into account when considering large penetration depths. In the edge-on measurement of a narrow layer of gold bearing ore the absolute concentration in the sample to be measured decreases as the sample dimension normal to the layer increases beyond the layer thickness, thus including waste rock in the sample. Because the gold concentrations that have to be determined are at trace levels, the measurement phenomenon to be detected manifests itself only weakly and it is therefore advantageous not to include much waste rock in the sample so that the phenomenon may appear relatively stronger. A high efficiency in the utilization of measuring radiation is desirable for such a weak phenomenon and this can be attained only with an uncollimated or wide-angle measurement geometry. With this geometry the measurement penetration should ideally be similar in value to the ore layer thickness and the

measuring head should be a similar distance away from the sample surface. This would indicate an optimum rock penetration depth of a few millimetres for most of the Witwatersrand deposits, but this would be impractical. There would be no point in employing a method with an effective sample penetration depth less than about 20mm, as it would be difficult to discern a layer and to guide a small measuring head, in scanning rapidly along a rough stope face, with a precision better than this.

From a penetration and concentration point of view the gamma-ray excited, gold K X-ray fluorescence method is thus ideal for the evaluation of most of the Witwatersrand gold deposits: the gold K X-rays have a half-range in rock of 13mm, i.e. they lose half of their intensity in going through 13mm of rock, and any exciting gamma radiation for these X-rays has a half-range in quartzite longer than this. In solid gold the half-ranges of gold K X-rays and of exciting gamma rays are respectively 0,2mm and greater than 0,04mm, thus most of the larger gold particles that may be encountered are easily penetrated so that the mass of gold particles, rather than their surface area is represented in the fluorescence measurement.

2.2 Description of the fluorescence system

Gamma radiation from a radioisotope source is used to excite the characteristic K X-rays of gold in a stope face sample. These in turn are detected by a germanium detector and the detector signals are processed to give a quantitative indication of the gold concentration.

Cadmium-109 emits 88 keV gamma rays which can be efficiently absorbed by the K electrons of gold which are then emitted with that energy less their K-shell binding energy of 80.7 keV, i.e. as 7 keV electrons. The vacant gold K atomic shell is subsequently filled with an electron from the L, M or N shell and in this process may isotropically emit a fluorescent gold K X-ray.

The 88 keV gamma rays are also scattered in all directions by electrons in the rock matrix. In the coherent scattering process the energy of the incoming and outgoing photon remains unchanged whereas in the incoherent scattering process some energy is lost to an electron. The probabilities of scattering in a given direction vary with the scattering angle and are different for the two types of scattering . Whereas the gold fluorescence X-ray spectrum is the same in all directions (except for differences from absorption through the matrix), the matrix scatter spectrum has different profiles at different scattering angles. Cadmium-109 was chosen primarily because its 88 keV photons excite gold efficiently while at close to a 180° scattering angle the scattering spectrum has a very low intensity in the region of the gold K X-rays.

A miniature point source in combination with a wide angle tungsten collimator shield was developed for mounting concentrically in front of a germanium detector so that a source-sample-detector scattering angle close to 180° could be achieved in all forward directions of the source-detector probe even for sample to probe distances as short as 25mm.

The 22 keV silver X-rays, emitted abundantly by

Cadmium-109, were filtered out to reduce the potential radiation hazard and so as not to take up any useful count rate handling capability of the detection and analysing system.

A hyperpure germanium photon detector, cooled by liquid nitrogen, was specified because of its high energy resolution and efficiency for photons in the gold Kβ X-ray energy region. The size of 200mm^{2}x7mm deep was evaluated for optimum data acquisition rates.

Instead of relying on conventional empirical approximations for spectrum evaluation, a fundamental study was undertaken to allow quantitative comparison of different methods of spectrum evaluation. An optimised single channel scheme for the two correlated gold Kβ' peaks was developed on this foundation. This provides efficient spectrum evaluation with instrumental simplicity needed in a portable instrument.

Two important developments for quantitative in situ gold determination were i) the derivation of a method of ratioing the measured gold peaks and their immediate background to cope with the variable geometry measurement of rough surfaces, and ii) for conversion of mass to area concentration a method of feedback to control the probe to sample separation within predetermined limits. In the latter method the total spectrum count rate is interpreted as a probe to sample distance, the rate is continually displayed to the operator to guide him for human servo control of the distance and the rate is internally monitored to inhibit data acquisition when the rate is not within set limits i.e.

when the measuring geometry is not within corresponding distance limits. A South African patent (Rolle, 1974) and a United States patent (Rolle, 1977) were granted for this concept.

The basic concepts of extending and non-extending processing times in the analog processing of random signals were developed together with new concepts of pileup parameters to allow a quantitative description of the data acquisition rate of a complete analog pulse processing system. With this foundation the pulse processing times could be optimised for given detector resolution parameters to maximize the non-piled up data acquisition rate.

Digital data processing was trimmed to the simplest system that could automatically provide data in calibrated concentration units to the operator and for storage in an internal data memory for retrieval above ground. More sophisticated, microprocessor-based systems can, however, be expected in the near future.

The layout of the portable system was designed for maximum operational simplicity and operator convenience, particularly for rapid scanning of long stretches of stope face.

The instruments so far tested underground have developed from a stationary, mains-operated model through three prototype versions of portable instruments. At the close of the writing of this thesis a number of instruments of the third prototype were in the stages of accumulating data in ore valuation field trials at various mines.

3 EXCITATION OF FLUORESCENT X-RAYS

For the determination of trace amounts of a heavy metal in a light matrix by XRF spectometry, it is necessary to choose a source which will excite the X-rays of interest as efficiently as possible. However, efficiency of excitation is not the sole criterion, because the excited X-rays must be detected against a background signal caused by the scattering of photons by the matrix or by photons in the source of energies other than those which excite the fluorescent X-rays most efficeintly. Accordingly the source of exciting radiation must be chosen not only on the grounds of the efficiency of excitation, but also so that it may minimize the background radiation seen by the detector. Excessive background radiation can reduce the efficiency of the detection system, increase the potential radiation hazard, and may reduce the signal-to-noise ratio in the energy regions in which the fluorescent X-rays of interest occur.

In what follows, therefore, all possible means for exciting the gold K and L X-rays are considered first, and then the various potential sources for K level excitation are compared not only on the grounds of the efficiency with which they can excite these X-rays, but also on grounds of the reduction in the total flux received by the spectrometer; the maximisation of the signal-to-noise ratio in the energy region of interest; and the practicability of

the various types of source when used in a portable underground instrument, which is the ultimate intended practical outcome of this work.

3.1 Particle induced X-ray emission

For X-rays below about 5 to 15 keV (1eV=1,602x10^{-19}J), charged particle excitation, e.g. by means of protons or alpha particles, offers good fluorescence cross sections while producing a relatively low scatter background in the recorded X-ray spectrum. Excitation cross sections of charged particles in the 1 to 50 MeV range lie in the region of 0,1 to 1m^2/kg which is comparable with that for photon excitation. The bremsstrahlung intensity depends on the square of the charge (z) per mass (m) of the incident particle i.e. on $(z/m)^2$ so that, with proton or alpha excitation as compared with direct electron excitation, problems of the associated background in the recorded spectrum are reduced by the order of the square of the proton/electron mass ratio. Charged particle excitation has, however, three drawbacks:-

i) their range in air is limited;

ii) apart from alpha particles emitted during radioactive decay, they have to be produced in accelerating machines and thus are unlikely to be practical underground and iii) secondary electrons are emitted and may result in an increase of the relevant background.

3.2 Photon excitation

In the past it was found that for X-rays above 5 to 15 keV, photon excitation offered superior detection limits (Woldseth, 1973).

The fluorescence excitation efficiency of photons of energy E decreases approximately as E^{-3} above the X-ray absorption edge of the element, i.e. 80,7 keV for the gold K level. Photons of energy below the absorption edge cannot excite the relevant group of X-rays.

Photon sources can be classified into three main groups depending on the mode of production of the principal radiation emitted, namely bremsstrahlung- , X-ray- and low energy gamma sources.

3.2.1 Bremsstrahlung sources

Bremsstrahlung is produced by the deceleration (or acceleration) of electrons. X-ray tubes for XRF are essentially operated as bremsstrahlung sources. The photon spectrum is continuous up to the maximum of the electron energy. The continuum spectrum is suitable for the simultaneous excitation of a whole range of elements but is not optimised for any particular element.

3.2.2 X-ray sources

Primary X-radiation is produced by atoms ionized through electron bombardment, nuclear recoil or internal conversion.

The photon spectrum consists of a group of characteristic X-ray lines which may be particularly suited for the selective excitation of some individual element. If a certain interfering element is to be discriminated against, then a filter, or a secondary target of either that element or one of slightly higher atomic number Z, may be placed in the primary photon beam. This can remove all radiation capable of exciting the interfering element,

partially converting it to X-rays of energies more efficient in exciting still lower-Z elements, thus allowing these to be selectively excited. More efficient use of radiation is, however, made by excitation with direct primary radiation.

In a well-designed, low energy source the intensity of the group of X-ray lines may constitute 90% of the total radiation from that source. At higher energies, scattering effects are relatively more important, and typically only 30 to 60% of the total radiation appears as the X-rays of interest.

3.2.3 Low energy gamma sources

Gamma radiation is produced in the decay of excited nuclear states to lower states of the nucleus. Most radioisotope decay schemes are complex and involve several gamma energies usually initiated by a charged particle. However, some decay schemes are simple with practically no charged particle emission and only one or two gamma energies, or all but the energy transitions of interest are of very low intensity.

Gamma sources for XRF are potentially monoenergetic sources that can give optimum excitation for individual elements.

A near perfect gamma source for XRF excitation of a particular element would exhibit the following characteristics -

a) decay by electron capture (EC) or isomeric transition (IT) with little internal conversion; other modes of decay are accompanied by a bremsstrahlung

continuum and internal conversion reduces the intensity while producing unwanted X-rays.

b) an intense gamma transition near the a .orption edge of the element of interest with no high energy gammas. The high energy radiation increases background in the detected spectrum and aggravates radiation problems.

c) a sufficiently long halflife to obviate tne need for frequent calibration of the instrument and replacement of the source.

d) an acceptable production cost - most of these isotopes are accelerator-produced and thus costly.

Gamma-ray sources are particularly convenient for the excitation of the high energy X-rays of the heavy elements.

3.3 Comparison of X-ray tubes and radioisotope sources

The primary advantage of X-ray tubes is the availability of a flux having an intensity orders of magnitude greater than is produced by radioisotope sources. The versatility of a tube through choice of operating conditions, and the simple fact that a tube with its potential radiation hazard, can be switched off, are secondary advantages.

Radioisotope sources have the advantage of being lightweight, having a very stable, predictable output and offering simple high energy XRF excitation.

3.4 Radioisotope sources for excitation of gold K X-ray

The gold K absorption edge lies at 80,.7 keV and only source photons of higher energy will excite the K X-rays effectively.

3.4.1 Primary emissions of potential radioisotopes

A number of potential radioisotopes and their primary radiations are listed in Table 3.1. The probability of producing a primary photon of particular energy during the decay of an atom depends on the decay scheme and often is not 100%. Furthermore the primary photon may be internally converted without emerging from the atom. The percentages in the fifth and sixth columns of Table 3.1 refer to the number of atoms decayed. Percentages above 100% are feasible from complex decay schemes and consecutive decays. The photoelectric cross section μ_{ph} for K level excitation is $0,71 m^2/kg$ Au for photons barely exceeding 80,7 keV. As the photon energy E increases, the excitation efficiency decreases approximately as E^{-3}, and the parameter $(E/80,7)^{-3}$, with E in keV, shown in the 7th column of Table 3.1 is an indication of the gold K-level excitation efficiency of the primary emission relative to that of 80,7 keV photons.

3.4.2 Secondary emissions from sources

If the radioisotopes could be mounted on a thin film then only the primary radiation would be observed. For practical applications the radioisotopes need to be encapsulated and shielded from the detector. Besides the primary radiation the source spectrum therefore contains X-rays and scatter peaks from the source backing and window and from the source material. As source scatter peaks are relatively small because the heavy metal backings, such as Ta and W used in these applications, attenuate photons in the 80 to 200 keV region predominantly by photoelectric absorption. At these

Table 3.1 Potential radioisotopes for gold determination

ISOTOPE	HALF LIFE days	DECAY MOD.	PRINCIPAL PHOTONS keV	INT. CONV. %	EMISSION %	REL.EXCIT. EFFICIENCY (max)
Ba-133	2628	EC	81*	57	34	0,99 (1)+
			356	2	62	0,01 (0,16)
			276;303;384	1	25	0,02 (0,2)
			54;80;160	12	5	0,09 (0,55)
Tm-170	128	$\bar{\beta}$	84	21	3,4	0,88 (1)
			brems(968)			0,00 (1)
Cd-109	453	EC	88	96	3,8	0,77 (1)
			AgKX 22;25		102	0
Gd-153	241	EC	97	8	30	0,57 (1)
			103	30	20	0,48 (1)
			70	11	3	0
			EuKX 41;47		110	0
Co-57	271	EC	122	1	85	0,29 (0,94)
			136	1	11	0,21 (0,75)
			14		9	0
			FeKX 6,4;7		55	0
Te-123m	120	IT	159		83	0,13 (0,56)
			TeKX 27;31		50	0
Pm-147	957	$\bar{\beta}$	brems(225)		50	0,05 (1)
			target PtX		<1	0,56 (1)
Ce-139	140	EC	166	20	80	0,12 (0,52)

* underlining indicates the photon of interest

\+ figures in brackets indicate the maximum relative excitation efficiency after incoherent scattering through an optimum angle

energies the usable primary radiation emitted from a source may thus constitute 50% or less of the total radiation.

Typical source spectra measured with a hyperpure Ge detector are shown in Figure 3.1.

3.4.3 The excitation spectrum in thick samples

For gold determination in a light geological matrix the excitation spectrum above 81 keV needs to be considered.

Photons at these energies are predominantly scattered, with less than 20% being photoelectrically absorbed. In a 'thin' sample the scattered radiation leaves the sample but in a 'thick' sample this radiation is available for further interaction with the sample.

Above 81 keV, scattering in a light matrix is largely incoherent so that inside a sample not only the intensity of the exciting radiation diminishes exponentially with depth, but the energy of the radiation is lowered as well. The energy E' of a photon scattered from a free electron at rest is a function of the scattering angle θ and the incident photon energy E. It is given by the Compton (1923) equation for conservation of momentum and energy

$$E' = E/[\ 1 + (1-\cos\theta)E/(mc^2)\ ]$$

The maximum angle through which a photon may be incoherently scattered before its energy is reduced below that required for the excitation gold K X-rays (81 keV) is shown in Figure 3.2. The reduction in the energy of an incoherently scattered photon, if it is still above 81 keV, results in an enhanced efficiency for the excitation of gold. The maximum relative efficiency for Au K-level

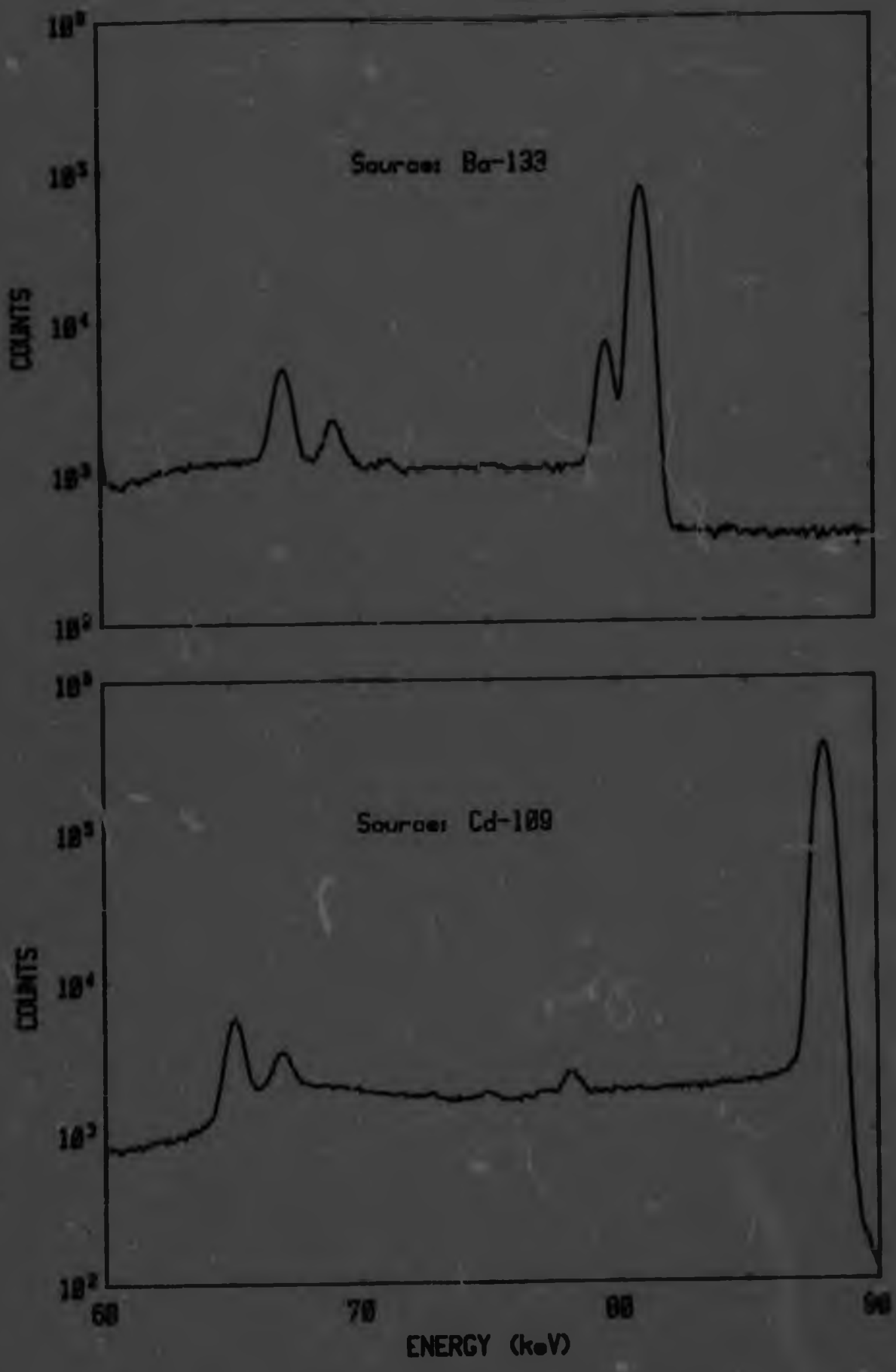


Fig. 3.1 Spectra of sources for gold K X-ray fluorescence

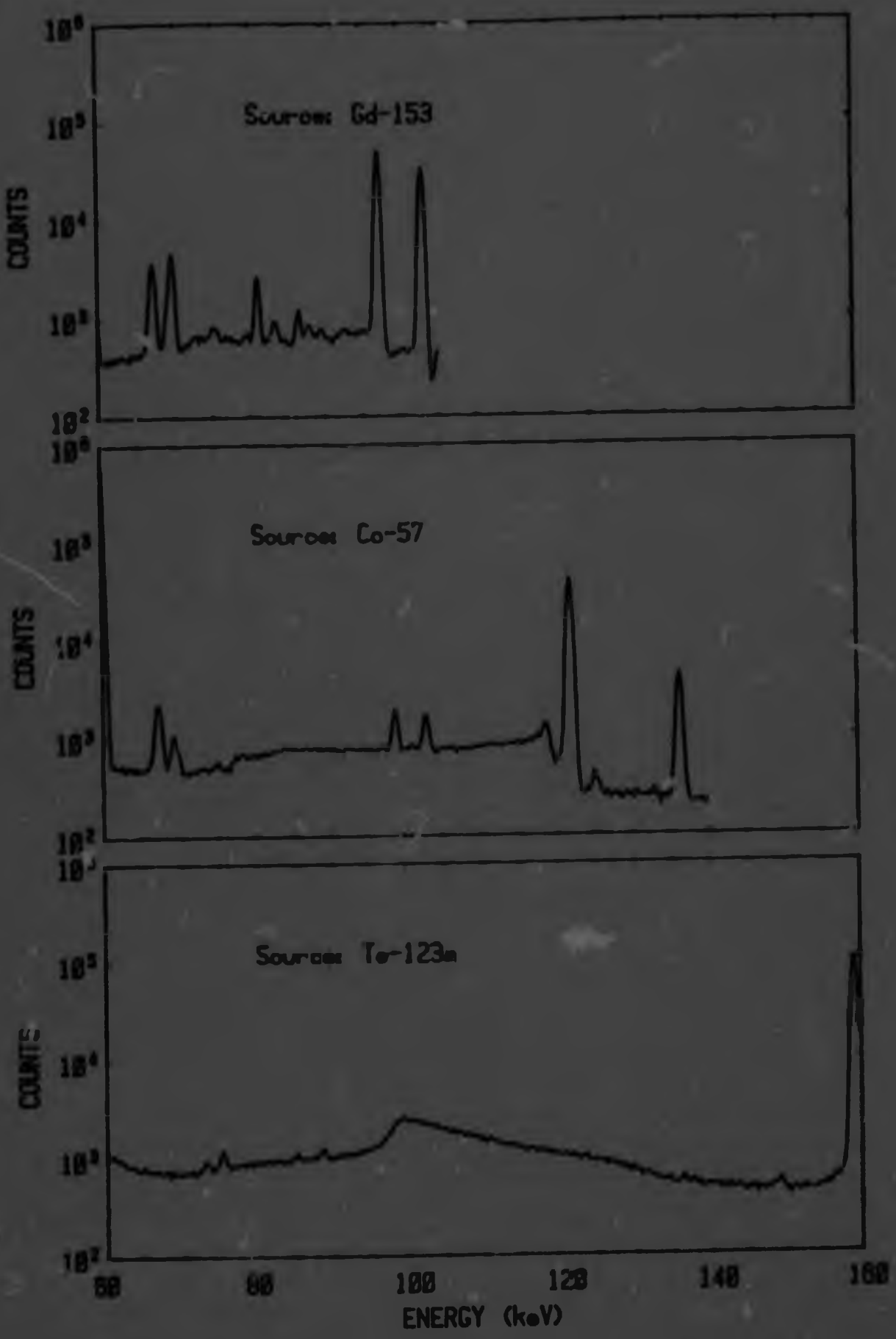


Fig. 3.1 (continued)

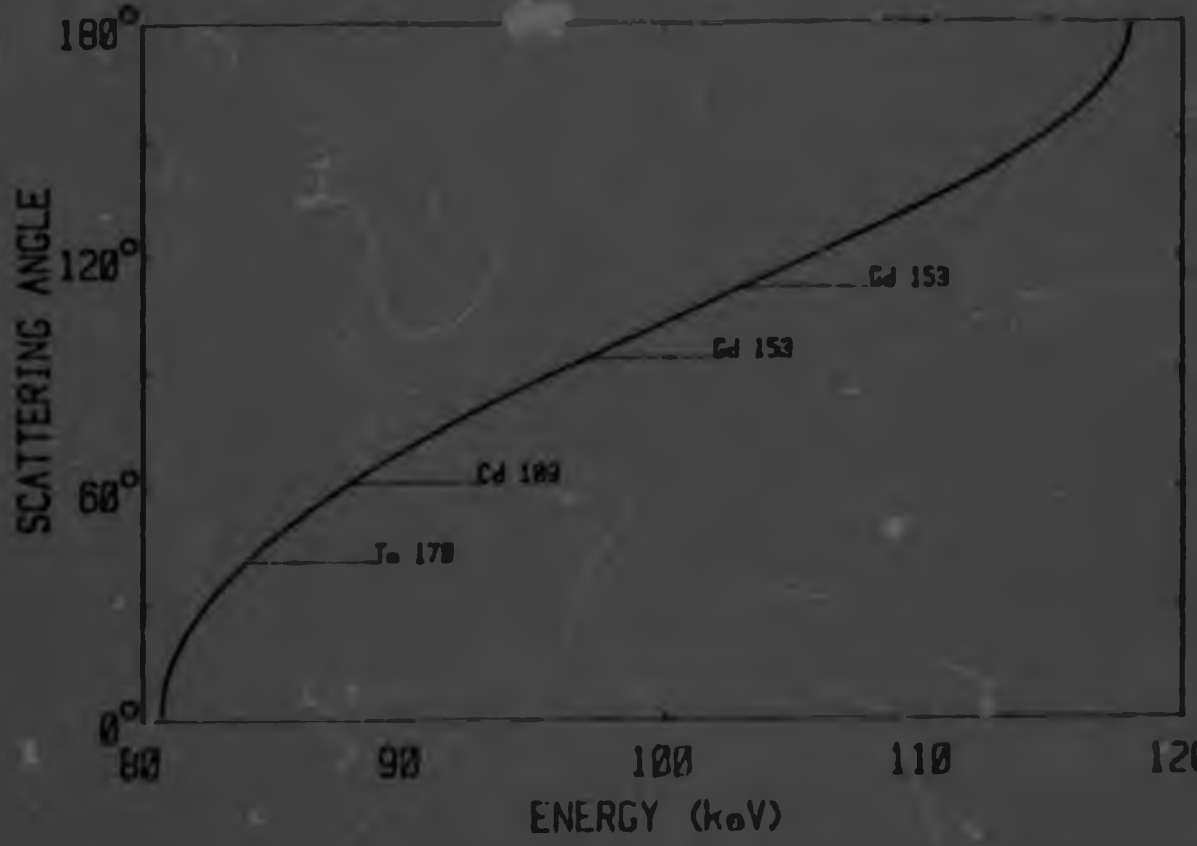


Fig. 3.2 Angle required in incoherent scattering to reduce energy of primary photon to 81 keV

excitation of singly scattered photons is given in parentheses in Table 3.1. This is analogous to the enhancement effect in XRF at lower energies, except that there, instead of being geometry dependent, it depends on the presence in the matrix of elements of atomic number Z a little higher than of the element of interest, because the effect occurs through fluorescence. The average excitation efficiency in a thick sample lies between the two values given in the table; multiple scattering, sample depth dependence and measuring geometry dependence as well as variations in matrix composition make precise calculation difficult.

In an 'infinitely' thick sample, photons scattered in a

forward direction remain in the sample for further interaction but those scattered backward have a lower probability of further interaction because they may also leave the sample. During scattering, the photons are polarized, and from the second scattering event, a photon tends to be focused to the plane defined by the first event, thus, compared to independent processes, the probability that a multiply scattered photon may leave the sample is enhanced.

3.4.4 Excitation of other heavy elements

X-rays of other heavy elements could possibly interfere with the measurement of trace amounts of gold. Elements from hafnium to radon have K X-rays in the vicinity of the gold X-rays. Only lead has a significant concentration among the heavy metals in Witwatersrand gold ores. All the sources listed in Table 3.1 can excite lead X-rays. At the start of this investigation the reported energy of 87,7 keV for the Cd-109 gamma transition (Lederer,1967) indicated that lead with a K absorption edge of 88,0 keV would not be excited, but experiments soon showed very efficient excitation of this element, and subsequently the gamma energy was reported at 88,023 keV (Dragun,1976).

Uranium is an economically important element associated with gold. Its K absorption edge lies at 115,6 keV. For direct excitation of U only sources emitting photons of energy higher than this can be used.

Measurement of lead, a decay product of uranium, may prove to be a useful measurement for uranium valuation in the Witwatersrand deposits where hardly any leaching is

forward direction remain in the sample for further interaction but those scattered backward have a lower probability of further interaction because they may also leave the sample. During scattering, the photons are polarized, and from the second scattering event, a photon tends to be focused to the plane defined by the first event, thus, compared to independent processes, the probability that a multiply scattered photon may leave the sample is enhanced.

3.4.4 Excitation of other heavy elements

X-rays of other heavy elements could possibly interfere with the measurement of trace amounts of gold. Elements from hafnium to radon have K X-rays in the vicinity of the gold X-rays. Only lead has a significant concentration among the heavy metals in Witwatersrand gold ores. All the sources listed in Table 3.1 can excite lead X-rays. At the start of this investigation the reported energy of 87,7 keV for the Cd-109 gamma transition (Lederer,1967) indicated that lead with a K absorption edge of 88,0 keV would not be excited, but experiments soon showed very efficient excitation of this element, and subsequently the gamma energy was reported at 88,023 keV (Dragun,1976).

Uranium is an economically important element associated with gold. Its K absorption edge lies at 115,6 keV. For direct excitation of U only sources emitting photons of energy higher than this can be used.

Measurement of lead, a decay product of uranium, may prove to be a useful measurement for uranium valuation in the Witwatersrand deposits where hardly any leaching is

thought to have taken place.

Excitation of the platinum group metals is very similar to that of gold and the same sources can, therefore, be considered for their determination in ores.

Good shielding materials are by their nature efficiently excited and possible interference by these X-rays needs to be held to acceptably low levels.

4 THE BACKGROUND SPECTRUM

A spectrum of 88 keV Cd-109 radiation backscattered from a blank rock is shown in Figure 4.1. It was measured with a system resolution of 600eV full width half maximum (FWHM) at 88 keV and the scattering angle from source to sample to detector was greater than 165°. Direct radiation from the source or source shield to the detector was negligible.

The most prominent feature in the spectrum is the intense incoherent or Compton scattered peak C. A much smaller peak marked A, approximately 1/100 of the peak

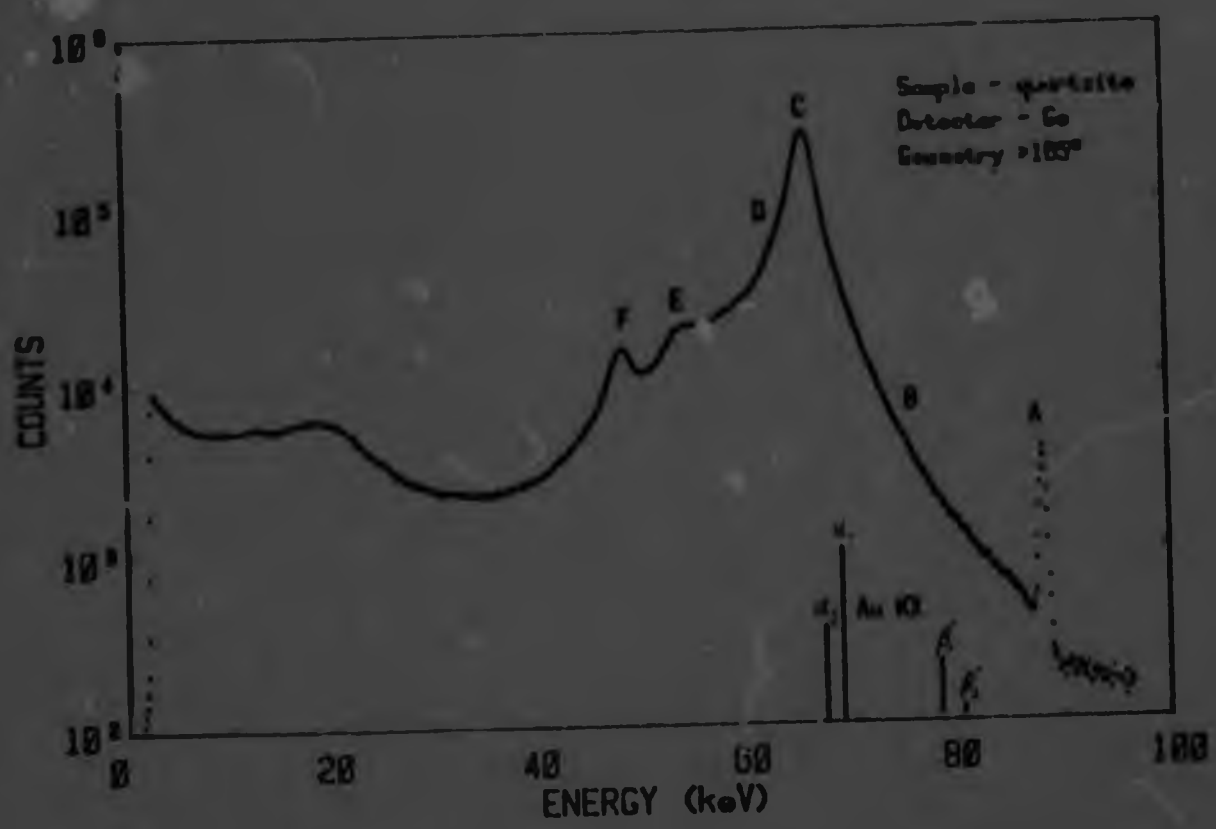


Fig. 4.1 Cd 109 backscatter spectrum from blank rock

intensity of C, arises from coherent scattering of the 88 keV source radiation. Peaks E and F are tungsten K X-rays from the source shield, backscattered by the sample. Our main concern is with the continuum region B where the gold K X-rays have to be measured or with region D when higher energy sources are used for which the prominent Compton peak C lies above the energy of the gold K X-rays.

The true sample spectrum is degraded by the resolution of the detection system so that sharp lines appear in the recorded spectrum as narrow Gaussian peaks of specific width. Minor, usually insignificant, deviations from a perfect Gaussian shape occur as a result of imperfections of the system.

The background under a peak determines the detection limit for the peak, and the total background flux taxes the pulse handling capability of the measuring system, thus limiting the speed with which a detection limit can be attained.

An understanding of the scattering processes is important if possible optimisation of the background spectrum is contemplated.

4.1 Photon scattering

Quartz with up to 5% pyrite may be considered the typical matrix for Witwatersrand gold-bearing conglomerate. The relevant photon interaction data, adapted from Gwozdz et.al.(1973), for SiO_2 and SiO_2 + 5% Fe_2O_3 are plotted vs. energy in Figure 4.2. Below 50 keV photoelectric absorption is the dominant mechanism for the attenuation of the photon intensity. Scattering here has a much lower

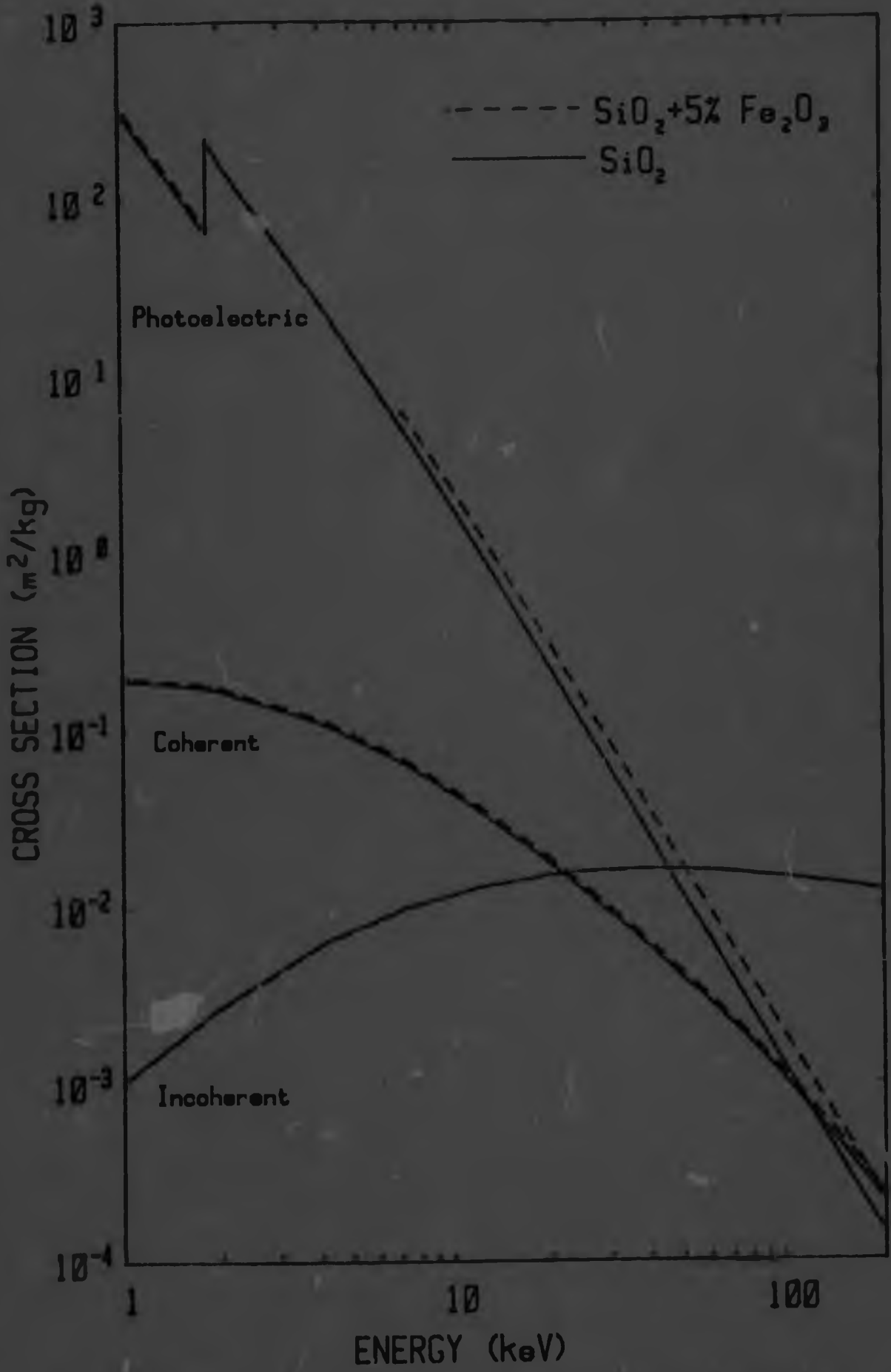
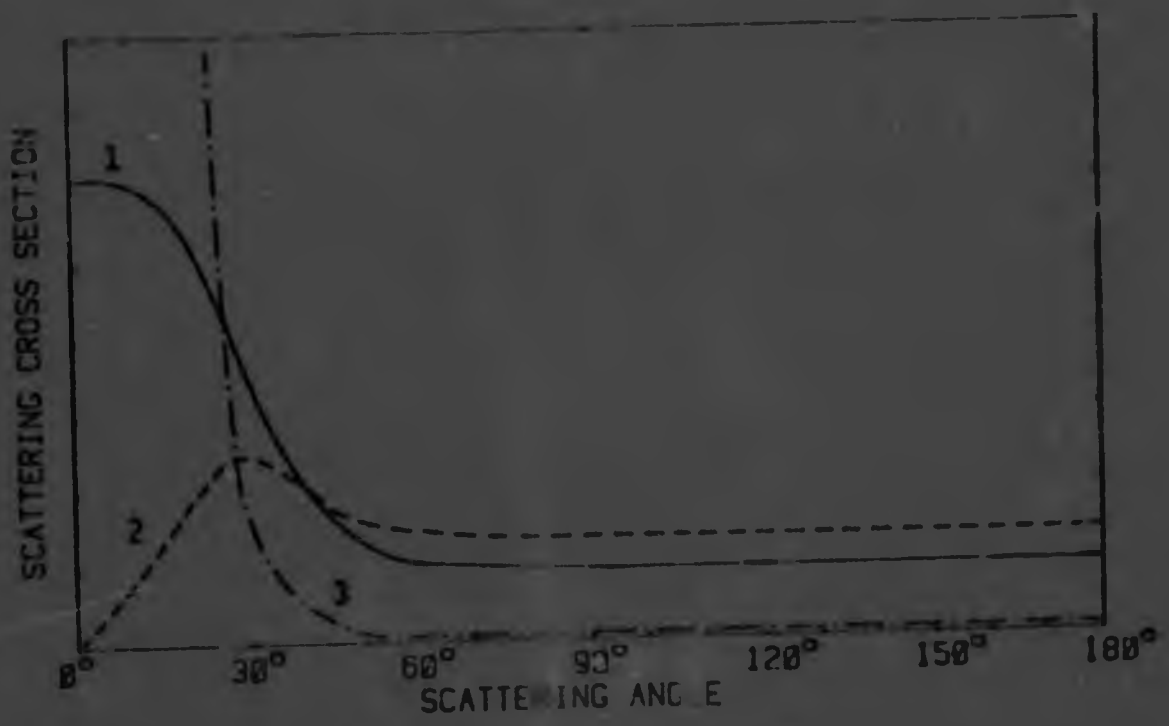


Fig. 4.2 Photon interaction data for 'rock'



4.2 Shape of differential cross sections per unit solid angle for scattering of 98 keV photons from iron. (1)-Compton free electrons, (2)-incoherent and (3)-coherent (after Davisson, 1963).

probability so that the background is low relative to the intensity of the X-ray peaks. Furthermore, the background spectrum below about 20 keV resembles that of the source radiation because scattering more occurs essentially coherently, i.e. without energy loss. The major attenuation of the photon intensity in the energy region above 50 keV comes from the incoherent scattering effect. At 80 keV the coherent scattering cross section is smaller by a factor of 7 or more. The energy loss in this incoherent scattering process results in a translation of the source radiation spectrum to lower energies and considerable modification of this spectrum.

Whereas fluorescent X-rays are emitted in all directions with equal probability, scattering of photons is

anisotropic. The cross sections shown in Figure 4.2 are the values integrated over all directions. The recorded background is thus dependent on the measuring geometry.

The energy dependence on scattering angle Θ for a Compton electron (i.e. stationary electron) was given in 3.4.3 -

$$E' = E/[\ 1 + (1 - \cos\Theta)E/(mc^2)\ ]$$

Klein and Nishina (1929) derived the cross sections in Compton scattering. The differential cross section per unit solid angle is illustrated for iron in Figure 4.3 for unpolarized 88 keV photons.

Bound electrons have specific momentum, and for incoherent scattering at a given angle the photons have an energy distribution known as the Compton profile. Only the peak energy corresponds to the above scattered energy equation. Compton profiles have been calculated from atomic wave functions (Clementi, 1965) and have been measured for a number of gases by Eisenberger et al.(1972). Most of the intensity in regions B and D of Figure 4.1 can be accounted for as the Compton profile. Some of the intensity, however, results from multiple scattering (discussed in the next section) and from instrumental pulse pileup discussed in chapter 9.

Coherent scattering would not be possible from unbound electrons. The peak A at 88 keV in Fig.4.1 is clear evidence that 88 keV photons can be scattered coherently through angles $>165^{o}$ by elements in the sample whose electrons have binding energies well below 10 keV.

An interesting feature of the scattering cross sections

is illustrated in the spectra for photons scattered from iron shown in Figure 4.4. There is a marked step about 7 keV below the 88 keV excitation energy - this energy difference corresponds exactly to the Fe K electron binding energy. The incoherent cross section drops sharply in favour of coherent scattering for energy transfers lower than the binding energy. This is shown qualitatively in Figure 4.3, in which the variation of differential cross sections with unit solid angle is given. A variable iron concentration would result in a variable step in the background spectrum at 81 keV and would reduce the precision with which the background in the gold Kβ peak region could be determined. The percentage of pyrite in Witwatersrand gold bearing conglomerates is, however, low and can cause only a very small step. Furthermore the intensity in the spectral region affected by the step forms only a small fraction of the background intensity useful for the evaluation of the gold Kβ′ peaks so that deterioration in precision would hardly be noticeable in this application.

4.2 Scattering spectrum from thick samples

In thick samples additional intensity in the spectral region between the coherent and Compton peaks arises from incoherent followed by coherent scattering, or vice versa. The incoherent process changes the energy of the photon with a corresponding change in scattering angle which may be insufficient for the photon to return to the detector and the coherent process further changes the direction so that the photon may reach the detector.

The process of combined coherent and incoherent

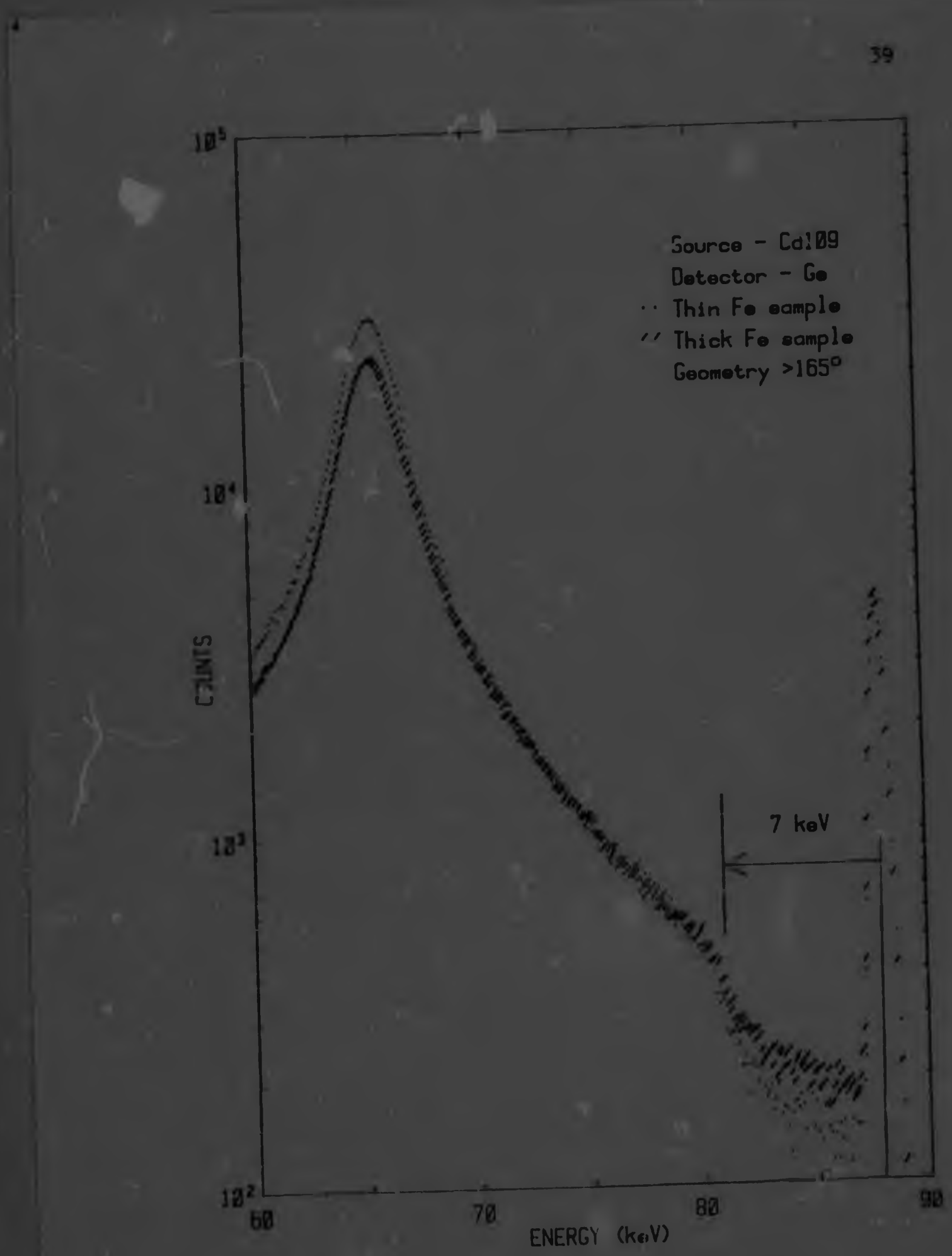


Fig. 4.4 Backscatter spectra from iron samples

scattering in thick samples is confirmed by the relative intensities of the superimposed spectra in Fig.4.4. These have been normalized to the same 88 keV integral peak intensity. The 'thin' sample consisted of a single disc 25mm diameter, 0,5mm thickness; the 'thick' sample consisted of 40 similar discs stacked behind the 'thin' sample. The intensity slightly below 88 keV is about 50% higher for the 'thick' sample from combined scattering, instead of being lower, as might have been expected from the preferential absorption of lower energy photons indicated by the relatively lower intensity of the Compton peak at 65 keV. The explanation for the higher intensity is that the probability for multiple scattering, to give a background contribution in the region between the incoherent and coherent scatter peaks, increases faster with sample thickness than the probability for single scattering represented by the coherent scatter peak.

Although the Compton profile is symmetrical, the intensity at energies below the Compton peak is generally higher than above it, as is evident in Figure 4.1. The additional intensity arises from incoherent scattering, mostly $>90^{o}$, in the source, scattered once more by the sample; source shield X-rays also are scattered by the sample.

4.3 Source-sample-detector (SSD) geometry

As shown later (chapters 6 and 7), in order to optimise the measurement of low gold concentrations in the reef, it is necessary to select both the gold X-ray peaks to be measured and the source so that the peak-to-background ratio is

maximized and the total background itself minimized. Because the background varies with the source-sample-detector geometry, some consideration must be given to the optimum geometry.

For a co-planar source and detector, increasing the SSD angle lowers the energy of the Compton peak thus reducing the background intensity at higher energies while increasing the intensity below it, and vice versa.

For Co-57 and higher energy sources, scattering angles considerably less than 180° would appear to be preferable while for Cd-109 and lower energy sources angles closer to 180° are more favourable.

Limiting the scattering angle to less than 180° implies that the sample should be small relative to the radiation path lengths, defined by the collimation of the source and/or the detector. This is a rather inefficient measuring geometry. Without collimation, a massive sample would subtend between source and detector a range of angles from a minimum all the way up to 180° and decreasing the minimum angle would, therefore, have little effect in reducing the background intensity at energies below the Compton peak; the reduction would be greater above the Compton peak when increasing the angle towards 180°.

Gold determination in situ requires the measurement of rough-surfaced samples* where the distances of samples from

---

* A rough surface may be defined as one where, over the sample area, the root mean square deviation from a flat plane is of the same order of magnitude as the radiation path lengths.

the source and detector cannot be accurately controlled. The minimum scatter angle may thus fluctuate causing an energy shift of the Compton profile as well as changes in the shape of the background from multiple scattering. The variation in the shape of the background contributes a variance to the measurement of fluorescent gold peaks. The closer the minimum scattering angle is to 180^{o} the smaller will be its fluctuation for a given change in sample distance; the finite dimensions of detector and source preclude a scattering angle equal to 180^{o}.

For Cd-109 a number of SSD configurations were tested. In the earliest experiments only a 3mCi Cd-109 source was available and a high geometrical efficiency was sought by placing the source directly on the rock with the detector a few cm behind the source shield. This gave a relatively lower peak-to-background ratio for gold Kβ′ peaks than was observed for the gold Kα peaks excited by Co-57. The source in contact with the sample allowed radiation emerging sideways (in a slighly forward direction) to be scattered by the sample through as low as 90^{o} towards the detector, thus greatly increasing the background under the gold Kβ′ peaks relative to that from a larger minimum scatter angle.

Subsequent measurements with the Cd-109 source placed close to the detector, and away from the sample, to increase the minimum scatter angle improved the gold peak-to-background ratio for Cd-109 so that it exceeded the ratio for Co-57.

In Figure 4.5 the Kβ spectral regions of a gold ore sample, of homogeneous concentration, are shown for central

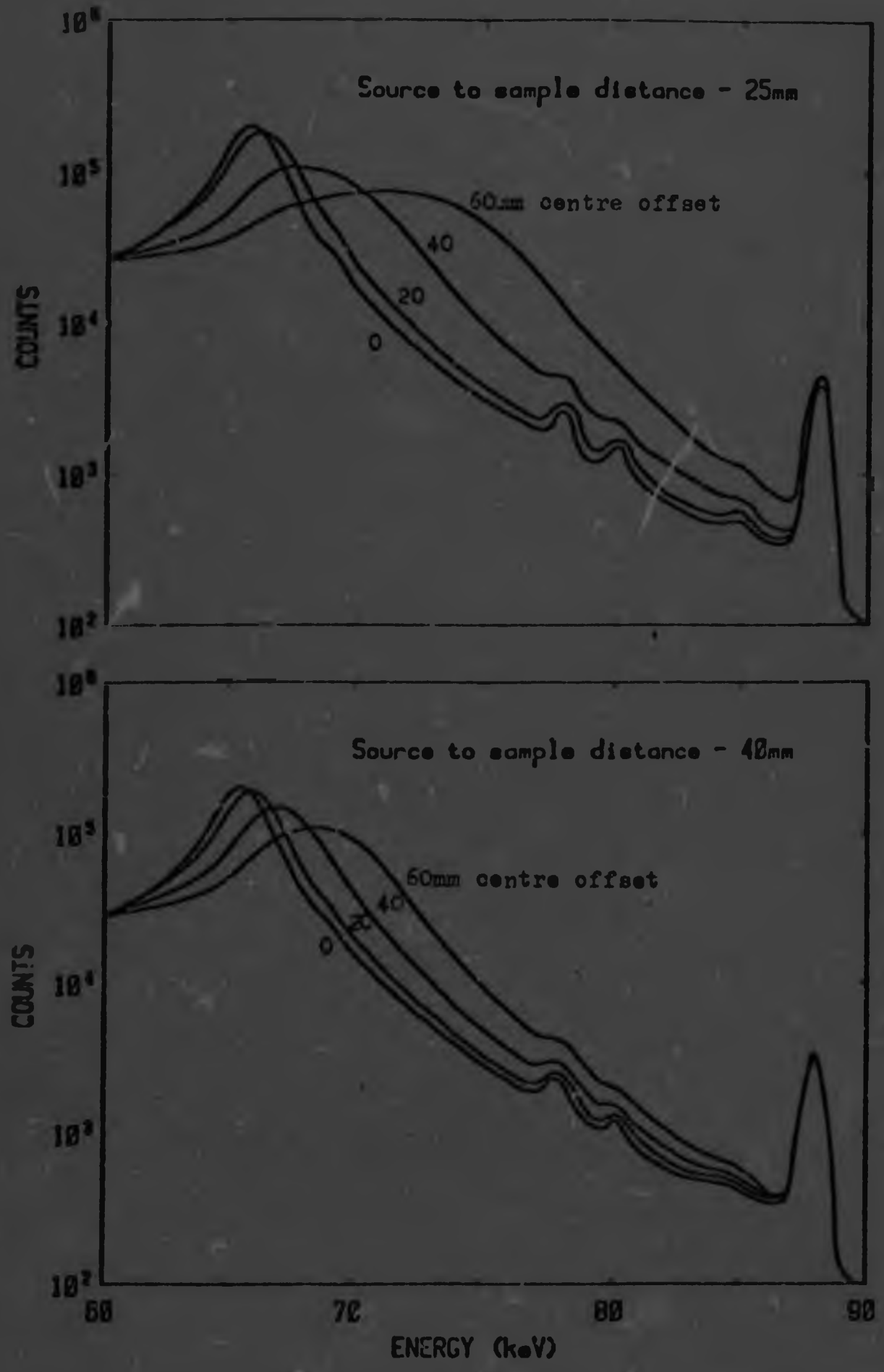


Fig. 4.5 Backscatter spectra from large sample of standard ore for different measuring geometries

and peripheral-source geometries. A 1,5mm diameter Cd-109 source was placed 3mm in front of and from 0mm to 60mm from the axis of a 16mm diameter x 10mm deep Ge detector; the surface of the standard ore sample was at distances of 25mm and 40mm from the detector, and source shield collimation was 120° towards the sample. Annular sources are often used for peripheral-source geometries but a set of point sources at the annulus radius gives the same results.

The spectra in figure 4.5 were normalized to the Au $K\beta_1'$ peak intensity. A change in the slope of the background in the gold Kβ region may be observed. The highest peak-to-background ratio was obtained for the central source geometry.

In figure 4.6 the relative increase of the backscatter

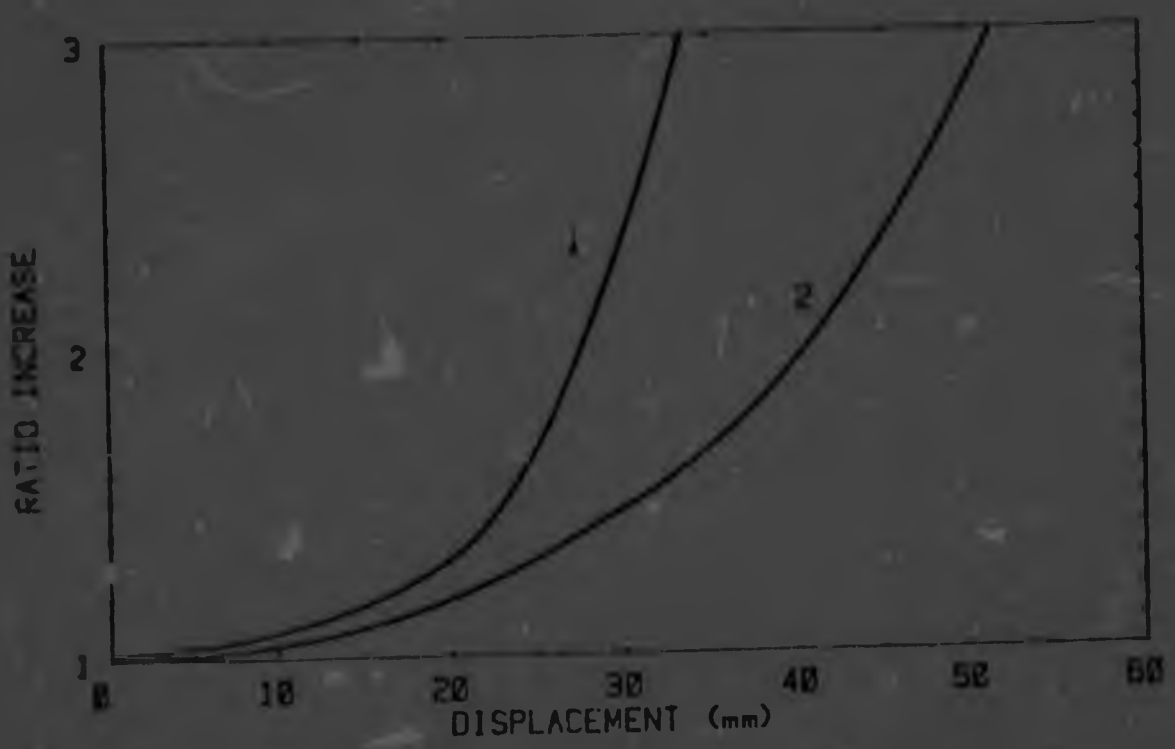


Fig. 4.6 Increase in backscatter intensity at 80keV from peripheral sources relative to that from a central source. Probe-to-sample distance: (1)-25mm, (2)-40mm

intensity at 78 keV (Au $K\beta_1$) is shown relative to that from a central source geometry as a Cd-109 source is moved away form the detector axis. It will be shown in chapters 6 and 7 that, for a fixed peak intensity the measuring time required to attain the same precision of estimation for the peak-to-background ratio is directly proportional to the background intensity in the peak region, other conditions being equal.

For small displacements from the axis of the detector, shadowing from the source decreases the measuring efficiency. A tiny Cd-109 source and shield of 5,5mm outside diameter was developed, so that this shadowing amounted to 12%. Consequently a peripheral Cd-109 source would have to be less than 18mm from the detector axis to show a better performance than a central source of the same strength. Peripheral sources this close to the detector axis hardly offer any manufacturing advantage over a central source system. Moreover, the system for gold determination is limited by the electronic count-rate-handling capability of the measuring system, so that a central source of higher intensity can be employed to compensate for its shadowing effect.

In the second prototype of the portable gold analyser, in an attempt to produce a reliable source shutter, a peripheral source geometry was designed with three sources mounted at 26mm from the detector axis. When the full implication of the increase in measuring time with reduction in the minimum scattering angle was realised the design reverted to a central source geometry for the third prototype.

5 DETECTION OF FLUORESCENT SPECTRA

For rapid determination of gold the photon flux in the gold K X-ray region that emerges from the sample must be detected efficiently and with high energy resolution. The detector parameters which affect efficiency and resolution are evaluated below. In chapter 9 a balance is struck between high efficiency and high resolution, which leads to an optimum measuring time for the determination of gold.

5.1 Geometrical detection efficiency

A few cm away from a large rock sample irradiated by an uncollimated point source, located a similar distance away, the flux spreads over many tens of square centimetres and encompasses directions in a solid angle somewhat less than 2π steradians. With increasing detector area the efficiency increases as more of the flux is detected. However, only the return flux near the source has been scattered through a large angle, which is necessary to give a spectrum of the desired low background. An uncollimated detector of a few cubic centimetres volume located behind the source, should thus have an optimised geometrical efficiency together with the large angle scattering desired.

Detectors commercially available for X- and low energy gamma ray measurement are gas proportional tubes, sodium iodide scintillators and cryogenically cooled silicon and germanium semiconductors.

5.1.1 Detector thickness

For uncollimated measurement the linear absorption coefficient of the detector should be high enough to detect most of the gold K X-rays within a volume close to the source, i.e. within a detector thickness not much greater than its radius. The intensity of 80 keV photons is reduced by half every 310mm, 0,6mm, 13,6mm and 1,37mm in Xe(gas), NaI, Si and Ge respectively, showing that the absorption coefficients of proportional tubes and silicon detectors are too low for this application.

With Cd-109 excitation most of the backscattered radiation has lower energy than the gold Kβ lines. It is thus desirable to use a detector thickness where the gold Kβ lines are detected at close to 100% quantum efficiency since the lower energy radiation is detected with higher efficiency. On the other hand, if Co-57 (122 keV) or Te-123m (159 keV) excitation were to be used a thinner detector having a lower efficiency for this higher energy radiation would discriminate against the unwanted radiation, i.e. the detector filters the desired X-rays.

With Cd-109 excitation and Ge detectors the linear detection efficiency for 80 keV and 65 keV photons and their ratio is shown in Figure 5.1. There is little improvement in the 80 keV/65 keV efficiency ratio for detectors thicker than three to four millimetres. However, the electronic noise resolution of the detector system improves with the lower capacitance of thicker detectors. A limitation on increasing the thickness is the maximum

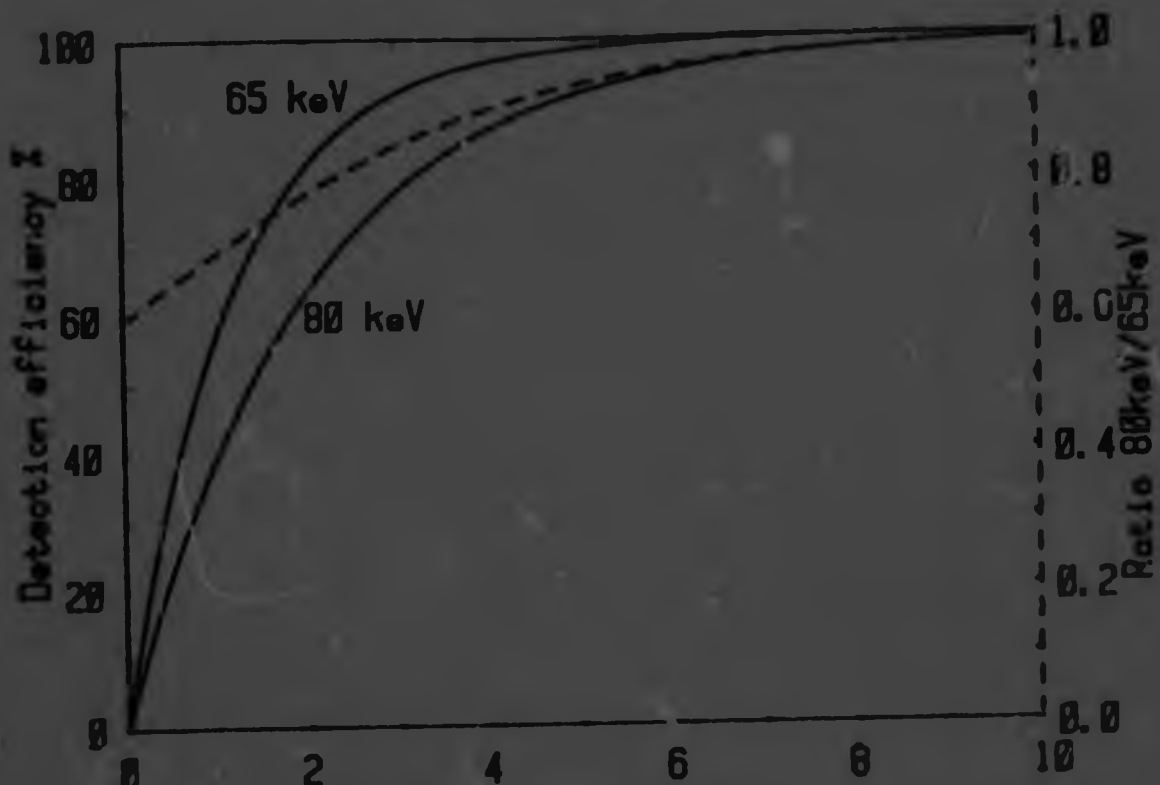


Fig 5.1 Linear detection efficiencies and their ratio vs. Ge detector thickness

desirable charge collection time, which amounts to 10ns/mm in the detector, since this proportionally affects the pulse-pair-resolution time for amplifier pileup rejection.

From these considerations, a Ge detector thickness of 7mm appears near optimum.

5.2 Energy resolution

In the X-ray region below 30 keV excellent line resolution can be attained with crystal diffractometers, i.e. wavelength dispersive systems. Their geometrical efficiency is, however, extremely low because only radiation from the sample collimated to fractional millisteradians is measured. The low geometrical efficiency requires a complementary high flux which is in practice available only

from X-ray tubes. In the gold K X-ray energy region, the crystals of wavelength dispersive systems also have a low diffraction efficiency and in fact have a poorer resolution than germanium detectors.

Sodium iodide (thallium activated) would be the most convenient type of photon detector because it requires no cooling and is highly efficient, but its energy resolution is rather poor in the X-ray region and additional energy discrimination would be required such as crystal diffraction or a pair of balanced filters which, by selective absorption, allow the determination of single elements in paired measurements.

Semiconductor detectors have inherently a high energy resolution for X-rays and may be used without additional energy discrimination. An inconvenience, particularly for portable applications, is that this resolution is realized only at cryogenic temperatures, conventionally at $77^{o}K$ (liquid nitrogen). The development in recent years of hyperpure germanium has, however, greatly reduced the cooling problem which prior to this meant lifetime cooling of the detector to prevent undrifting of compensating lithium ions. Warmup of these detectors between daily operation no longer has a deleterious effect on the resolution.

The energy window of a pair of platinum/iridium balanced filters (whose thicknesses are balanced to exhibit the same absorption characteristics outside their energy window) for the measurement of the gold $K\beta_1$ lines is 2,28 keV, while the resolution of a thin NaI scintillator crystal for associated

background measurement is about 11 keV FWHM. These parameters may be compared to the 0,6 keV FWHM resolution of a germanium detector, which permits simultaneous measurement of peak and background and thus enables gold to be determined with a germanium detector at least ten times, and probably closer to a hundred times faster, than with balanced filters and a thin NaI crystal.

5.2.1 Resolution of germanium detectors

The energy resolution of a germanium detector is a function both of the photon energy and of the electronic noise of the detector system.

The FWHM energy resolution of the system is given by (Woldseth, 1967)

$$\Gamma = \sqrt{(5{,}55\ F\varepsilon E + \Gamma_n^2)} \qquad 5.1$$

where

F = Fano factor $\sim 0{,}125$ for Ge

ε = energy per hole electron pair $\sim$ 2.93eV in Ge

E = photon energy (in eV)

Γ_n = FWHM system noise resolution

The constant 5,55... converts squared units of FWHM to standard deviations.

In what follows, the approximate resolution of a germanium detector is taken at 80 keV (the energy of the gold $K\beta'_2$ lines) and a preliminary evaluation of the noise resolution is made. Further calculations of the noise resolution are given in chapter 9.

The inherent resolution for germanium at 80 keV, i.e. if there were no electronic noise (Γ_n=0), is 406eV (i.e. 5,55x0,125x2,98x80000eV). Cooled field effect transistors

and pulsed-optical-feedback circuits are commercially available with an electronic noise performance which matches the still smaller inherent resolution at lower photon energies. At 80 keV, however, resistive feedback provides adequately low noise performance, and at the same time permits operation at higher count-rates than does pulsed-optical feedback.

The noise resolution Γ_n depends on the amplifier time constant TC, the capacitance of the detector system and on the baseline instability of the amplifier at high count rates.

Integration over time of the equivalent series and parallel noise gives respectively an inverse and direct square root dependence on the system time constant TC for the two noise components -

$$\Gamma_n(\text{series}) \propto 1/\sqrt{TC}$$

and $\Gamma_n(\text{parallel}) \propto \sqrt{TC}$

while $$\Gamma_n^2 = \Gamma_n^2(\text{series}) + \Gamma_n^2(\text{parallel}) \qquad 5.2$$

This is indicated by the dashed lines in Figure 5.2. For time constants TC shorter than 2μs the total noise resolution is predominantly caused by serial noise and the parallel noise contribution may be disregarded. In this figure the resolution of a typical Ge detector 200mm^{2}x7mm thick measured at several time constants TC is shown as well as the noise resolution of the system with a pulser.

The noise resolution is proportional to the capacitance of the detector system. For a planar detector the capacitance is given by the permittivity x area/thickness. Thus a 7mm thick Ge detector has a capacitance of about

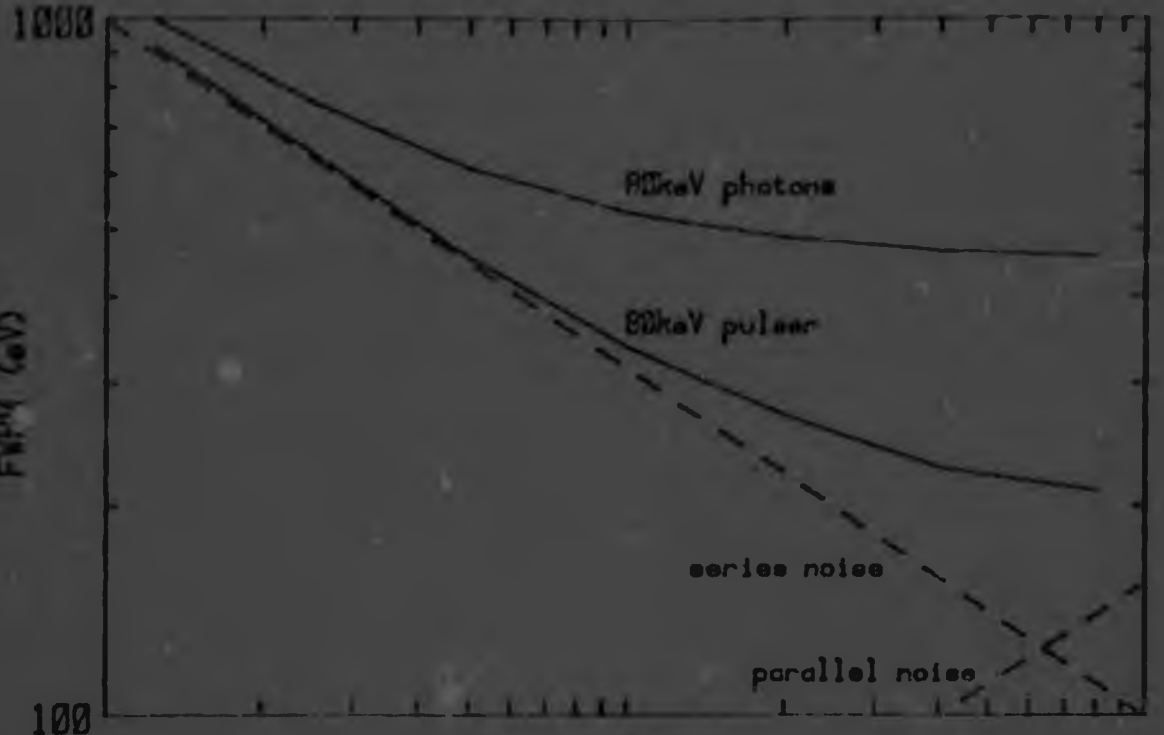


Fig. 5.2 Energy resolution of a 200mm² x 7mm Ge detector

22,5pF/mm² and the stray capacitance in a typical detector system is about 5pF. This gives the noise resolution as -

$$A\Gamma_n \sim {}_{100}\Gamma_n(0,0225A + 5)(2,25 + 5) = (0,003A + 0,7)\,{}_{100}\Gamma_n \quad 5.3$$

where A = area of detector in mm²; thickness 7mm

${}_{100}\Gamma_n$ = noise resolution of 100mm² detector

Combining this with ${}_{200}\Gamma_n \sim 310/\sqrt{TC}$ eV the approximate noise resolution at time constants shorter than 2μs is given by

$$A\Gamma_n \sim (0,003A + 0,7)310/1,3\sqrt{TC}\ \text{eV}$$

$$\sim (0,73A + 163)/\sqrt{TC}\ \text{eV} \quad 5.4$$

and with equation 5.1, the system energy resolution at 80 keV is

$$\Gamma \sim \sqrt{[406^2 + (0,73A + 163)^2/TC]}\ \text{eV} \quad 5.5$$

Degradation of the resolution and peak shift at high count rates is largely caused by instability of the

amplifier baseline which is additive to the amplifier peak height. With good baseline restoration, amplifier duty cycles as high as 95% can be tolerated, whereas with poorer restoration, instability may be noticed at duty cycles of 40% or even lower. In the gold detector duty cycles are maintained below 30% so as to keep the signal processing efficiency high. Degradation of the resolution and peak position with highly varying count rates, as encountered in scanning rough rock faces, should, therefore, be low.

It has been shown above that, for gold determination with Cd-109 excitation, the detection efficiency of a germanium detector is closely proportional to its area and the energy resolution is a function of the area and system time constant given by equation 5.5. These relationships will be used in chapter 9 to derive the optimum detector size and system time constant for gold determination.

6 FUNDAMENTALS IN SPECTRUM EVALUATION

In previous chapters, optimisation of the throughput of a detector amplifier sub-system was discussed. All too often a great deal of attention is paid to the throughput of this sub system while the evaluation of the output spectrum is treated rather poorly, resulting in reduced total system performance. In this chapter, handling of the amplifier output in the portable instrument is discussed. Although highly efficient spectral evaluation is desired, at the present time instrument simplicity may dictate a slightly reduced efficiency. Advances in technology may in the future lead to more complex portable instruments less restricted in the evaluation of the amplifier output. It is shown, however, that the benefits to be gained from additional complexity are likely to be small.

The output from the amplifier is a spectrum of pulse heights. A finely differentiated pulse height or energy spectrum can be obtained by employing an analog-to-digital converter - multichannel system. In this type of system the height of a pulse is analysed by small incremental steps. Alternatively, selected parts of the spectrum can be coarsely differentiated into a few channels by means of separate pulse height discriminators in a set of single channel systems.

In a finely differentiating system, the processing time

or deadtime of the pulse-height-analysis sub-system can sometimes adversely affect the total system output rate. For gold determination, the backscatter spectrum from a rock face would, however, require fine differentiation over only a limited region. This region has a very low count rate relative to that of the total spectrum and fine differentiation in this case need not reduce the useful output rate by more than one percent at the highest practical rates.

The spectral features of importance here are peaks and the background under and adjacent to the peaks. The instrumental response to a monoenergetic line may be considered as purely Gaussian. Although intense single peaks may also show non-Gaussian tails, these are usually small and need not concern us here. The background in the peak region can be considered as a smooth function with no peak structure.

The extent of the spectral region suitable for the evaluation of a peak and its background is normally limited by neighbouring peaks and by the correlation of the background away from the peak to that under the peak.
In the following sections the evaluation of a single peak and its background will be treated analytically. In the following chapter the theoretical results will then be applied to the gold region of the backscatter spectrum.

6.1 Gaussian peak on a constant background

A single Gaussian peak on a constant background will be considered here. Other smooth background functions can readily be related to this simple constant function. For

this case, spectrum evaluation involves the separate determination of peak and background intensities from two or more measured intensity values of various parts of the spectrum. At a given background rate, the standardized variances obtained are directly proportional to the measurement times which would be required to obtain the same measurement precision by the different evaluation schemes. These variances thus form a basis for the objective optimization of the spectrum evaluation.

6.2 Generalized evaluation

For comparison of different evaluation methods a normalized co-ordinate system, shown in Figure 6.1, is chosen, where the peak resolution is given by the Gaussian parameter $\sigma = 1$. The total peak intensity, when integrated from $-\infty$ to $+\infty$, is defined as P units, while the background has an intensity B per unit peak standard deviation. The peak to background ratio R can then be defined as $R = P/B$.

In this normalized co-ordinate system the peak height is $P/\sqrt{(2\pi)}$ and the FWHM resolution is $\sqrt{(8\ln 2)} = 2,35..$. When the normalized R needs to be converted to peak-height ratio, R should be multiplied by $1/\sqrt{(2\pi)} = 0,398..$, while for conversion to FWHM peak area per FWHM background area, R should be multiplied by $\sqrt{(2/\pi)} \int_0^{\sqrt{(2\ln 2)}} \exp(-t^2/2)\,dt = 0,429..$.

Measurements in a spectral region can be performed in a number i of independent measuring channels, each bounded by lower and upper discriminators at energies $_{i}t$ and $_{i}u$ respectively, as illustrated in Figure 6.2. For fine differentiation a large number of contiguous channels

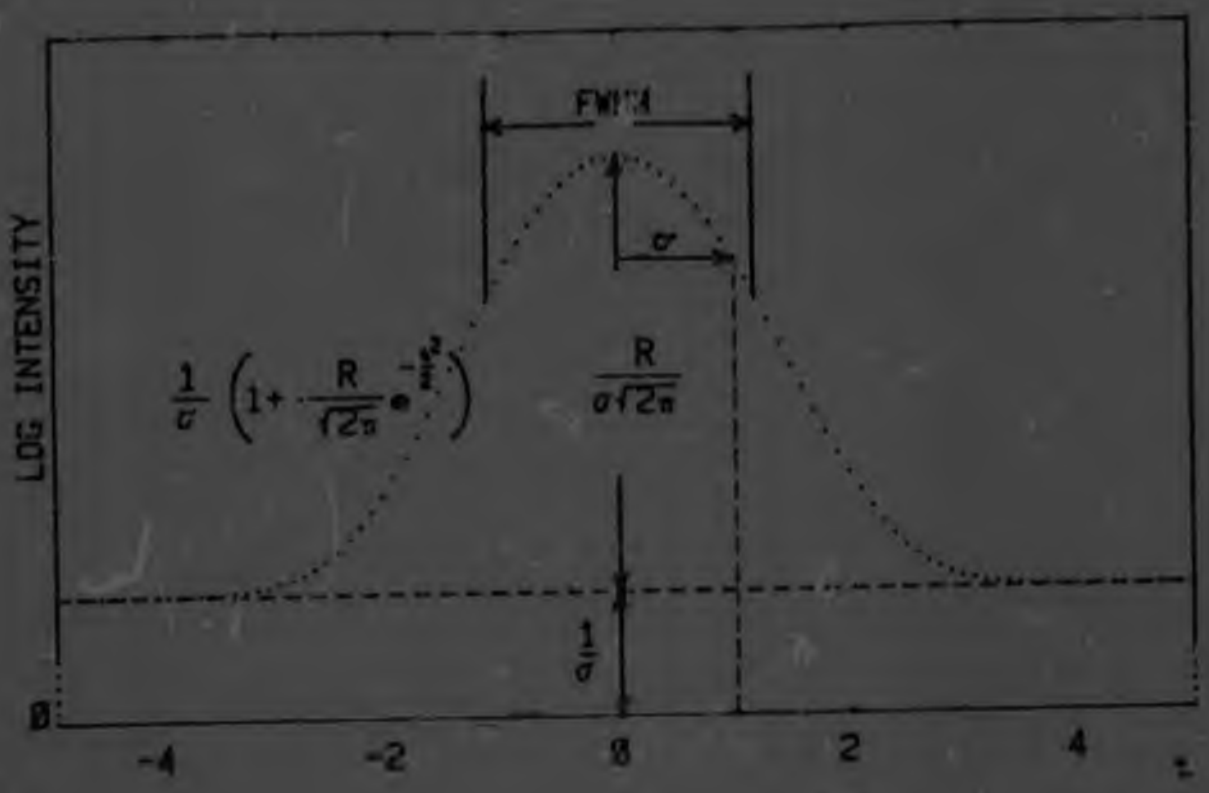


Fig. 6.1 Normalized Gaussian peak and background

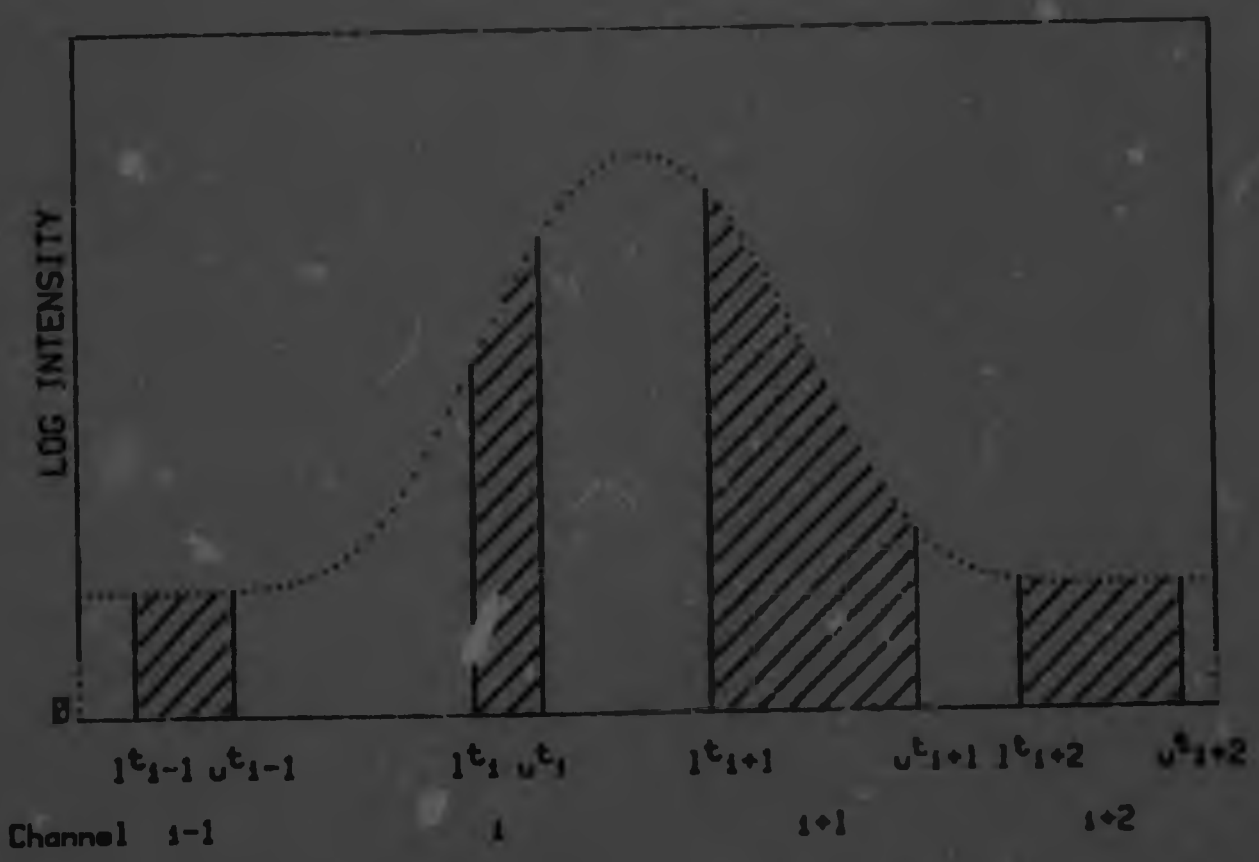


Fig. 6.2 General peak and background measurement

$({}_u t_i - {}_l t_{i+1})$ of equal energy increments $({}_u t_i - {}_l t_i = {}_u t_{i+1} - {}_l t_{i+1})$ are employed so that there are several channels per peak standard deviation. In coarse differentiation a minimum number of two channels, of non-equal energy increments, or spaced asymmetrically about the peak, is required.

At a true peak and background intensity $\hat{P}$ and $\hat{B}$ the expected intensity in each measuring channel is given by -

$$\begin{aligned} Y_i &= \hat{B}\,({}_u t_i - {}_l t_i) + \hat{P}\,({}_l t_i \int^{{}_u t_i} \mathrm{Exp}(-t^2/2)\,dt/\sqrt{(2\pi)} \\ &= \hat{B}\,t_i + \hat{P}\,G_i \\ &= \hat{B}\,(t_i + \hat{R}\,G_i) \end{aligned}$$

The intensities are Poisson variables, and the expected mean and variance thus have the same value -

$$\begin{aligned} V[Y_i] &= \hat{Y}_i \\ &= \hat{B}\,t_i + \hat{P}\,G_i \\ &= V[Bt_i] + V[PG_i] \end{aligned}$$

A solution for P and B can be obtained from measured intensities by the following weighted least squares calculation

$$\begin{vmatrix} P \\ B \end{vmatrix} = \begin{vmatrix} \sum_i G_i^2 W_i & \sum_i t_i G_i W_i \\ \sum_i t_i G_i W_i & \sum_i t_i^2 W_i \end{vmatrix}^{-1} \begin{vmatrix} \sum_i Y_i G_i W_i \\ \sum_i Y_i t_i W_i \end{vmatrix}$$

$$= \frac{1}{D} \begin{vmatrix} \sum_i t_i^2 W_i & -\sum_i t_i G_i W_i \\ -\sum_i t_i G_i W_i & \sum_i G_i^2 W_i \end{vmatrix} \begin{vmatrix} \sum_i Y_i G_i W_i \\ \sum_i Y_i t_i W_i \end{vmatrix}$$

where the determinant is -

$$D = \frac{1}{2} \sum_i \sum_j (t_i G_j - t_j G_i)^2 W_i W_j$$

The solution of maximum likelihood would be obtained with weighting factors W_i equal to the reciprocal of the true variance of Y_i i.e. for

$$W_i = 1/V[Y_i]$$

$$= 1/\hat{Y}_i$$

In a measuring situation the true means and variances are unknown. If, however, the measured intensities are high enough then they can be taken as a good approximation for the true values -

$$Y_{i\ >>1} \rightarrow \bar{Y}_i$$

When the measured intensities Y_i are small, the least squares calculation can be performed without the weighting factors w_i - usually with little deterioration in accuracy of the results. The first calculation can be followed by one or two iterative calculations using improved weighting factors.

In two-channel analysis the same means are obtained with or without weighting factors but the variance is affected by the weighting factors.

6.3 Variance of the peak to background ratio

In the present analytical evaluation with a priori knowledge of the P and B, the true values of $1/\hat{Y}_i$, even at low intensities, are available as weighting factors for the variance analysis of expected P and B.

The variance of P and B are given by the diagonal elements of the square covariance matrix -

$$V[P] = \frac{1}{D} \sum_i t_i^2/\bar{Y}_i$$

$$V[B] = \frac{1}{D} \sum_i G_i^2/\bar{Y}_i$$

The variance of the peak-to-background ratio, derived by the delta method (Hawkins, 1975), involves all the elements -

$$V[P/B] = \frac{1}{D}\left(\sum_i t_i^2/\bar{Y}_i + 2R \sum_i t_i G_i/\bar{Y}_i + R^2 \sum_i G_i^2/\bar{Y}_i \right)$$

$$= \frac{\bar{M} \sum_i (t_i + \hat{R} G_i)}{\frac{1}{2} \sum\sum_{ij} \frac{(t_i G_j - t_j G_i)^2}{(t_i + RG_i)(t_j + RG_j)}}$$

The last equation, in various forms, was applied to the differential multichannel and to the three single channel-schemes for spectrum-evaluation shown in Figure 6.3. The background intensity was standardized to a single (Poisson) count per peak standard deviation, i.e. B=1, to allow comparison of variances. Only the region t>=0 was considered because peak and background are symmetrical about t=0. This one-sided analysis facilitates adaptation of the evaluation scheme to pseudo two channal situations where the spectrum on one side of a peak often differs from that on the other side.

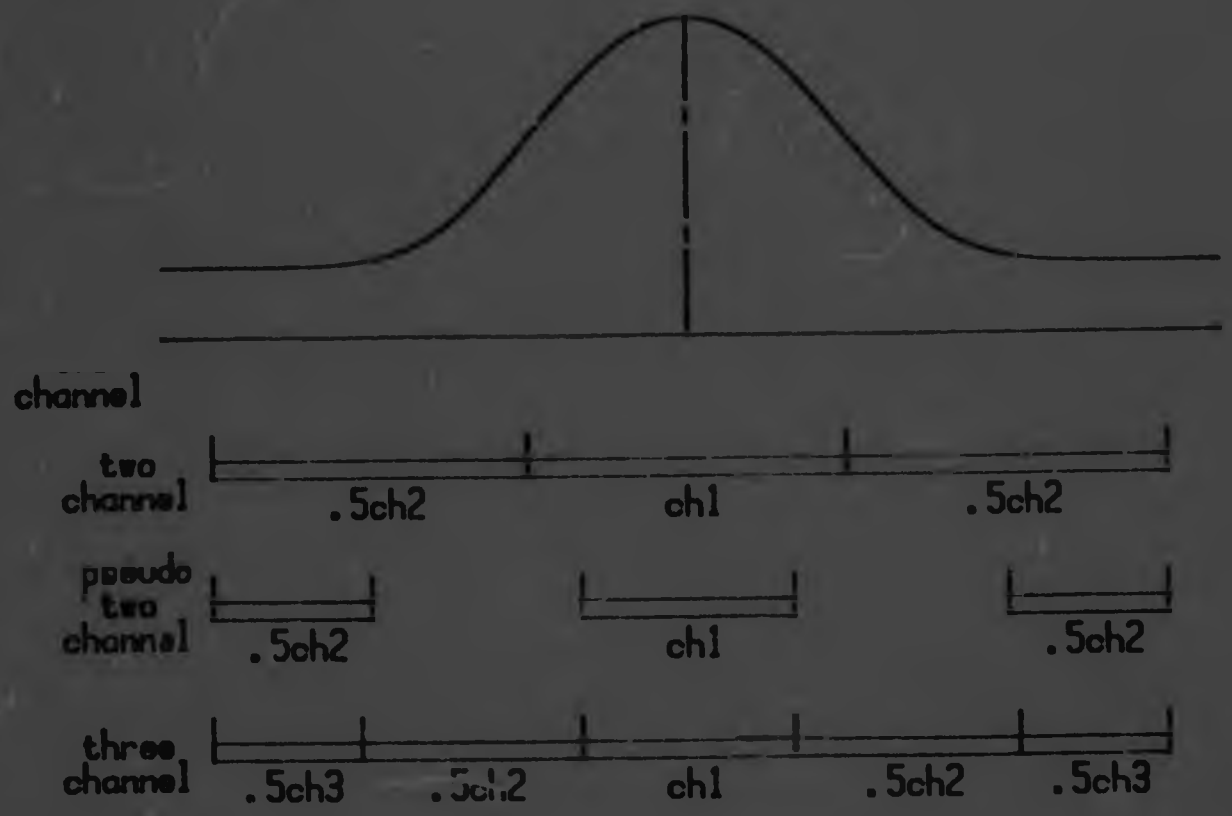


Fig. 6.3 Single channel schemes for peak evaluation

Variances were computed for a series of peak to background ratios R from 1000 to 0,01 and R=0, and for a range of maximum available background regions, t_{max} from infinity to 1σ, where the highest discriminator would be positioned.

In Figure 6.4 the standardized background multichannel (superscript m) variance ${}^{m}_{R}V_{t_{max}}$ of the peak-to--background ratio with an unlimited background region, i.e. $t_{max} \longrightarrow \infty$, is shown for the above series of peak-to-background ratios. For R=0 we have ${}^{m}_{0}V_{\infty} = 4\sqrt{n} = 7,09$ and a logarithmic scale of ${}^{m}_{R}V_{\infty} / {}^{m}_{0}V_{\infty} - 1$ was chosen for clarity in presentation of the variance. In Figure 6.5 the standardized multichannel variance at limited background regions divided by those at unlimited background, from the previous figure, ${}^{m}_{R}V_{t_{max}} / {}^{m}_{R}V_{\infty}$ are given. The relative variances are plotted on a logarithmic scale of ${}^{m}_{R}V_{t_{max}} / {}^{m}_{R}V_{\infty} - 1$ while the maximum available background region is plotted on a log scale of $(t_{max} - 0,67\sigma)$, the constant 0,67 relating to the probability of 0,5, since $\sqrt{(2/\pi)}\int_{0}^{0,67} Exp(-t/2)dt = 0,5$. These curves illustrate the ultimate improvement factor possible in differential multichannel evaluation if an unlimited background region were available.

In single channel schemes the variance for a given R and t_{max} depends on the position(s) of the intermediate discriminator(s). The variance equations when partially differentiated with respect to the intermediate discriminator position(s) and equated to zero, lead to transcendental equations involving normal integrals. The minimum variances were, therefore, computed by successive

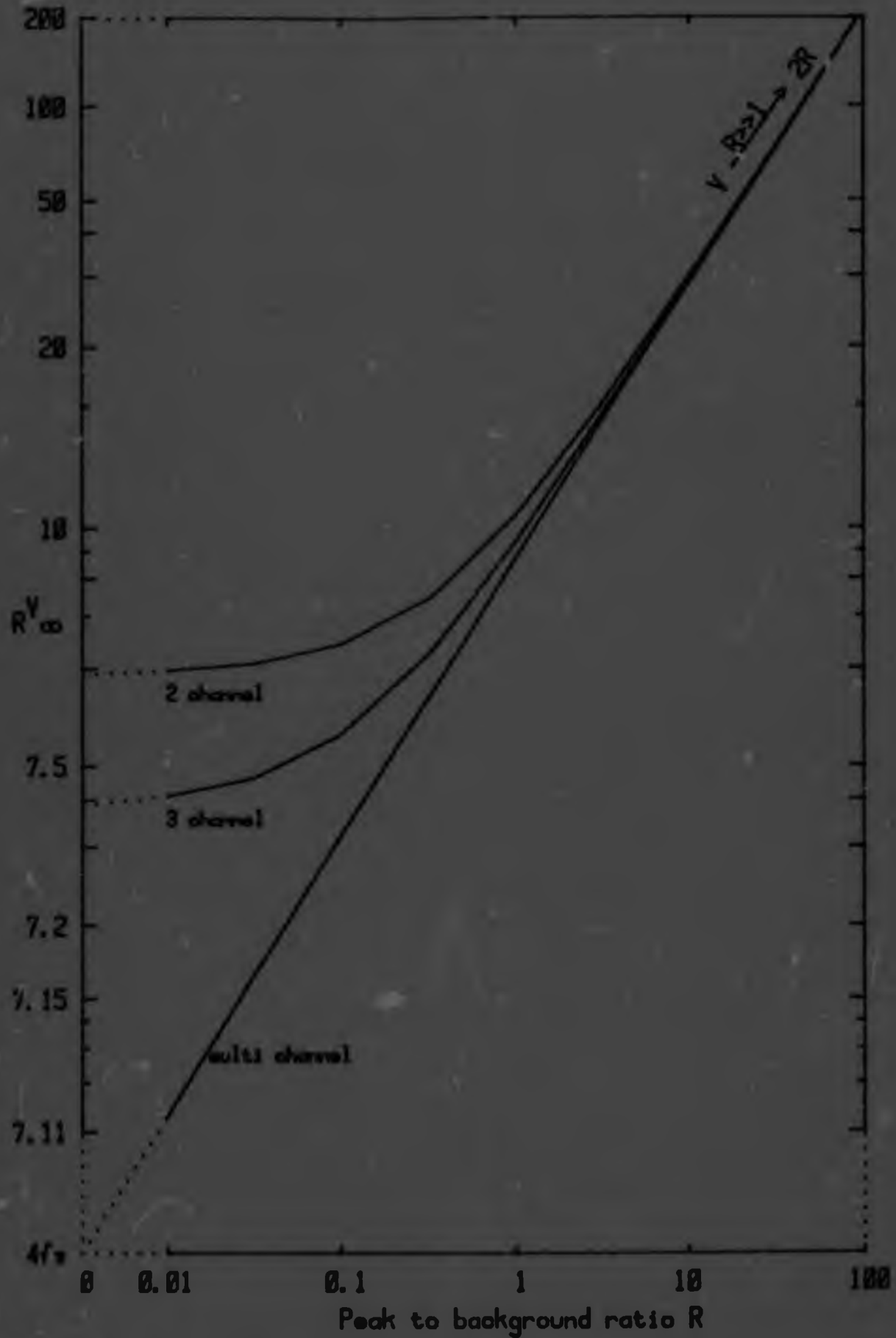


Fig 8.4 Standardized background variances of R ; background region unlimited

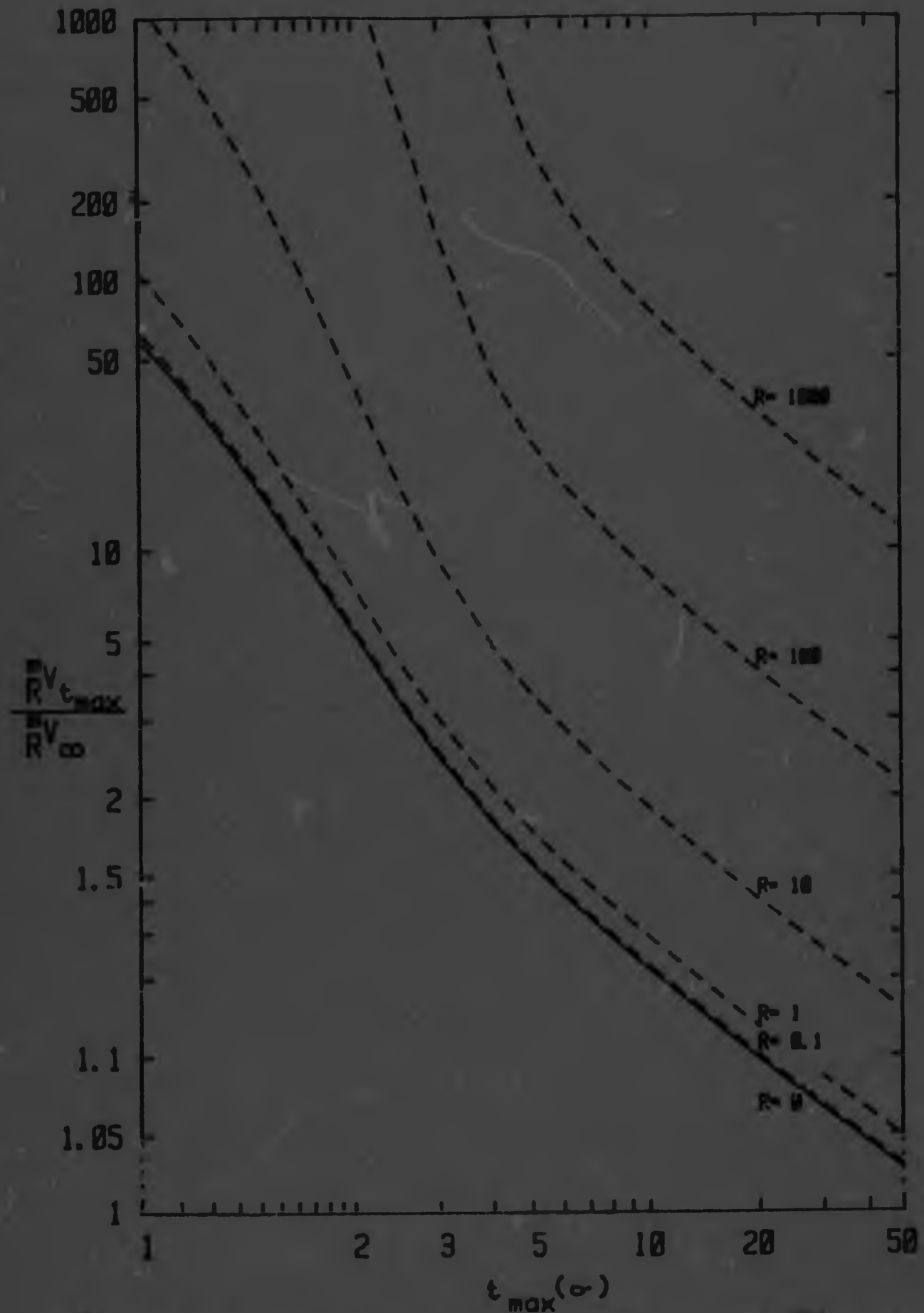


Fig. 6.5 Standardized multichannel variance ${}^{m}V_{t_{max}}$ relative to ${}^{m}V_{\infty}$

approximation of the intermediate discriminator position(s).

Single channel schemes for spectral peak-to-background ratio evaluation employ two or more counting channels. Usually an even number of pulse-height-discriminators is used. A discriminator at the peak centre serves no purpose. An odd number of discriminators would thus be unevenly distributed between the two sides of the peak. This special situation need not concern us here. Mention should, however, be made of the lowest scheme of two contiguous counting channels with 3 discriminators - this can be useful where the background is highly asymmetrical about the peak or where it is imperative to use the lowest posible number of discriminators.

With the same number of discriminators on both sides of the peak the corresponding spectral regions can be counted in the same counting channel. In this analysis only one side of the peak and background region was considered, with the same number of counting channels and half the number of discriminators as used in the whole region. Variances of the peak-to-background ratio were computed for the three single-channel schemes illustrated in Figure 6.3 -

a) ^{2}V for 2 discriminators on a side with two contiguous counting regions - this will be referred to as the 2 channel scheme;

b) ^{3}V for 3 discriminators with three contiguous counting regions - referred to as the 3 channel scheme, and

c) $^{3:2}V$ for 3 discriminators with two non-contiguous counting regions referred to as the pseudo 2 channel scheme; data between the two regions is discarded.

The attraction of using only two counting channels lies

approximation of the intermediate discriminator position(s).

Single channel schemes for spectral peak-to-background ratio evaluation employ two or more counting channels. Usually an even number of pulse-height-discriminators is used. A discriminator at the peak centre serves no purpose. An odd number of discriminators would thus be unevenly distributed between the two sides of the peak. This special situation need not concern us here. Mention should, however, be made of the lowest scheme of two contiguous counting channels with 3 discriminators - this can be useful where the background is highly asymmetrical about the peak or where it is imperative to use the lowest posible number of discriminators.

With the same number of discriminators on both sides of the peak the corresponding spectral regions can be counted in the same counting channel. In this analysis only one side of the peak and background region was considered, with the same number of counting channels and half the number of discriminators as used in the whole region. Variances of the peak-to-background ratio were computed for the three single-channel schemes illustrated in Figure 6.3 -

a) ^{2}V for 2 discriminators on a side with two contiguous counting regions - this will be referred to as the 2 channel scheme;

b) ^{3}V for 3 discriminators with three contiguous counting regions - referred to as the 3 channel scheme, and

c) ^{312}V for 3 discriminators with two non-contiguous counting regions referred to as the pseudo 2 channel scheme; data between the two regions is discarded.

The attraction of using only two counting channels lies

in the simplicity of calculating P and B by the linear algorithms -

$$\begin{vmatrix} P \\ B \end{vmatrix} = \frac{1}{D} \begin{vmatrix} t_2 & -t_1 \\ -G_2 & G_1 \end{vmatrix} \begin{vmatrix} Y_1 \\ Y_2 \end{vmatrix}$$

where $D = G_1 t_2 - G_2 t_1$

and $\frac{P}{B} = (t_2 Y_1/Y_2 - t_1)/(-G_2 Y_1/Y_2 + G_1)$

If a preset count is accumulated in channel 1 or 2 then P, B and P/B can be calculated from the count Y in channel 2 or 1 respectively by $A_1 Y + A_2$, where in the case of P and B the A's are constants and in the case of P/B the A's are functions of Y, but can usually be taken as constants for small values of P/B or over limited ranges of P/B.

When more than two counting channels are used then calculation of the algorithms becomes slightly more laborious and, as indicated in section 6.2, weighting factors $w_i = 1/V[Y_i]$ ought to be used.

In Figures 6.6a to 6.8a the standardized variances of the peak-to-background ratio in single channel analysis relative to those in multichannel analysis are shown. The corresponding positions of the intermediate discriminators, at which the minimum variance occurs, are shown in the (b) parts of the figures. The maximum available background region t_{max} is again plotted on a log scale of $(t_{max}-0,67\sigma)$.

The absolute values of the standardised variances can readily be obtained by multiplying the relative variances in these figures by the appropriate factors from Figures 6.4 and 6.5.

These variances have to be halved when combining the evaluation of both (symmetrical) sides of a peak and have to

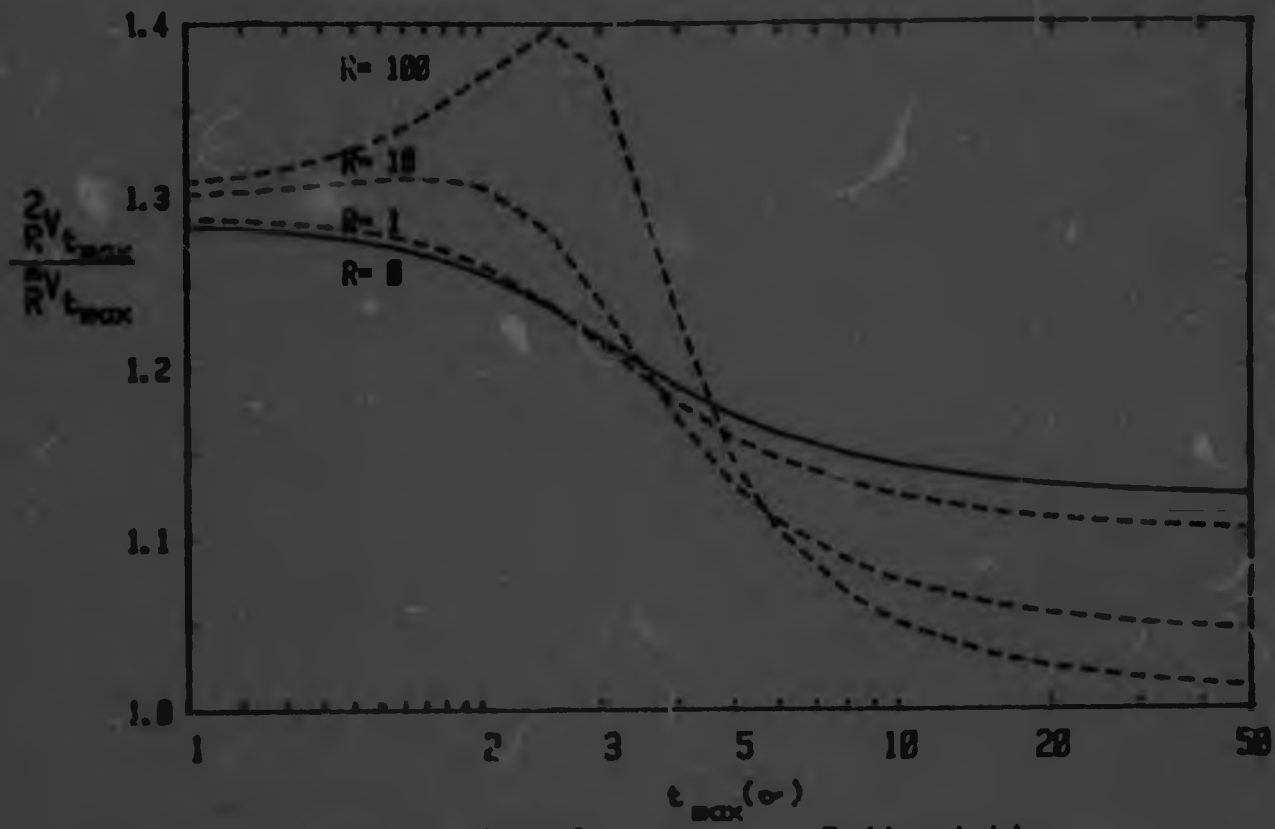


Fig. 6.6a Minimum two channel variance in R (divided by multichannel variance)

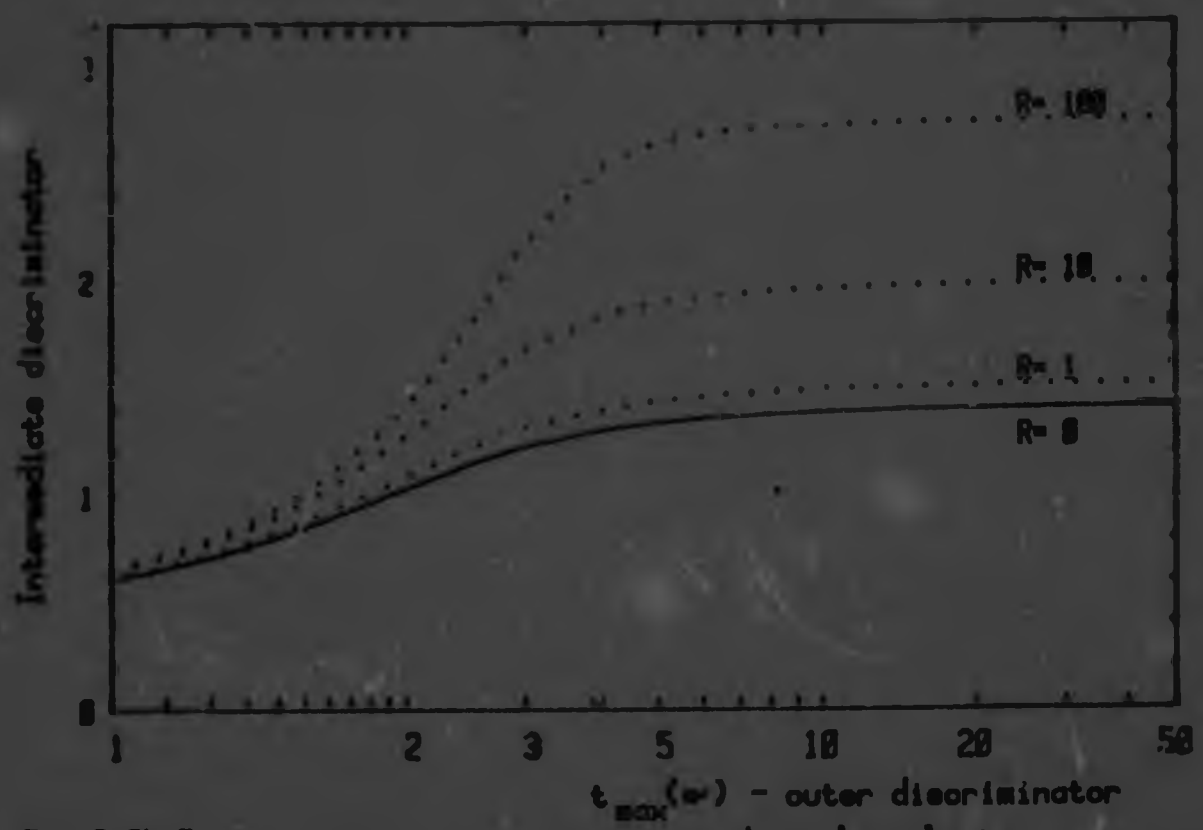


Fig. 6.6b Discriminator positions in two channel analysis for minimum variance in R

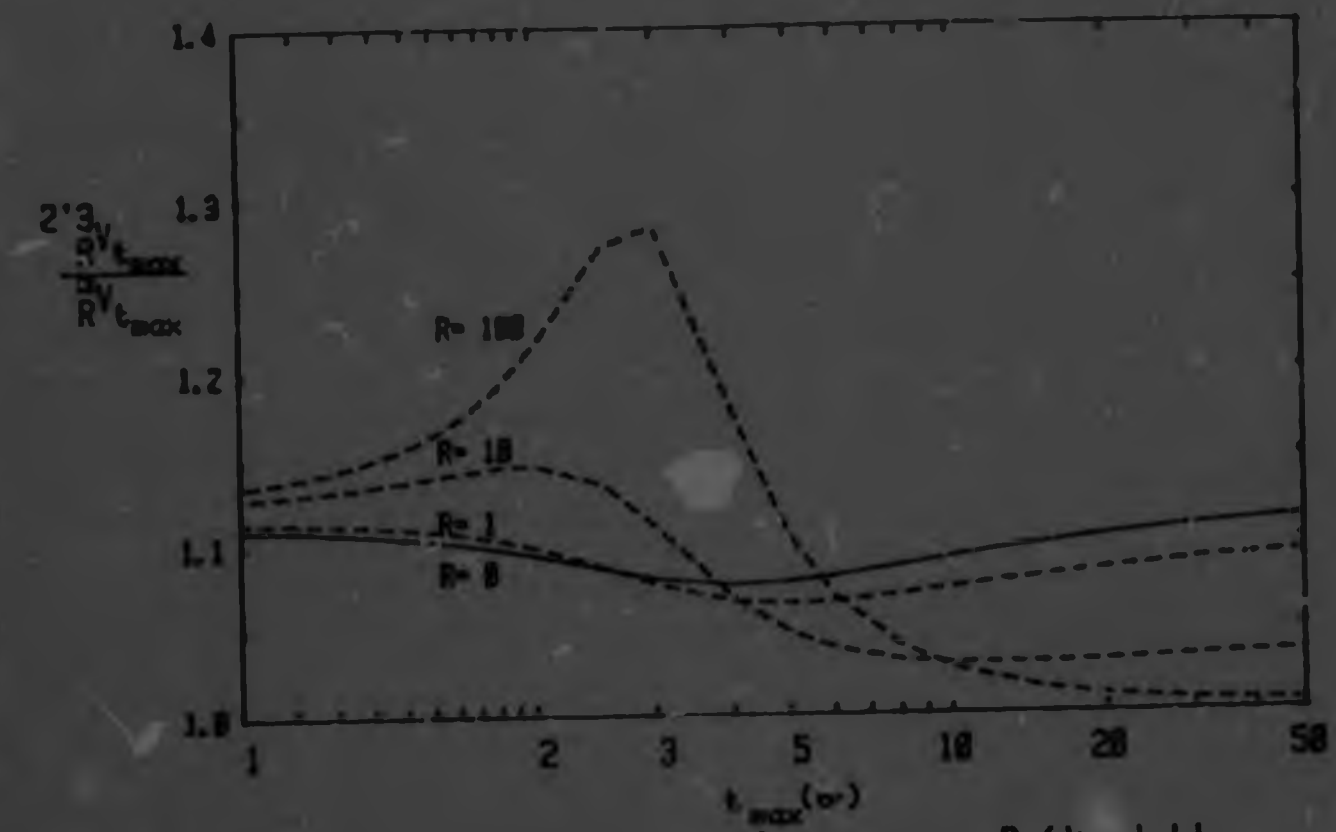


Fig.6.7a Minimum pseudo two channel variance in R (divided by multichannel variance)

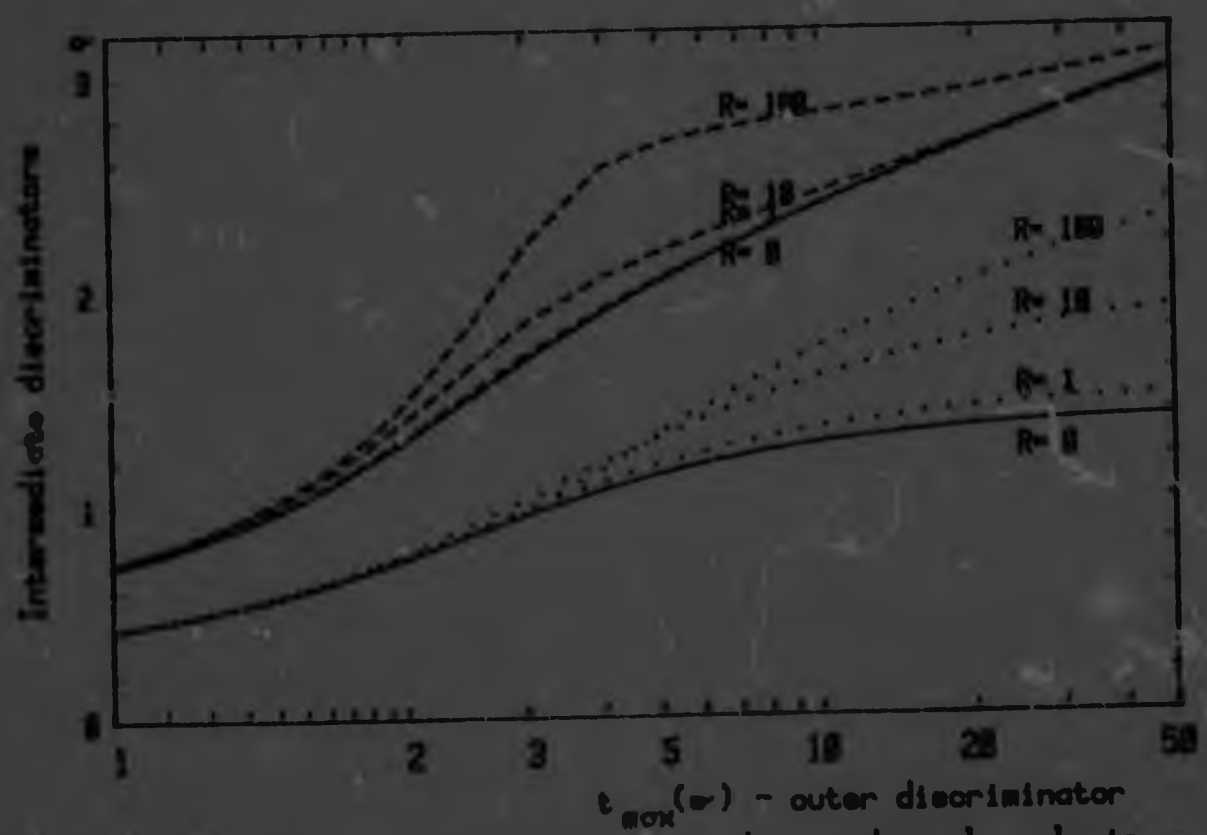


Fig.6.7b Discriminator positions in pseudo two channel analysis for minimum variance in R

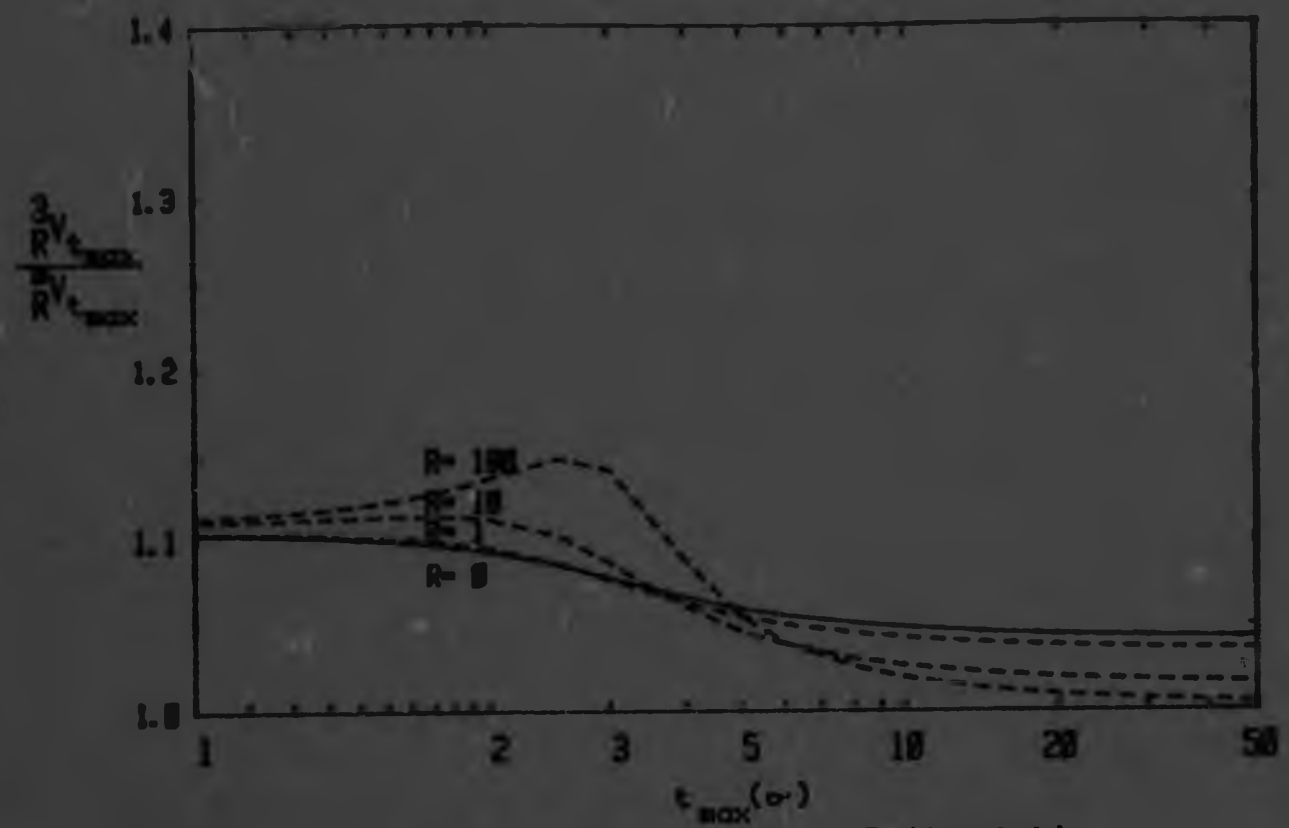


Fig. 6.8a Minimum three channel variance in R (divided by multichannel variance)

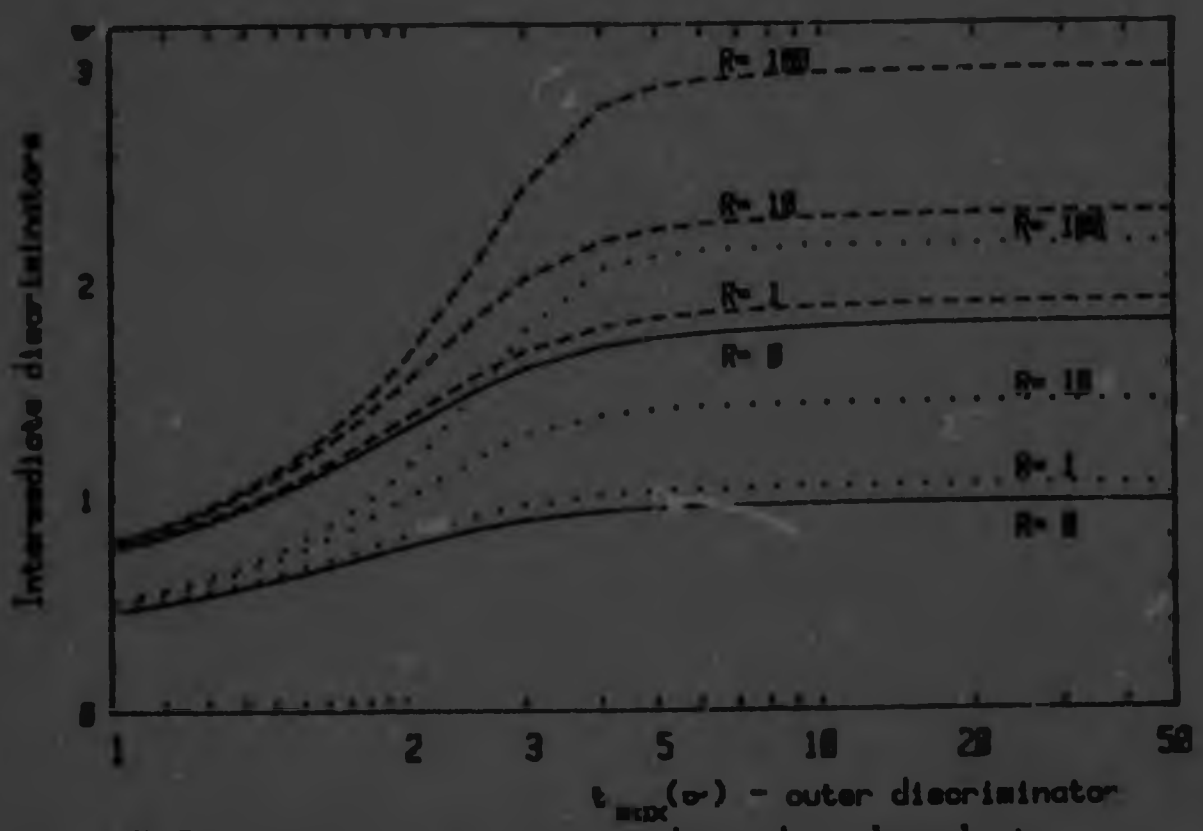


Fig. 6.8b Discriminator positions in three channel analysis for minimum variance in R

be divided by B for non-standardised background conditions. The relative presentation permits ready comparison of the different evaluation schemes.

6.4 Comparison of multichannel and few channel methods

The multichannel variances shown in Figure 6.4 may be considered as the inherent standardised variances of the peak-to-background ratios under standardised background conditions. It may be seen that when ^{m}R increases from 0 to 1 the variance increases by only 32% (from 7,09 to 9,4) because it is dominated by the standardised background, whereas at high ratios the increase is much greater as the inherent variance tends to the value 2R. At high ratios, the peak intensity on its own is usually more important than the peak-to-background ratio but at low ratios the opposite is often the case, as it is in the gold detection problem.

From Figure 6.5, it may be seen that, for ratios below R=1, little improvement in variance is to be gained by using background regions beyond $t_{max}=10\sigma$ (i.e. 4 FWHM from the peak centre position). The standardised multichannel variances for $t_{max}=8\sigma$, i.e. $_{R<1}{}^{m}V_{B}$, are only about 30% higher than the inherent variances $_{R<1}{}^{m}V_{\infty}$ requiring an infinite background region; doubling the background region to $t_{max}=16\sigma$ results in only 15% reduction in variance.

It should be pointed out that these theoretical improvements in $^{m}V^{B}$ with larger background regions rest on the assumption that all parts of the background region are perfectly correlated. In real spectra, however, the further a particular background region lies away from a peak, usually the poorer will be its correlation with the

background directly under the peak. This diminishing correlation in real spectra soon balances out the small improvements in variance that theoretically could be gained by greatly increasing the total background region.

On the other hand, when the available background region is reduced below $t_{max} \sim 4\sigma$ the variances deteriorate very rapidly. When this happens on one side of a peak then the other side should be more heavily relied upon for the combined two sided evaluation of the peak. Evaluations for $t_{max} < 2\sigma$ are made usually when there are overlapping or unresolved peaks that are uncorrelated. This case need not be treated here.

Comparison of the various single-channel schemes, Figures 6.6a to 6.8a show that the variances $3:2_V$ of the pseudo-two-channel scheme in very restricted background regions ($t_{max} < 2\sigma$) tend to those of the three channel scheme and at very wide background regions approach the variances 4_V of the two-channel scheme.

It may be seen that, as is to be expected, the variances decrease as more discriminators and counting channels are added. The biggest decrease occurs at the first addition and further additions give rapidly diminishing returns. The total possible decrease is not very large. For $R <= 1$ and $t_{max} => 4\sigma$ the variance even in the two-channel scheme is never more than 18% higher than that in the multichannel scheme; the same holds for large ratios $R>1$ and $t_{max} => 5\sigma$. In single-peak evaluation the simplicity of calculation in two counting-channel schemes leaves little incentive, as far as variance improvement is concerned, for using schemes with

more than two counting channels.

The most widely used scheme is the pseudo-two-channel scheme. Even in the majority of multichannel measurements the peaks are still evaluated according to the pseudo-two-channel scheme. The only basic difference between the little-used two-channel and the pseudo-two-channel schemes is that at a substantial saving of two discriminators the two channel scheme has a slightly higher variance, as shown in Figure 6.6a and 6.7a, particularly at low values of t_{max}. The wide acceptance of the pseudo-two-channel scheme cannot be ascribed to the above difference. It probably stems from the misconception that the pseudo two channel scheme is much more precise or it may have been adopted to simplify calculation. Certainly there is a general unawareness that a two-channel scheme can be implemented by placing both a wide and a narrow single-channel analyser window symmetrically over a peak, the wider counting channel including the narrower counting channel. The algorithms for this overlapping two channel scheme are still just as simple -

$$\begin{vmatrix} P \\ B \end{vmatrix} = \frac{1}{D} \begin{vmatrix} t_1+t_2 & -t_1 \\ -G_1-G_2 & G_1 \end{vmatrix} \begin{vmatrix} Y_1 \\ Y_1+Y_2 \end{vmatrix}$$

where $D = G_1 t_2 - G_2 t_1$

$$\frac{P}{B} = \frac{(t_1+t_2)Y_1/(Y_1+Y_2) - t_1}{-(G_1+G_2)Y_1/(Y_1+Y_2) + G_1}$$

In the pseudo-two-channel scheme the outer counting channel pair is normally placed by inspection far enough for the assumption that $G_2=0$; in the two-channel scheme a similar, somewhat better, approximation $G_1+G_2=0,5$ (per side)

can be made for large enough t_{max}.

In conclusion it can be stated that with an appropriate setting of two pairs of discriminators, the simple two-channel scheme leaves little room for improvement in single-peak evaluation. The far more widely used pseudo-two channel scheme at a 50% increase in the number of discriminators can yield variances in R only marginally better.

7 EVALUATION OF SPECTRA FOR GOLD ANALYSIS

In this chapter the foregoing theoretical results for a single Gaussian peak on a uniform background are applied to the measured spectrum. In gold ore analysis, the relevant part of the spectrum for detailed evaluation consists of a number of gold K X-ray peaks and interfering peaks on a sloping background.

The basis for comparison of spectra is introduced below. Thereafter the spectra from Ba-133, Cd-109, Gd-153, Co-57 and Te-123m excitation are semiquantitatively compared and finally the Cd-109 spectrum will be treated qualitatively in more detail.

7.1 Comparison of different peaks and backgrounds

In the previous chapter, variances were obtained which permitted the comparison of evaluation methods for a single peak on a normalized background. For comparison of the precision or detection limits of different peaks on their particular backgrounds, either the coefficient of variation of the ratios, $CV[R] = \sqrt{V[R]}/R$ i.e. the relative standard deviation at equivalent background counts, or the relative measurement times at a constant background rate to obtain a constant $CV[R]$ may be used. This is basically the same approach as in the previous chapter, although previously standardised conditions allowed some simplification.

At low peak-to-background ratios, i.e. $R<1$, $V[R]$ was

shown to be nearly independent of R because it is dominated by the background so that CV[R] is inversely proportional to R i.e.

$$CV[R] \propto 1/R \qquad \text{(for small R)} \qquad 7.1$$

because the variance of the mean of a number of independent measurements is equal to the variance of the individual measurements divided by the number of measurements, the coefficient-of-variation of a given R is inversely proportional to the square root of the background count B, or the square root of the measurement time at a constant background rate T_B i.e.

$$CV[R] \propto 1/\sqrt{B} \qquad \text{(R constant)} \qquad 7.2a$$

$$\text{or } CV[R] \propto 1/\sqrt{T_B} \qquad \text{(R constant)} \qquad 7.2b$$

It follows that, for different ratios, the same CV will be obtained with background counts B, or measurement times at a constant background rate T_B, that are inversely proportional to the square of the ratio i.e.

$$B \text{ and } T_B \propto 1/R^2 \qquad \text{(CV constant; R small)}. \qquad 7.3$$

Similarly the same CV will be obtained with peak counts P, or measurement times at a constant peak rate T_P, that are inversely proportional to (the first order of) the ratio i.e.

$$P \text{ and } T_P \propto 1/R \qquad \text{(CV constant; R small)} \qquad 7.4$$

These relationships emphasise that the more prominent peaks generally have a lower CV[R]. The ratio has a stronger influence on the coefficient-of-variation than the actual counts. When there are two or more intensity-correlated peaks in a spectrum, it is usual to analyse only the most prominent peak in single-element analysis. When highly efficient spectral evaluation is desired, it may be

worthwhile to look also at the less prominent correlated peaks in order to reduce the total coefficient-of-variation.

7.2 Comparison of spectra from different sources

Sources of five radioisotopes, Ba-133, Cd-109, Gd-153, Co-57 and Te-123m, were used for XRF excitation of the same gold ore sample. The relevant spectra are shown in Figure 7.1. Ba-133, Cd-109, Co-57 and Te-123m showed prominent gold Kα or Kβ' peaks. With Gd-153 the background in the peak regions was much higher and the peaks were no longer discernible above the background noise.

If sources of sufficient strength are available, then the measuring instrument can be operated at its optimum count-rate-handling capability, irrespective of the type of source used. An objective comparison of measurement times required to achieve the same precision when using different types of sources can then be made by normalizing the spectra to the same total count. The count rate handling capability of a measuring instrument, however, depends to some extent on the average energy of the photon flux. Cobalt-57 and Te-123m spectra have average photon energies about 30% and 50% higher than a comparable Cd-109 spectrum. The comparisons below referring to spectra of the same total count, will thus be biased conservatively against Cd-109.

The source excitation efficiency shown in chapter 3 (Table 3.1), when multiplied by the relative intensity of the gold K line from Table 7.1, gives a rough indication of the relative peak height to be expected in a normalized spectrum. Additional source lines, matrix enhancement, and different absorption of Kα and Kβ lines, modify the relative peak height somewhat.

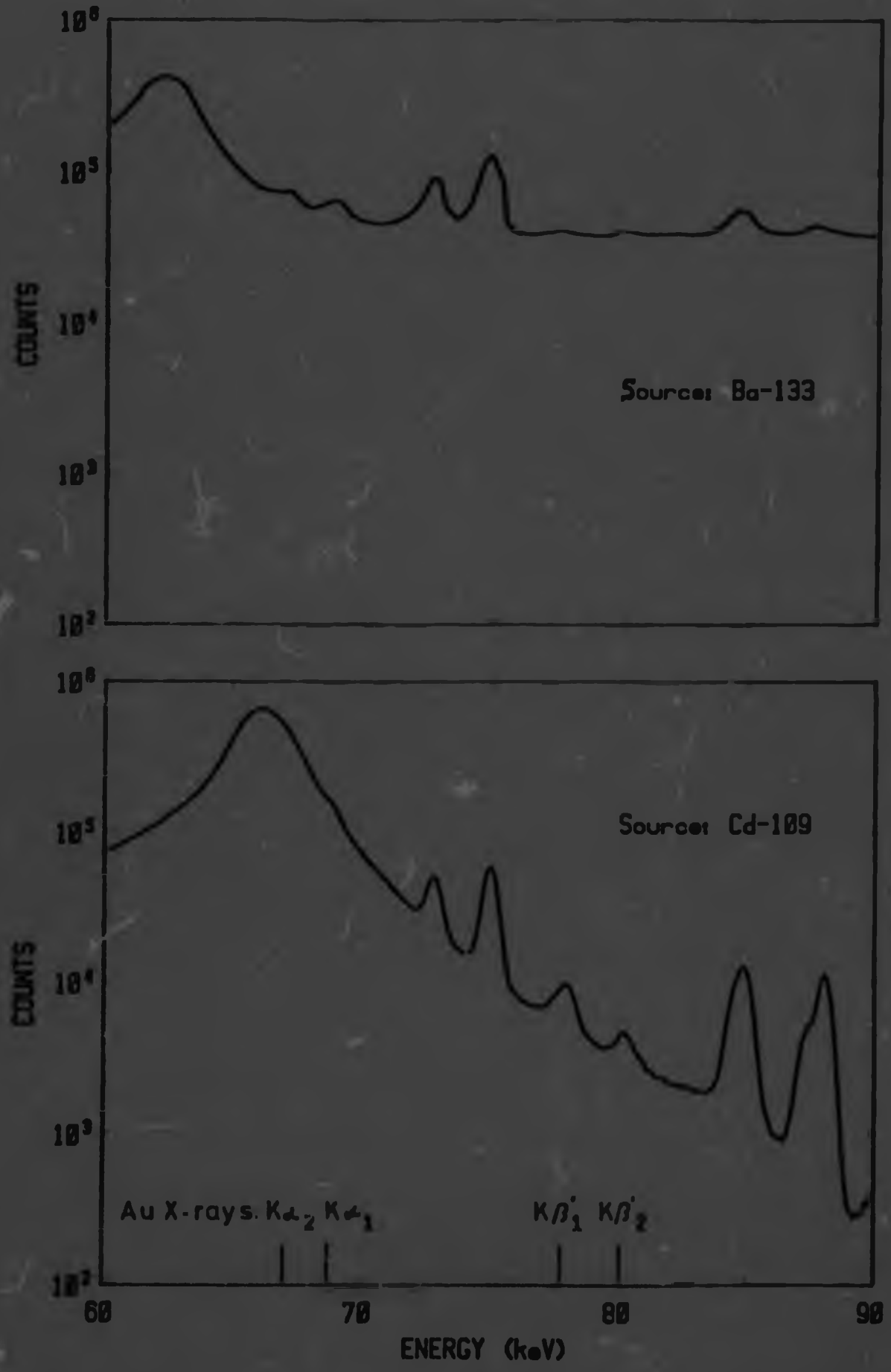


Fig. 7.1 Fluorescence spectra of a standard gold ore sample

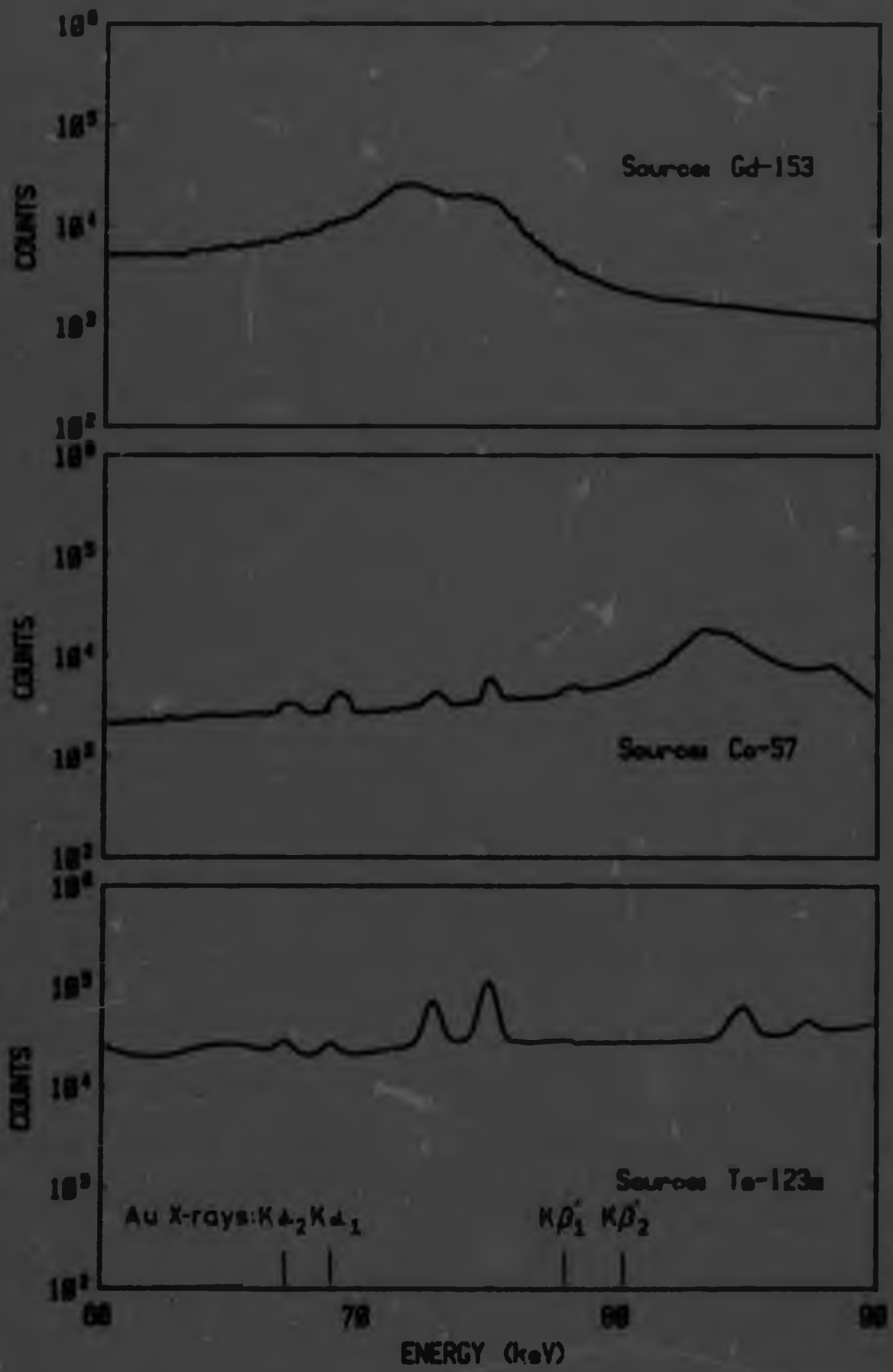


Fig. 7.1 (continued)

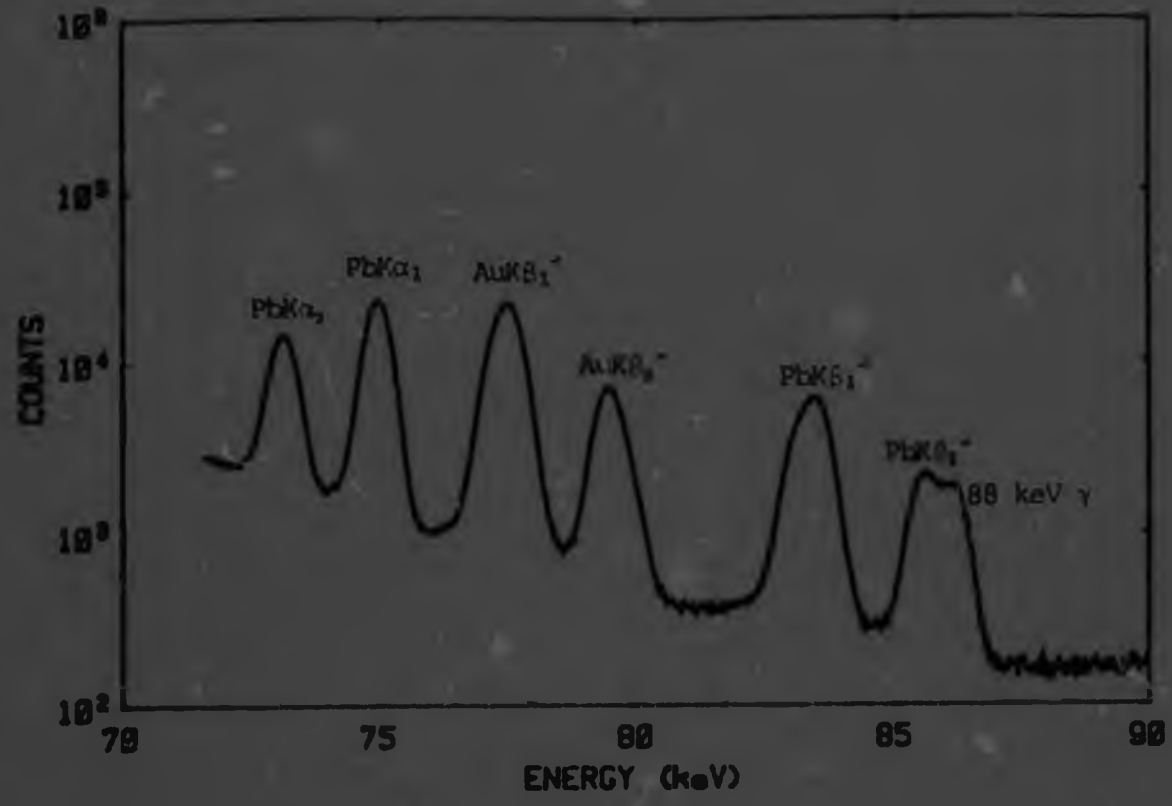


Fig. 7.2 Fluorescence spectra of pure gold and lead

Table 7.1 Energy and relative intensity of the K X-rays of gold and lead

Element	$K\alpha_2$	$K\alpha_1$	$K\beta_1'$	$K\beta_2'$
gold	66.99(55*)	68,8 (100)	77,9(35)	80,1(9)
lead	72,80(55)	74,97(100)	84,8(35)	87,3(10)

* Measured relative intensities from 'infinite' sample differ a few percent from the listed values because of matrix absorption.

Experimentally it was found that the most prominent gold peak in the normalized Co-57 spectrum i.e. the Au $K\alpha_1$ peak, had a net peak height slightly lower than the Au $K\beta_1'$ peak in the comparable Cd-109 spectrum. The peak-to-background ratio for the same gold concentration was more than three times higher in the latter spectrum i.e. $R_{Cd} \Rightarrow 3R_{Co}$. From equation 7.4 for similar peak heights, therefore, Co-57 requires a measuring period more than three times longer than that for Cd-109, to attain the same coefficient-of-variation of the peak-to-background ratio at the same gold concentration.

Although in the Te-123m spectrum the Au $K\alpha_1$ peak had about 1,3 times the intensity of the $K\beta_1'$ peak in the Cd-109 spectrum, the background under the $K\alpha_1$ peak was 2,2 times higher than that under the $K\beta_1'$. Equation 7.4 shows a 2,2 times longer measuring period for Te-123m if the peaks had been equal, but the increased intensity of the $K\alpha$ peak requires that equation 7.3 be used, so that the actual measuring period is $2,2/(1,3)^2 = 1,3$ times longer than that for Cd-109.

For <u>in situ</u> gold ore valuation, where rapid measurement is required, the much shorter measuring time using Cd-109 easily compensates for its higher cost relative to Co-57 and Te-123m.

7.3 <u>Measurement of the Cd-109 gold ore spectrum</u>

The optimum scheme for evaluating the spectrum characterized by the relevant spectral region has two gold $K\beta'$ peaks on a nearly exponentially decreasing background needs to be determined. Lead $K\alpha_1$ and $K\beta_1'$ peaks are situated on either

side of the Au Kβ′ peaks. The only other elements whose Kβ lines lie closer to the Au Kβ lines than the Pb Kβ lines, namely Ir, Pt, Hg, and Tl do not occur in significant quantities in the Witwatersrand gold deposits. Interfering Kα peaks for elements heavier than lead cannot occur in this region because the K lines of such elements are not excited by the 88 keV photons of Cd-109.

Although a positive correlation between gold and uranium, and its associated natural radioactivity and lead, is known to exist in the deposits, the correlation often is poor and cannot be relied upon. The lead peaks must, therefore, be considered as an uncorrelated interference that limits the spectral region available for the evaluation of the background under the gold Kβ′ peaks.

Similarly in the measurement of rough samples where the measuring geometry may vary widely the background beyond the lead K lines is not well enough correlated with the background under the gold peaks and cannot, therefore, be used in the evaluation of the gold region.

The 70 to 90 keV region of the fluorescence spectrum of pure gold and lead is shown in Figure 7.2. The energies and relative intensities of the K lines are listed in Table 7.1 (Lederer, 1967).

Measured relative intensities from thick samples differ a few percent from the listed values because of matrix absorption.

In preliminary measurements, a pseudo-two-channel scheme was employed for the evaluation of the Au Kβ′1 peak only. One window was placed arbitrarily over the peak while two

background windows which were counted in the same register, were placed between the Pb $K\alpha_1$ and Au $K\beta_1'$ peaks and between the Au $K\beta_1'$ and Au $K\beta_2'$ peaks. System energy resolution gave some concern as it was thought necessary for the Au $K\beta_1'$ and the Au $K\beta_2'$ peaks to be well enough resolved to allow an adequate "clear background" window between them.

The Au $K\beta_1'$ peak was certainly the most prominent peak and the listed K line intensities and observed background intensities seemed to indicate that it would hardly be worthwhile to include the Au $K\beta_2'$ peak in the evaluation. When it came to optimising the six discriminator positions, however, closer investigation showed that, when background intensity per mean peak width is considered, the peak to background intensity ratios for the Au $K\beta_1'$ and $K\beta_2'$ peaks are about the same. It was found that since the $K\beta_2'/K\beta_1'$ peak intensities had a ratio which was approximately 9/35, measurement times would have been increased by about 9/35 [illegible], by not including the $K\beta_2'$ peak. Since inclusion of the $K\beta_2'$ peak would involve little or no added instrumental complexity, this change was considered worthwhile.

Detailed analysis of the two peak measurement will be deferred (chapter 9) so that it may be combined with the optimisation of signal processing parameters.

8 FUNDAMENTALS IN RANDOM SIGNAL PROCESSING

In routine application where as much rock as possible should be sampled in a given time and valued to a given precision, it is important that all parts of the valuation system should be optimised as a whole. Data acquisition for trace elements is an inherently slow process, and the processing of detector signals thus must be efficient and of high quality to reduce the time for data acquisition to a minimum. In most discussions on random signal processing times only the fundamentals of the basic processes are dealt with. In this chapter comprehensive equations, including new concepts of pileup overlap parameters, developed from first principles, are presented. These permit optimisation of the signal processing system as a whole.

The efficiency of signal processing can be expressed as the usable output count-rate divided by the detected event rate for any one spectral component; it is synonymous with the probability P that an event will be analysed without pileup distortion, and with the true livetime fraction. In what follows, P* with the asterisk will indicate the probability that a randomly detected event is processed inclusive of pileup distortion. In a complementary way percentage deadtime is a measure of inefficiency. Energy resolution and freedom from spectral distortion are measures of system quality rather than efficiency.

8.1 Extending and non-extending processing times

Every detected photon gives rise to a signal sequence which must be above the noise threshold for the finite time required to process the signal. In the processing of signals from randomly occurring events, there are two types of processes, extending and non-extending. Extending processes, variously known as self-prolonging, paralysable or retriggerable, occur for every event irrespective of other events, e.g. the amplifier pulse width w^* in solid state detector systems. Non-extending processes occur if signals that have met certain conditions are processed a particular way, e.g. analog-to-digital conversion of duration t^* in pulse height analysis.

When simply counting above the noise level is required, the probability that a randomly detected event gives rise to an extending pulse is given by the familiar expression

$$p^* = 1/\mathrm{Exp}(rw^*) \qquad 8.1$$

where r = total detected event rate

and w^* = pulse width for a single event.

For purely non-extending processes of duration t^* the expression would be:-

$$p^* = 1/(1 + rt^*) \xrightarrow[0]{rt^*} 1/\mathrm{Exp}(rt^*) \qquad 8.2$$

When both types of processes occur for the same event they do not usually commence simultaneously, e.g. in energy analysis the optimum point for analysing the height of a pulse occurs a time ℓ^* after the event, ℓ^* usually being the leading edge of a pulse or the time-to-peak, for a pulse from a single event. It is at this point where non-extending processes of duration t^* usually start; part or all of t^*

may run concurrently with the trailing edge $w^*-\ell^*$ of the amplifier pulse, i.e. with part or all of the extending processing time. These parameters are illustrated in Figure 8.1.

The leading edge of a pulse normally is shorter than the trailing edge i.e. $\ell^* <= w^*/2$. The opposite situation, however, would not alter the processing efficiency.

8.2 Processing overlap parameters

The random occurrence of detected events inevitably leads to the overlap of the processing times of different events.

If any two events follow each other very closely, and if this can be detected, then one or both events may be rejected from final signal processing which could in this

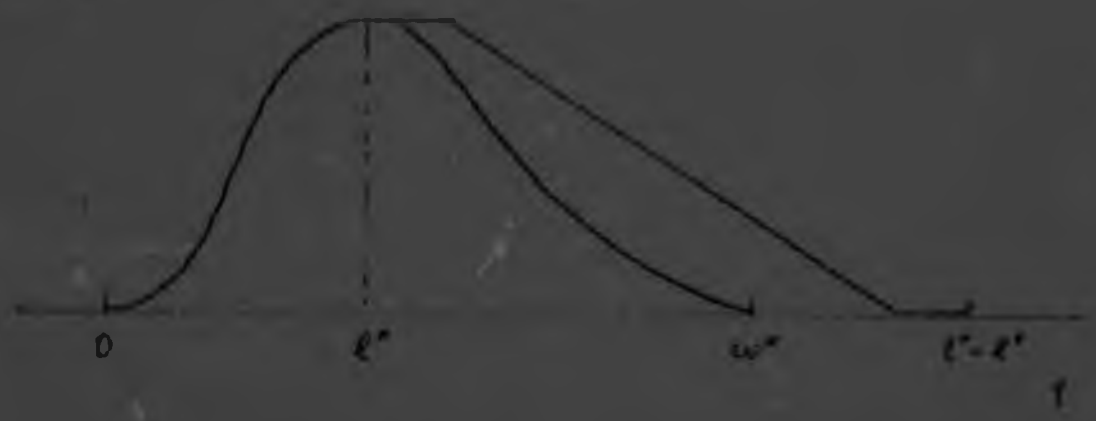


FIGURE 8.1 ANALOG PULSE PROCESSING TIMES

case possibly be perturbed. Such rejection would thus reduce spectral distortion. Whether or not a specific event will undergo final processing depends on timing conditions which can be defined by three overlap parameters , namely p , α and β as follows:

- p - In any processing systems there is always a lower time limit p within which two or more randomly occurring events cannot be recognised separately and will be processed as a single pulse. The parameter p is normally referred to as the pulse-pair-resolution time for pileup rejection. In energy analysis, if p is small relative to w^* and the height of the amplifier pulse is nearly constant over a time p near its peak, then practically full summing of analysed pileup events will result from peak-on-peak pileup. Larger values of p will also allow analysis of leading edge and trailing edge pileup pulses. This overlap parameter always has a finite value that cannot exceed w^*, i.e. $0 <= p <= w^*$,

- α - If the time between a current event and the next event is greater than $\ell^* + \alpha$ then the current event will not be rejected by the next event; in pulse height analysis if $-\ell^* <= \alpha < 0$ then spectral distortion will be caused by amplifier leading pileup - hence α will be referred to as the leading overlap limit, and

- β - If the time between the end of the processing time of a previous event and a current event is greater than $\beta - \ell^*$ then the current event will not be rejected by the previous one; if $-(w^* - \ell^*) <= \beta < 0$ then spectral distortion will be caused by trailing edge pileup - thus β will be

referred to as the trailing overlap limit.

Negative leading and trailing overlap limits are mutually exclusive with p so that $-w^* <= \alpha + \beta - p$. Positive values cause unnecessary rejection but do not cause pileup distortion of the spectrum.

The introduction of these overlap parameters greatly simplifies the derivation of the signal processing efficiency P.

8.3 Effective processing time and efficiency

The probability P that a randomly detected event will be processed without pileup distortion can still be expressed simply with the following effective parameters

$w = w^* + \alpha + \beta + p$ = effective extending processing time

$l = l^* + \alpha$ = effective leading edge 8.3

and $t = t^* + \beta + p$ = effective non-ext. processing time

For extending processes

$$P = 1/Exp(rw) \qquad 8.4$$

and for purely non-extending processes

$$P = 1/(1 + rt) \qquad 8.5$$

The absence of the asterisk indicates that effective parameters are used and that the probability excludes the pileup distorted part of the processed spectrum. P is a more realistic measure of system efficiency than P* particularly in signal processing not followed by data processing that unfolds pileup spectra.

When both extending and non-extending processes occur the probability becomes (see Appendix 8.6) -

$$P = 1/[e^{rw} + e^{rl}(1-e^{-rt'}) + rt''] \qquad 8.6$$

where t' and t" depend on how much the non-extending process

lengthens the extending process as given in Table 8.1.

Equations 8.4 and 8.5 are readily seen to be the limiting conditions of equation 8.6. If the total detected event rate r consists of spectral components r_n (i.e. $r = \sum^{n} r_n$) where the subscript n refers to events of energy between n and n + 1, and if the effective non-extending processing time t varies as t_n, as for example in ramp type analog to digital conversion systems, then the probability, this time in original parameters, becomes

$$p = 1/[e^{r(w^{o}+\upsilon+\delta+p)} + e^{r(t^{o}+\upsilon)}(1-\sum_{0}^{n} rt_{n}^{o} r_n/r) + \sum^{n} r_n t_n^{u}] \qquad 8.7$$

the summations extending over all detected components.

Table 8.1 Effective non-extending processing times

Process relationship	$t^{'}$	t^{o}
$t_n \leq w - i$	0	0
($t_n^{o} \leq w^{o} - i^{o}$	0	0)
$w - i < t_n \leq w$	$t_n - w + i$	0
($w^{o} - i^{o} < t_n^{o} \leq w^{o} + \upsilon$	$t_n^{o} - w^{o} + i^{o}$	0)
$w < t_n$	1	$t_n - w$
($w^{o} + \upsilon < t_n^{o}$	$i^{o} + \upsilon$	$t_n^{o} - w^{o} - \upsilon$)

The foregoing equations have wide applicability in random event processing systems. They can be used from the simplest counting systems to high-rate coincidence spectrometry and pulsed-optical feedback detection systems to provide a precise measure of the efficiency of data acquisition. Their analytical nature forms a basis for evaluating systematic errors in a wide variety of timing

systems used in present-day random-event processors.

8.4 Relative importance of various processing parameters

In most pulse processing systems, only the familiar parameters w* and ℓ* are specified.

The extending parameters w* and ℓ* are usually expressed in time constants TC, w* ranging down to 5,5TC or even lower, and ℓ* usually around 2,2TC for modern semi-Gaussian amplifiers.

For high-energy (MeV) analysis with solid-state detectors of about 0,1% resolution at full-width half maximum (FWHM) the optimum TC at low count rates is about 2 µs (i.e. w*≈10 µs) while for low energy (keV) analysis with detectors of ≈3% FWHM resolution, time constants up to 10 µs (i.e. w*≈50 µs) are often recommended by the manufacturers.

The non-extending time t* in ramp-type pulse-height-convertors of 100 MHz rundown frequency ranges from around 50 µs at 0,1% FWHM resolution to about 5µs at 10% FWHM resolution.

Table 8.1 shows that only the portion of the non-extending processing time that is not already taken up by extending processing time reduces the processing efficiency P. At low energies where t* is usually less than w*-ℓ*, the non-extending time t* hardly influences P; although at high energies P can be reduced substantially more by t* than by w* if t* is greater than w*-ℓ* for most of the detected spectral components. However, if only one or two minor spectral components are of interest then, as equation 8.6 shows, the extending processing time can become the dominant one even at high energies. For the analysis of

a single element at trace concentrations, the signal processing efficiency with ramp-type pulse-height-converters can thus be practically the same as with discrete pulse-height-discriminators having much smaller t*.

In most commercial spectrometry systems the combined overlap times $\alpha + \beta + p$ can readily amount to $w^*/2$ and influence P by an additional half as much as w^*.

Whereas negative values of α and β result in pileup distortion of the spectral background and positive values of α and β cause unnecessary rejection of good amplifier pulses, zero values allow the highest signal processing efficiency with the lowest pileup distortion.

In systems without specific pileup rejection, trailing-edge pileup distortion can be overcome simply by analysing only the first peak in a pulse starting from the noise threshold. In these systems $\beta \Rightarrow \ell^*$, an excessive positive value, and because $\alpha = -p = -\ell^*$ leading-edge pileup distortion occurs.

In systems with specific pileup rejection p is considerably smaller than ℓ^* and $\alpha \Rightarrow 0$. However, almost always it is found that $\beta \Rightarrow \ell^*$ whereas practically zero values could readily be implemented for both α and β.

Commercially available systems are thus seen to be somewhat wasteful in rejecting amplifier pulses unnecessarily. At low count rates, i.e. for $rw < 0{,}1$, where most systems tend to be operated, this hardly matters, but at increasingly higher rates this aspect becomes progressively more important.

For a given effective extending processing time w, the

spectrum acquisition rate for any component $r_n P$ reaches a maximum at a total detected rate $r = 1/w$. At higher rates the signal processing is very inefficient i.e. $P = 1/e = 0{,}368$, and well before the efficiency has dropped this low it may be advisable to trim w^*. Reductions in w^* must, however, be carried out judiciously as they worsen the system energy resolution; a compromise between efficiency P and FWHM energy resolution is called for.

8 Pileup rejection

The need to reject amplifier pulse pileup is not always clearly understood. In systems where non-extending processing times t_n^* exceed the trailing edge $w^* - \ell^*$, non-rejected pileup pulses unnecessarily add to the total non-extending processing time, but in most cases the reduction in P is not significant. When for all spectral components $t_n^* <= w^* - \ell^*$, pileup rejection has no effect on the signal processing efficiency whatsoever.

Without rejection, pileup causes a count-rate-dependent background of relatively low intensity over the whole spectrum. For most spectral components where this pileup background slightly augments an intense natural background, pileup hardly affects the spectral quality. The real need for pileup rejection, however, arises for minor and trace spectral components that lie in a natural background region of low intensity which might be overshadowed by pileup background.

The total pileup intensity in spectrum acquisition, relative to the total natural spectrum intensity is given by $(e^{-r(\alpha+\beta-p)} - 1)$ where positive values of α and β are taken

as zero, because with positive values there is no pileup distortion. The pileup components of a spectrum are made up of (partial) energy summations of the natural spectral components. The relative spectral distortion in a particular spectral region of low intensity can thus be far more severe than the mean value for the total spectrum indicated by the above expression.

To sum up, the signal processing efficiency P of a system can be completely described in terms or the total detected event rate r, the familiar parameters w^*, t^*, and t_n^* and the three overlap parameters p, α and β. The pulse width w^* or, more correctly, the system time constant TC influences the energy resolution, while the overlap parameters determine the degree of spectral distortion from pulse pileup.

8.6 Appendix: Derivation of equations

Mean of the number (1 + c) of events occurring for each analysed event.

In a PHA system every detected event is followed by an extending processing time:

w^* = amplifier pulse width

The point of optimum resolution for analysing the pulse height occurs at

t^* = leading edge (time to peak)

after the event.

Only analysed events cause non-extending processing time

$t_n^* = n/f + mc$

where

n = channel number

f = ADC rundown frequency

mc = ADC stretcher + resetting time + memory storage cycle time

If p is the pulse pair resolution time for pileup rejection and if the pulse peak of an event has to occur at least an interval β after the end of the processing time of the previous event, and at least an interval α before the next event, in order not to be rejected, then:

$w = w^* + \alpha + \beta + p$ = effective extending processing time

$\ell = \ell^* + \alpha$ = effective leading edge

and $t_n = t_n^* + \beta + p$ = effective non-ext. processing time

When $-w^* <= \alpha < 0$, spectral distortion is caused due to trailing edge pile-up and when $-\ell^* <= \alpha < 0$, spectral distortion is caused due to leading edge pile-up. Values of α and β equal to zero are the optimum for pile-up rejection, whereas positive values cause unnecessary rejection.

The non-extending processing time of non piled-up events starts at a time ℓ or ℓ^*, whichever is the larger, after the event. The trailing edge of the amplifier pulse overlaps with t_n^*.

The following equations are derived for $\ell^* <= \frac{1}{2}w$; symmetrical results would be obtained for $\ell^* => \frac{1}{2}w$.

Let

$$t = \begin{cases} w - \ell & \text{for } t_n <= w - \ell \\ t_n & \text{for } w - \ell < t_n <= w \\ w & \text{for } w < t_n \end{cases}$$

r = random event rate

Q(i) = probability that there will be i events between any two successive analysed events

A) Then for a fixed non-extending processing time $t_n <= w$ the Q(i)'s can be derived as:

$$Q(0) = e^{-rt}$$

$$Q(1) = (1-e^{-r(t-1)})e^{-rw}$$

$$Q(2) = (1-e^{-r(w-1)})(1-e^{-r(t-1)})e^{-rw} + (1-e^{-rt})e^{-r(w-1)}e^{-rt}$$

Let $W = (1 - e^{-r(w-1)})$

and $L = (1 - e^{-r1})e^{-r(w-1)}$

then

$$Q(2) = W\,Q(1) + LQ(0)$$

$$Q(3) = W^2Q(1) + W\,LQ(0) + LQ(1)$$

$$Q(4) = W^3Q(1) + W^2LQ(0) + 2W\,LQ(1) + L^2Q(0)$$

$$Q(5) = W^4Q(1) + W^3LQ(0) + 3W^2LQ(1) + 2WL^2Q(0) + L^2Q(1)$$

etc.

For i and j > 0 the jth term of Q(i) is

$$Q(i,j) = \begin{cases} \dfrac{(i-\frac{j}{2}-\frac{j}{2})!}{(i-j)!(\frac{j}{2}-\frac{j}{2})!} W^{i-j}L^{\frac{j}{2}-\frac{j}{2}}Q(1) & \text{for odd } j \\ \dfrac{(i-\frac{j}{2}-\frac{j}{2}+1)!}{(i-j)!(\frac{j}{2}-1)!} W^{i-j}L^{\frac{j}{2}}Q(0) & \text{for even } j \end{cases}$$

Substituting

$$k = \begin{cases} \frac{j}{2}+\frac{j}{2} & \text{for odd } j \\ \frac{j}{2} & \text{for even } j \end{cases}$$

and $m = i - j$

the zeroeth statistical moment becomes

$$\sum_{i=0}^{\infty} Q(i) = Q(0) + \sum_{i=1}^{\infty}\sum_{j=1}^{i} Q(i,j)$$

$$= Q(0) + \sum_{k=1}^{\infty}\left[\{L^k\,Q(0) + L^{k-1}Q(1)\}\left[\sum_{m=0}^{\infty}\frac{(k+m-1)!}{m!(k-1)!}W^m\right]\right]$$

$$= Q(0) + \sum_{k=1}^{\infty}\left[\{L^kQ(0) + L^{k-1}Q(1)\}(1-W)^{-k}\right]$$

$$= Q(0) + (e^{rx}-1)Q(0) + e^{rw}Q(1)$$

$$= 1 = \text{the total probability}$$

and the first statistical moment becomes

$$\sum_{i=0}^{\infty} iQ(i) = \sum_{k=1}^{\infty}\left\{(L^k\,Q(0)\sum_{m=0}^{\infty}(m+2k)\frac{(k+m-1)!}{m!(k-1)!}W^m\right\}$$

$$+ (L^{k-1}Q(1)\sum_{m=0}^{\infty}(m+2k-1)\frac{(k+m-1)!}{m!(k-1)!}W^m)\}$$

$$= \sum_{k=1}^{\infty} \left[\left(\frac{L}{1-W}\right)^k Q(0)^k \frac{2-W}{1-W} + \left(\frac{L}{1-W}\right)^{k-1} Q(1) \left(\frac{k}{(1-W)^2} + \frac{k-1}{1-W} \right) \right]$$

$$= \left[Q(0)\frac{2-W}{1-W} + Q(1)\frac{1}{1-W} \right](1-e^{-r\ell})e^{2r\ell} + Q(1)\frac{1}{(1-W)^2} - e^{2r\ell}$$

$$= e^{rw} - 1 + e^{r\ell} - e^{r(w-t)}$$

$$= E[c] = E[1 + c] - 1$$

= the mean number of events between successive analysed events.

B) For a fixed non-extending processing time $t_n > w$ the events occurring during the trailing, non-extending interval $(t_n - w)$ are Poisson distributed with parameter $r(t_n - w)$. The above mean is thus increased by $r(t_n - w)$.

$$E[c] = e^{rw} - 1 + e^{r\ell} - e^{r(w-t)} + r(t_n - w)$$

C) For a variable non-extending processing time t_n where

r_n = rate of component n requiring a non-extending processing time t_n

Let

$$t' = t-w+ = \begin{cases} 0 \\ -t_n - w + \ell \\ \ell \end{cases} \quad \text{and} \quad t'' = \begin{cases} 0 & \text{for } t_n <= w-\ell \\ 0 & \text{for } w-\ell < t_n <= w \\ t_n - w & \text{for } w < t_n \end{cases}$$

then

$$E[1+c] = 1 + E[c]$$

$$= 1 + \sum^{p} (e^{rw} - 1 + e^{r\ell} - e^{r(\ell - t')} + rt'')r_n/r$$

$$= e^{rw} + e^{r\ell}(1 - \sum^{p} e^{-rt'} r_n/r) + \sum^{p} r_n t''$$

$$= 1/P \longrightarrow$$

which is the reciprocal probability that a detected event will be analysed without pileup distortion.

$$= \sum_{k=1}^{\infty} \left[\left(\frac{L}{1-W}\right)^{k} Q(0) \frac{k(2-W)}{1-W} + \left(\frac{L}{1-W}\right)^{k-1} Q(1) \left(\frac{k}{(1-W)^{2}} + \frac{k-1}{1-W} \right) \right]$$

$$= \left[Q(0)\frac{2-W}{1-W} + Q(1)\frac{1}{1-W} \right] (1-e^{-r\ell}) e^{2r\ell} + Q(1)\frac{1}{(1-W)^{2}} - e^{2r\ell}$$

$$= e^{rw} - 1 + e^{r\ell} - e^{r(w-t)}$$

$$= E[C] = E[1 + c] - 1$$

= the mean number of events between successive analysed events.

B) For a fixed non-extending processing time $t_n > w$ the events occurring during the trailing, non-extending interval $(t_n - w)$ are Poisson distributed with parameter $r(t_n - w)$. The above mean is thus increased by $r(t_n - w)$.

$$E[C] = e^{rw} - 1 + e^{r\ell} - e^{r(w-t)} + r(t_n - w)$$

C) For a variable non-extending processing time t_n where

r_n = rate of component n requiring a non-extending processing time t_n

Let

$$t' = t - w + \begin{cases} 0 \\ -t_n - w + \ell \\ \ell \end{cases} \quad \text{and} \quad t'' = \begin{cases} 0 & \text{for } t_n \leq w - \ell \\ 0 & \text{for } w - \ell < t_n \leq w \\ t_n - w & \text{for } w < t_n \end{cases}$$

then

$$E[1+c] = 1 + E[c]$$

$$= 1 + \sum^{n} (e^{rw} - 1 + e^{r\ell} - e^{r(\ell - t')} + rt'') r_n / r$$

$$= e^{rw} + e^{r\ell}\left(1 - \sum^{n} e^{-rt''} r_n / r\right) + \sum^{n} r_n t''$$

$$= 1/P \longrightarrow$$

which is the reciprocal probability that a detected event will be analysed without pileup distortion.

9 ANALOG SIGNAL PROCESSING IN THE GOLD ANALYSER

9.1 The gold Kβ' peaks

Quantitative evaluation of two intensity-correlated peaks would be straightforward if they were Gaussian. The $K\beta_1$ and $K\beta_2$ peaks are, however, an unresolved triplet and doublet respectively. Peak broadening can readily be observed in Figure 7.1 where only the Pb $K\alpha_1$ peak is a singlet. When the system has been adjusted for higher resolution, peak shoulders could be observed. For evaluation of peak-to-background ration the individual lines need to be defined more precisely.

The $K\alpha_1$ and $K\alpha_2$ lines correspond to monoenergetic transitions from two L atomic levels to the K level. However, the energies listed in Table 7.1 for the β' lines are averages of groups of transitions from three M atomic levels and two N levels. The Siegbahn notation for the individual lines and their energies, calculated from differences in binding energies (Lederer, 1967), is shown in Table 9.1.

A literature search for the relative individual intensities did not turn up reliable data. The values listed in ASTM DS46 (Johnson et al., 1970) do not total to the intensity means in Table 7.1 nor do they fit the observed peak shapes in Figure 7.1. It was, therefore, assumed that in the Siegbahn notation the lines had been numbered in

9 ANALOG SIGNAL PROCESSING IN THE GOLD ANALYSER

9.1 The gold Kβ' peaks

Quantitative evaluation of two intensity-correlated peaks would be straightforward if they were Gaussian. The $K\beta_1'$ and $K\beta_2$ peaks are, however, an unresolved triplet and doublet respectively. Peak broadening can readily be observed in Figure 7.1 where only the Pb $K\alpha_1$ peak is a singlet. When the system had been adjusted for higher resolution, peak shoulders could be observed. For evaluation of peak-to-background ratios the individual lines need to be defined more precisely.

The $K\alpha_1$ and $K\alpha_2$ lines correspond to monoenergetic transitions from two L atomic levels to the K level. However, the energies listed in Table 7.1 for the β' lines are averages of groups of transitions from three M atomic levels and two N levels. The Siegbahn notation for the individual lines and their energies, calculated from differences in binding energies (Lederer, 1967), is shown in Table 9.1.

A literature search for the relative individual intensities did not turn up reliable data. The values listed in ASTM DS46 (Johnson et al., 1970) do not total to the intensity means in Table 7.1 nor do they fit the observed peak shapes in Figure 7.1. It was, therefore, assumed that in the Siegbahn notation the lines had been numbered in

Table 9.1 Individual K X-ray lines of gold and lead

LINE	LEVEL TRANSITION	ESTTD. INTENSITY	ENERGY (keV) Au	Δ	Pb
$K\alpha_2$	L_{II} - K	55	66,99		72,80
$K\alpha_1$	L_{III} - K	(100)	68.81	2,61	74,97
$K\beta_1'$ $K\beta_3$	M_{II} - K	3 - 6	77,58	0,40	84,45
$K\beta_1'$ $K\beta_1$	M_{III} - K	26 - 32	77,98	0,45	84,94
$K\beta_1'$ $K\beta_5$	M_{IV} - K	0,5 - 3	78,43	1,03	85,42
$K\beta_2'$ $K\beta_4$	N_{II} - K	3 - 4,5	80,00	0,10	87,24
$K\beta_2'$ $K\beta_2$	N_{III} - K	4,5 - 6	80,10	4,27	87,36

order of decreasing intensity as expected from calculated transition probabilities; estimated intensities based on this assumption are included in Table 9.1.

Instead of treating the five gold lines individually, the $K\alpha_1'$ and $K\beta_2'$ peaks can be handled as approximately Gaussian peaks having effective peak resolutions wider than the Pb $K\alpha_1$ peak. Because the two gold peaks are correlated their ratios can be treated as one composite peak in calculating the peak-to-background ratio.

9.2 Maximum available background region

In deciding on the maximum available background region t_{max} in units of σ, available for the evaluation of the peak-to-background ratio, first the available energy region needs to be determined from the interfering Pb $K\alpha_1$ and $K\beta_3$ line energies and the system energy resolution Γ. Next the

effective energy resolution of the Au $K\beta_1$ and Au $K\beta_2$ peaks must be defined in terms of Γ. Compensation must be made for the change from a constant background to a sloping background. This is done by adjusting the t_{max}, determined from the energy resolution and separation of the gold and lead peaks, by the ratio of the background intensity under the gold peaks and the adjacent regions.

The FWHM system energy resolution was given in eq.5.1

$$\Gamma = \sqrt{[\ 5{,}5FcE \ + \ \Gamma_n^2\ ]} \qquad 9.1a$$

over the limited range between the Pb $K\alpha$ and $K\beta$ lines $\sqrt{E}$ is practically constant. Thus, taking an average energy of 80 keV, the system resolution is

$$\Gamma = \sqrt{(406^2 \ + \ \Gamma_n^2\ )}\ eV \qquad 9.1b$$

which can be written linearly as the fundamental resolution plus a noise term:-

$$\Gamma = 406eV \ + \ {}^*\Gamma_n \qquad 9.1c$$

where ${}^*\Gamma_n$ is the equivalent quadrature summed noise contribution. For detector systems under consideration ${}^*\Gamma_n$ ranges from about 50eV to 400eV.

Interference from lead peaks depends on the intensity of the lead peak tails included in the background evaluation. If exceptionally strong lead peaks are not to bias the measurement of small gold peaks ($R \sim 0{,}1$) by more than 10% (negatively) then the background region employed should not come within 4 σ (i.e. 1,7 FWHM) of the Pb $K\alpha_1$ and Pb $K\beta_1$ lines. The total energy region available is thus -

	Pb $K\alpha_1$		Pb $K\beta_1$		
from	74970 + 1,7 Γ	to	84450 - 1,7 Γ	eV	9.2a
i.e. from	75650 + 1,7*Γ_n	to	83770 - 1,7*Γ_n	eV	9.2b

working with the blank backscatter spectrum in Figure 4.1 the intensity in this region relative to the total spectrum intensity was found to be

$$\frac{I_n}{I} = 7{,}36\times10^{-3} - 3{,}84\times10^{-6} * \Gamma_n \qquad 9.2c$$

The effective resolution of the Kβ' peaks in this region is given by the system resolution Γ and broadening from the 400eV and 100eV separation of the dominant β lines. The broadening cannot exceed the separation at high resolution and tapers off at poorer resolution. Over the limited resolution range where Gaussian approximation of the multiplets is appropriate the effective resolution of the β' peaks was measured over a range of time constants, changing Γ, and was determined as

$$\Gamma\ (\beta_1') \quad 500 + 0{,}5\,\Gamma\,eV = 703 + 0{,}5*\Gamma_n\ eV \qquad 9.3a$$

$$\text{and } \Gamma\ (\beta_2') \quad 60 + \quad \Gamma\,eV = 463 + \quad *\Gamma_n\ eV \qquad 9.3b$$

The FWHM energy regions for the Au Kβ_1' and Au Kβ_2' peaks are based upon the data given in Table 9.1, thus:

$$77900\ \pm\Gamma(\beta_1') \quad \text{i.e. from } 77540-\tfrac{1}{2}*\Gamma_n \text{ to } 78251+\tfrac{1}{2}*\Gamma_n \qquad 9.4a$$

$$\text{and } 80100\ \pm\Gamma(\beta_2') \quad \text{i.e. from } 79868-\tfrac{1}{2}*\Gamma_n \text{ to } 80332+\tfrac{1}{2}*\Gamma_n \qquad 9.4b$$

The relative intensities of the background spectrum in Figure 4.1 for these regions were found to be

$$\frac{I_n}{I} = 8{,}24\times10^{-4} + 5{,}75\times10^{-7}*\Gamma_n \qquad 9.5a$$

$$\text{and } \frac{I_n}{I} = 3{,}03\times10^{-4} + 7{,}57\times10^{-7}*\Gamma_n \qquad 9.5b$$

respectively, giving a total FWHM $\beta_1'+\beta_2'$ relative background intensity

$$\frac{I_n}{I} = 1{,}13\times10^{-3} + 1{,}33\times10^{-6}*\Gamma_n \qquad 9.5c$$

The total available background region finally is given by the intensity relationship multiplied by $\sqrt{(2\ell n2)}$

$$t_{max} \sim 1,177 \frac{1,36\times10^{-3} - 3,64\times10^{-6}\cdot\Gamma_n}{1,13\times10^{-3} + 1,33\times10^{-6}\cdot\Gamma_n} \qquad 9.6$$

9.3 Two- and pseudo-two channel analysis

In Table 9.2 t_{max} is given at various resolutions. For two-channel evaluation the optimum position of the inner discriminator from Figure 6.6b is seen to be for this limited range of t_{max} and R ~ 0,1 at about 1,36 σ, which corresponds to a convenient setting at full width 40% peak height (i.e. FW4/10M) of prominent gold Kβ' peaks. The FW4/10M positions of six discriminators A to F for two channel evaluation of the gold Kβ' peaks are shown schematically in Figure 9.1. Counts from the two peak regions BC and DE are summed into one counting channel and AB + CD + EF into the other. In pseudo-two-channel evaluation, two discriminators each would be required for B, C, D and E, all in all ten discriminators instead of six.

Also shown in Table 9.2 are the standardised two-channel and pseudo-two-channel variances from Figures 6.6a and 6.7a for R = 0,1. In the double β' peak evaluation the variances or measurement times with a two-channel scheme are only 3 to 6% higher than with a pseudo-two-channel scheme at a saving of four discriminators in ten. An approximate comparison of the pseudo-two-channel evaluation for only the $K\beta_1'$ peak and the two-channel evaluation for both Kβ' peaks shows that the two-channel scheme would increase the measurement time per peak by about 7%, but this is more than compensated for by the 9/35th additional information contributed by the Au $K\beta_2'$ peak; the latter scheme thus permits at least 13% (i.e. 9/(35 + 9) - 7%) faster measurement with the same number (6)

Table 9.2 Spectral region and variances in gold ore analysis at various system resolutions

Γ(eV)	t_{max}(s)	σ_v^2	$2\sigma_v^2$
400	7,7	11,0	10,4
450	7,7	11,4	10,7
500	6,5	11,6	11,0
550	6,0	12,2	11,3
600	5,0	12,7	11,7
650	5,4	13,2	12,2
700	4,8	13,8	12,7

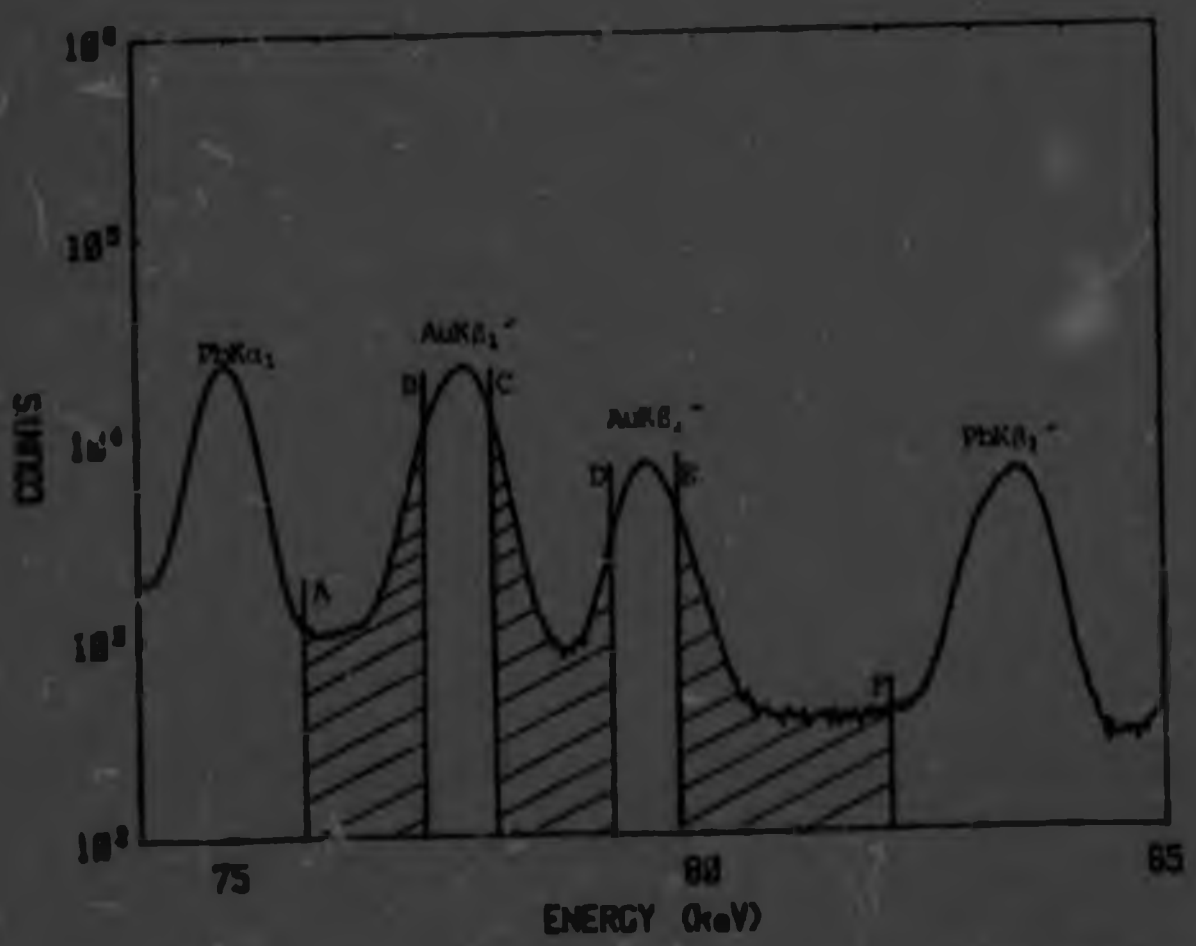


Fig. 8.1 Discriminator positions for two channel evaluation of gold Kβ' peaks

of discriminators.

From the above treatment it may be concluded that with six discriminator, two channel evaluation of both the Au $K\beta_1$ and Au $K\beta_2$ peaks is an optimum scheme for gold ore analysis with a simple field instrument. This is only 16% slower than is theoretically feasible with multichannel, weighted least-squares Gaussian evaluation.

9.4 The peak-to-background ratio detection limit

The variable parameter in the previous section, the system resolution Γ, is a function of the amplifier time constant TC. Longer time constants give better energy resolution but lower signal processing efficiency P. A combination of parameters is, therefore, sought which allows the shortest measurement time T_m for a specified precision.

At a given detector count rate, r, three factors varying with Γ influence the required measurement time T_m - the standardised variance V^B, the specified peak-to-background ratio R and the signal processing efficiency P.

A detection limit for a peak-to-background ratio of R = 0,1 may be provisionally specified at the fundamental peak resolution (Γ_n=0). If, according to Currie (1968), for 5% errors of the 1st and 2nd kind a 1,65 S.D. critical level and a 3,29 S.D. detection limit (i.e. coefficient of variation CV=1/3,29) is adopted, then the variance in R of a measurement at the limit has to be

$$V = (R \times CV)^2 = (0,1/3,29)^2 = 0,00092 \qquad 9.7$$

In the two-channel evaluation the standardised variance (B=1) at the fundamental resolution (for which t_{max}=7,7σ) is

$$v_{7,7}^{2} V^B = 11,0$$

The 2σ background count (for 2 sided evaluation) thus ought to be

$$B = V^B/V \qquad 9.8$$

From equation 9.5c the 2σ relative intensity in the spectrum of Figure 4.1 is

$$(r_B/r) = 1{,}13\times10^{-3}/\sqrt{(2\ell n2)} \sim 9{,}6\times10^{-4} \qquad 9.9$$

The total analysed count required for the specified detection limit (R=0,1 for Γ_n=0) is therefore

$$\frac{r}{r_B}\left(\frac{V^B}{V}\right) \text{ counts} \sim \frac{1044}{0{,}001} V^B \text{ counts}$$

$$\sim 939600 \times V^B \text{ counts} \qquad 9.10$$

As the resolution gets poorer the peak intensity remains constant giving a smaller but wider peak, the background intensity per unit energy remains unchanged, but the intensity per peak resolution increases so that the peak-to-background ratio decreases. For the gold Kβ' peaks the increase is proportional to the value given in equation 9.5c and the detection limit ratio can be specified at any resolution as

$$R = 1{,}13\times10^{-4}/(1{,}13\times10^{-3} + 1{,}13\times10^{-5}\Gamma_n) \qquad 9.11$$

The different R's correspond to the same gold concentration and if the CV of the measurement is to remain constant (at 1/3,29) then, according to equation 7.3, the total analysed count (eq. 9.10) has to be increased by 0,1/R.

At a detected count rate r the total analysed count is given by rT_mP where T_m is the measurement time and P the signal processing efficiency. The measurement time to accumulate the required number of counts at the specified detection limit is therefore

$$T_m = \left(\frac{r}{r_B}\right)\frac{1{,}1V^B}{\varepsilon PKV} \qquad 9.12$$

The signal processing efficiency in single element analysis is

$$P = \mathrm{Exp}(-rw) \qquad 9.13$$

where w is the effective pulse width (chapter 8) usually measured in system time constants TC. In efficient signal processing systems typically $w \sim 5,5TC$ or even smaller, but in less efficient systems w can readily exceed 12TC. The resolution Γ of a system depends mainly on TC and not on the factor w/TC. In Table 9.3 the system resolution (at 80 keV) and TC are given for a typical 200mm^2 germanium detector, and P has been calculated for a total detected rate of r = 50 kHz which amounts to a detected flux of 25 kHz/cm^2. The ratio R and $^2_R{}^B_{t_{max}}$ in Table 9.3 were calculated from equation 9.11 and were taken from Table 9.2. The time

Table 9.3 Data acquisition parameters for gold ore analysis for a typical 200m^2 Ge detector at r = 50 kHz

Resolution Γ(eV)	TC μs	P=Exp(-rw) w=5,5TC(12TC)	Limit R	$^2_R{}^B_{t_{max}}$	T_m(s)
400	—	—	0,1	11,0	--
450	2,8	0,46(0,19)	0,094	11,4	589(1467)
500	1,1	0,74(0,52)	0,089	11,8	402(573)
550	0,65	0,84(0,68)	0,085	12,2	385(477)
600	0,42	0,89(0,78)	0,081	12,7	396(455)
650	0,32	0,92(0,82)	0,077	13,2	421(468)
700	0,24	0,94(0,87)	0,074	13,8	451(488)

required to measure the specified R with a CV = 1/3,29 at r = 50 kHz calculated from eq. 9.12 is shown in the last column of the table and in Figure 9.2.

A minimum measurement time of T_m = 385 (455) seconds is indicated for the specified ratio detection limit at a system time constant of TC = 0,6 (0,4) µs.

9.5 System time constant and detector size

Similar calculations were performed for some larger and smaller planar detectors at a flux of 250 Hz/mm^2. The noise resolution (in eq.9.1a or b) was assumed to be directly proportional to the detector capacitance of 22,5 fF/mm^2 plus a stray capacitance of 5pF as discussed in chapter 5.2.1. The measurement times for the specified ratio detector limit (eq.9.11) are shown in Figure 9.2 and the minimum values are reproduced in Figure 9.3.

Figure 9.2 shows that the minimum measurement times at a total count rate of 250 Hz/mm^2 are attainable at TC ∿ 0,6µs for a wide range of detector sizes.

The measurement times for the specified ratio detection limit are inversely proportional to the detector size when the size is small but above 100mm^2 poorer resolution and lower signal processing efficiency counteract this trend. In Figure 9.3 the lowest measuring time of 293 seconds is shown for a 400mm^2 detector running at 100 kHz. The measurement time required with a 200mm^2 detector at 50 kHz is, according to this analysis, ∿ 30% higher than the minimum attainable with the larger detectors that cost disproportionately more. In most signal processing systems, however, count rates as high as 100 kHz would cause resolution degradation in

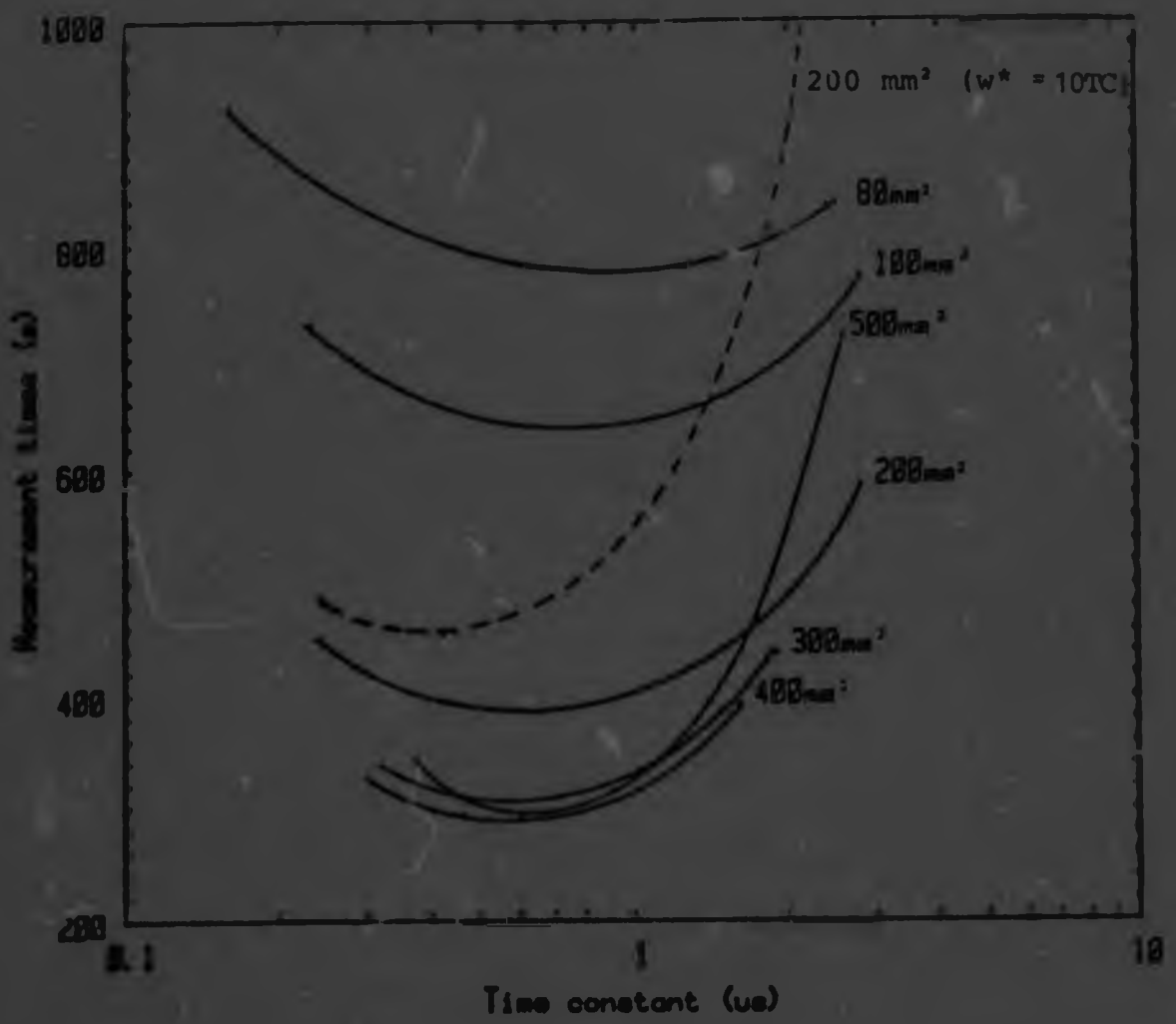


Fig. 9.2 Measurement times for specified ratio detection limit vs. TC for various detector sizes ($w^* = 5.5TC$).

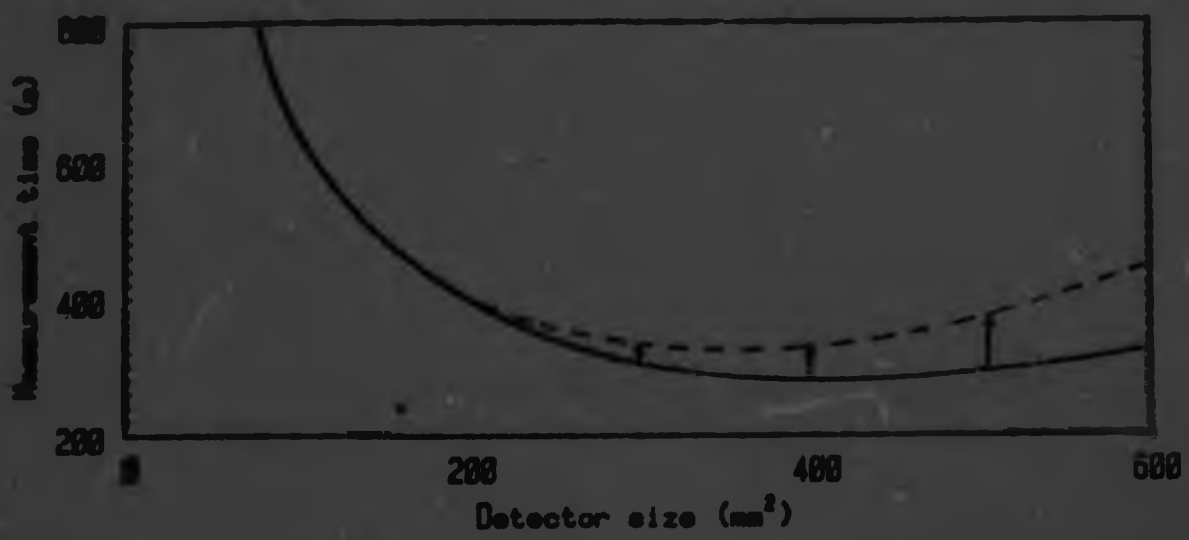


Fig. 9.3 Measurement times @ 250Hz/mm^2 vs. detector size

addition to the capacitance noise contribution already taken into account. This would increase the minimum measurement times of the larger detectors as indicated by the arrows in Figure 9.3, shifting the lowest point of the curve to smaller sizes.

This analysis has shown that a germanium detector size of 200mm^2 (a standard size in the industry) would be optimum for the measurement of gold ores.

9.6 The gold concentration detection limit

The ratio detection limit provisionally specified in section 1.4 (eq. 9.11) can be related to a certain gold concentration. Absolute derivation of the relationship from fundamental parameters is beyond the scope of this thesis as the differential scattering cross sections are not readily available. An empirical determination of the concentration detection limit follows below.

A powdered ore sample assaying approximately 400 p.p.m. gold was measured with a 200mm^2 Ge detector and a system time constant τ_c= 0,5 μs at r = 50 kHz. The total gold $K\beta_1'$ and $K\beta_2'$ peak counts above the interpolated background were determined as 58500 + 19200 = 77700 counts. The FWHM resolution of the system at 80 keV and 50 kHz was determined as 600eV, and from eq. 9.3, $\Gamma[\beta_1'] = 800eV$ and $\Gamma[\beta_2'] = 660eV$. The interpolated 1σ (i.e.Γ/2,355..) background counts were 27000 and 12000 respectively totalling 39000 counts. The peak to background ratio determined for 400 p.p.m. was therefore 77700/39000 = 2,0. The detection limit ratio specified by equation 9.11 and the parameters in Table 9.3 thus correspond to a concentration detection limit of (see

5th row of Table 9.3) -

400 x 0,081/2,0 = 16 p.p.m. gold

and a measurement S.D. = 5 p.p.m. gold.

with a 200mm^2 Ge detector and an efficient signal processing system (w = 5,51C) this limit can thus be measured in 385 seconds at a count rate of 50 kHz. For single measurement times up to a few hours, at this count rate, the detection limit is inversely proportional to the square of the measurement time, beyond this, long-term instrument instabiliy may result in measurement standard deviations that exceed these lower standard deviations derived from counting statistics alone.

9.7 Discussion

The values of several of the parameters used in this chapter were decided on from measurements with systems differing appreciably from an optimised system for gold valuation. They served to illustrate the procedure of arriving at optimised conditions, but they may be revised as the optimising criteria can be more precisely defined.

The choice between Cd-109 and other isotopes rests mainly on the need for rapid measurement of very low concentrations. If measurements are not performed *in situ* then slower measurement might be acceptable and a less costly isotope might suffice.

The choice of the energy region is determined by the occurrence of interfering elements in the ore. The decision to include the Au $K\beta_2$ peak in the evaluation was made in the interest of faster measurement, as it does not involve additional instrumental complexity.

The reason for optimising the evaluation for peak to background ratios below 1 is that for gold ore valuation the measurement of low concentrations, particularly of marginal grades, is considered more important than that of high concentrations. Ratios as high as R = 10 can be expected occasionally, but even their non-optimised evaluation would furnish a measurement precision in excess of requirements. The optimum precision to which an individual sample needs to be measured will depend on the use to which the measurement is put, and will be discussed in the next chapter. The detection limit of 16 p.p.m. in 385 seconds, arrived at in the previous section, can, by means of equation 7.3, readily be adjusted to any particular need, probably as low as fractional parts per million.

A count rate of 50 kHz average was assumed from estimates of the count-rate handling capability of a number of commercial systems. This rate, i.e. 250 Hz/mm^2, received in a 200mm^2 detector from a fluoresced sample 50mm away, gives an acceptable radiation dose rate at approximately 125mm behind the detector where a portable probe would be held. If this dose rate is not to be changed, then the count rate for different size detectors must be proportional to their area. However, the optimum sample distance depends to some extent on the thinness of the tabular deposit and the count rate would change considerably with a small adjustment of the measuring distance without a significant change in dose rate. It may thus be advisable to operate at a different count rate, most probably at a higher rate, depending on the types of deposit encountered.

Examination of Table 9.2 shows that an adequate interference- free region is available for evaluation of the gold Kβ's. The change in t_{max} with resolution is associated with a moderate linear change in the standardised variances. In Table 9.3 it can be seen that the latter change is slightly smaller than the change of the composite ratio of the Kβ' peaks and background. The exponential change in signal processing efficiency has a similar but opposite effect on the measurement time and this time thus has a pronounced minimum in the resolution range considered.

Comparison of an efficient signal processing system (TC/w = 5,5) with a less efficient system (TC/w = 12) in Table 9.3 shows that optimum measurement times are about 455/385 i.e. 18% longer with the latter system. It is possible to obviate this increase by careful design based on thorough understanding of the processes involved. The concept of pileup overlap parameters evolved in this thesis has greatly facilitated this. At lower count rates there would be less of a difference in measurement times, but at the more probable higher count rates the difference increases sharply.

In this chapter it has been shown that for in situ gold ore measurement a two channel scheme for the evaluation of the minor gold $K\beta_1'$ and $K\beta_2'$ peaks on the scattered background ensures good efficiency with an uncomplicated instrument. A $2cm^2$ detector and efficient signal processing at a time constant of TC = 0,6μs permit optimum measurement times at a constant detector flux. At 250 Hz/mm^2 the (3,29 S.D.) detection limit is 16 p.p.m. gold in a measurement time of

385 seconds. This limit is inversely proportional to the square of the measurement time and the square of the count rate.

10 QUANTITATIVE MEASUREMENT OF ROUGH ORE SAMPLES

In Chapter 4 consideration was given to the source-sample-detector geometry. In this chapter the geometry of the sample itself is considered. Geological samples normally require preparation before quantitative analysis, typically homogenisation of the sample and presentation in a reproducible measuring geometry. Such preparation is not feasible where mine stope faces are to be scanned for gold ore valuation. The samples, i.e. the areas on the face to be measured, have a rough surface, particularly in the gold containing regions where the rock may be more friable than in the waste rock above and below the reef.

Furthermore, the thin layered, sedimentary nature of the deposits requires that the area concentration of gold in g/m^2 (or related units) instead of the volume concentration in g/m^3 be determined. Accordingly it is necessary to determine the area concentration by viewing the layered deposit edge on, which is a difficult sample shape for quantitative measurement because of its heterogeneous nature.

10.1 Homogeneous concentrations

In the laboratory, where a constant measuring geometry can be assured, absolute counting of the gold peaks plus their background would give a quantitative measure of the gold concentration in homogeneous samples. Alternatively at variable count rates the counting of the gold peaks plus

their background relative to the easily measured Compton peak would give a quantitative measure.

Because the detected count rates vary approximately as the inverse square of the radiation path length, absolute counting of the gold peaks plus background would not be a quantitative measure. Moreover, for rough surfaced samples the finite dimensions of source and detector and the comparatively short radiation path lengths result in a backscatter angle at the sample from source to detector which is significantly smaller than 180°. With a smooth surfaced sample this angle may be held constant, but with a rough sample it varies with changing radiation path lengths. As shown in chapter 4 the background under the gold peaks is influenced by this angle. For rough surfaced samples the Compton peak and the background under the gold peaks, therefore, do not have a high enough correlation for the quantitative determination of very small gold peaks by the relative counting of these peaks.

The background adjacent to and between the two gold $K\beta'$ peaks is, however, well enough correlated with the background under the peaks for the determination of very small peak to background ratios even if the radiation path length and scatter angle vary appreciably.

Over the limited energy region from the lead $K\alpha_1$ peak to the lead $K\beta_3$ peak the mass absorption coefficient of the rock matrix decreases by about 15% but the mean mass absorption coefficient of the background energy regions adjacent to and between the gold $K\beta'$ peaks hardly differs from the mean mass absorption coefficient of the two $K\beta$

peak energy regions. With the same entrance and the same exit absorption coefficients, the singly scattered background photons thus follow the same radiation paths i.e. the same sample depths as the exciting and fluoresced photons.

The multiple scattered background photon follow slightly different radiation paths but they constitute only a small proportion of the total scattered photons.

The nett gold peaks and the regional background thus come from the same sample and, therefore, their ratio is a good measure of the gold mass concentration.

Because different parts from the sample contribute different proportions to the total detected intensity the (unweighted) ratio of gold to background is a measure of concentration only for a homogeneous sample. If the mean radiation path lengths vary greatly while scanning rough surfaces, the relationship between the ratio of gold to background and gold concentration may be poorer.

10.2 Thin layered sedimentary concentrations

The majority of the Witwatersrand gold deposits are thin, layered deposits. Although the 'reef' conglomerate may be several decimeters thick, the gold is often concentrated in a layer or layers less than 5cm thick, sometimes existing only between the contact of two sedimentary layers.

These deposits are mined edge-on, the complete thickness of the gold bearing layer being extracted with additional waste rock above and below it. For ore valuation the amount of gold per area mined needs to be determined, regardless of the thickness mined i.e. regardless of the stope 'width'.

The valuation unit most commonly used in the gold mining industry is the area concentration unit g/m^2 divided by the rock density (2,76)t/m^3 to give c.g/t, or more rationally cm.g/t. The advantage of this area concentration unit is that the values for several layers are additive and that on division by the stoping height (in cm) it gives the extracted or mill mass concentration in g/t, or divided by the sample height gives the homogeneous or average sample mass concentration in g/t.

In the horizontal direction, or rather in the plane of the reef, scanning with the fluorescence probe effectively homogenizes a sample; however, normal to the reef plane a heterogeneous sample is seen by the probe. When the distance between the probe and sample surface increases the effective sample height increases while the effective sample depth decreases, i.e. more waste rock above and below a gold bearing layer is seen by the probe, and the measured concentration (in g/t) decreases.

A 1cm thick cemented ore slab having a homogeneous gold concentration was sandwiched between large blocks of waste rock to simulate a narrow reef. Edge-on measurements at various distances of the probe from this sample and at various distances of the probe axis from the centre plane of the slab are shown in Figure 10.1. These illustrate the substantial effect the measuring geometry has on the precision in the quantitative measurement of heterogeneous samples.

To prevent wide fluctuations in measured concentrations of the same sample the variation in distance between the sample surface and the fluorescence probe may be limited

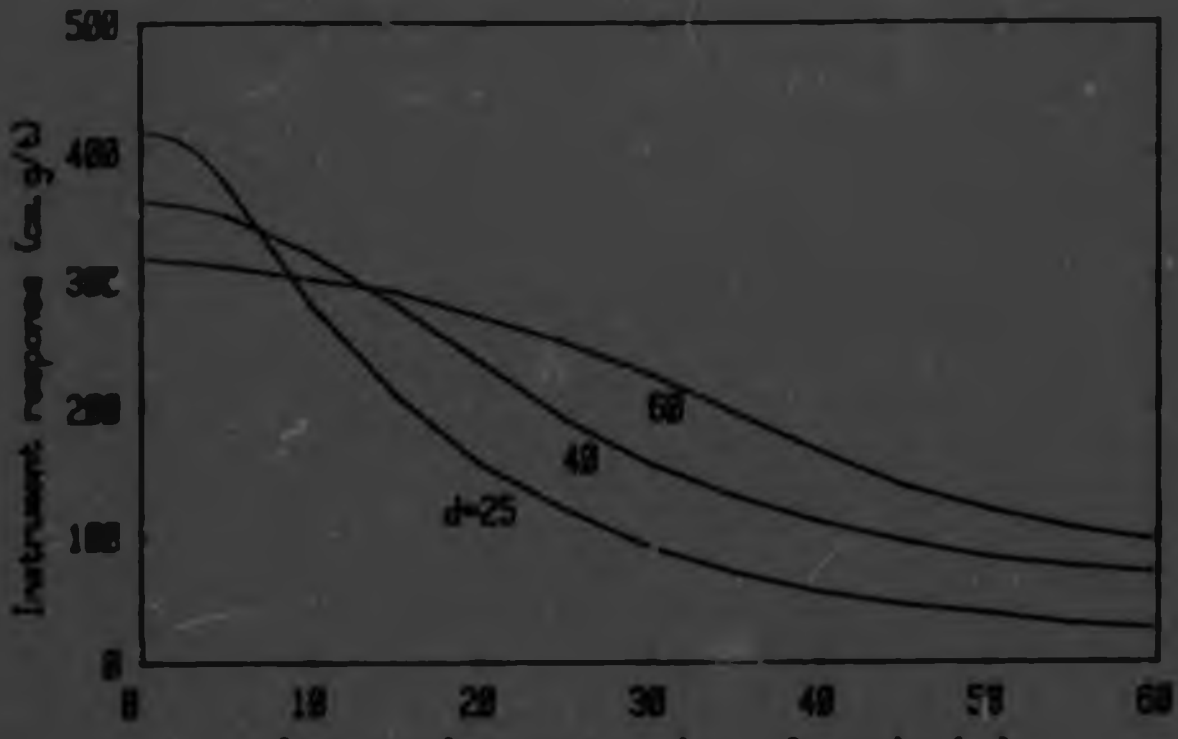


Fig. 10.1 Edge-on fluorescence measurements of a 'sandwich' ore sample; d = probe to sample distance (mm)

to a fixed range thus limiting fluctuations in the measured peak-to-background ratio from this source to acceptable values.

Restriction of short measuring distances to within a narrow range is mechanically not feasible on rough surfaces and another way was devised. It was found that the total count rate is inversely proportional to a low power ($\sim 1,4$) of the probe to sample distance. The count rate in the energy region between the Pb $K\alpha_1$ and $K\beta_1'$ peaks is a good measure of the distance to the centre of mass of the measured sample, but this rate is rather low. It was found that the total count rate above about 50 keV, which is far higher and therefore can be measured far more precisely over short periods, can give an accurate indication of the distance. In Figure 10.2 the regression of count rate and

probe-to-sample distance is shown, and the two standard deviation limits for measurements of five milliseconds are indicated.

In practice the effective distance was restricted by interrupting data accumulation for gold peak-to-background determination whenever the total count rate, measured with a ratemeter, fell outside two set count-rate limits. These count-rate limits could be chosen to correspond to limits in the probe-to-sample distance over which the maximum errors in a single measurement were acceptable. These limits would normally be ascertained from smooth-surfaced standard sandwich samples, but the somewhat larger variations in

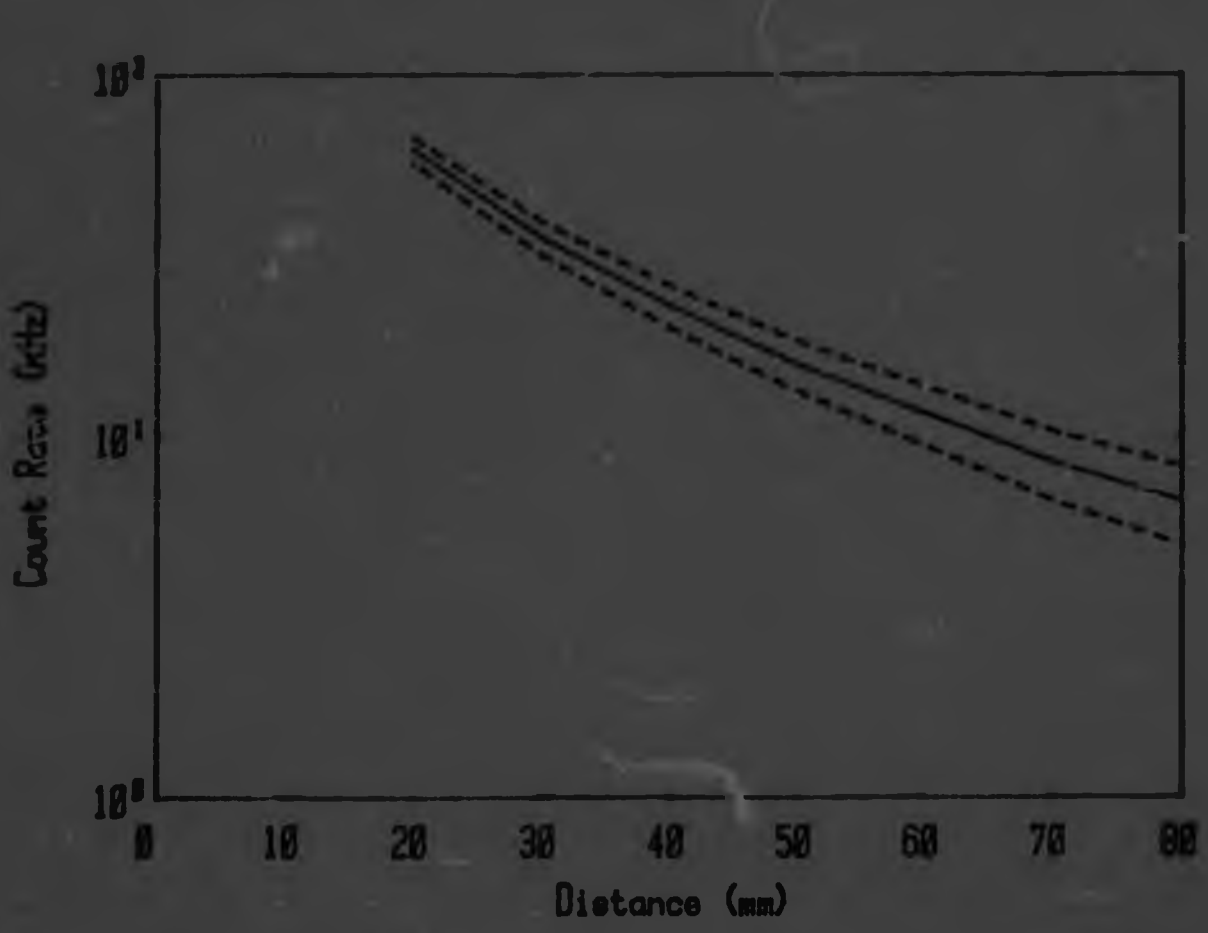


Fig. 10.2 Total count rate (>50 keV) vs. probe to sample distance; - - ± two st.dev. for 5ms

distance from particular small portions of rough samples needs to be taken into consideration in the final settings.

10.3 Shape of the fluorescence sample

The vertical profiles in Figure 10.1 reflect the effective sample shape in the determination of area concentration values.

With a co-axial source detector geometry a flat surfaced sample has a shape similar to that of a segment from a sphere. If the segment is viewed as a series of concentric shells, the different layers would contribute different proportions per unit (sample) mass to the measurement, i.e. the innermost layers, which are closest to the probe, have the highest measuring weight. With sources (or detectors) collimated to less than 2π steradians the edges of the deeper sample layers are truncated. With rough surfaces this layered sample is effectively distorted in the direction of the source radiation paths with slightly increased measuring weight being given to sample sections positioned closer to the source.

The effective sample depth is fixed by the sample's mass absorption coefficients for both the exciting and the excited radiation and these are constants for the relevant energies in the gold ore matrix. The sample depth, therefore, is a constant even if the sample surface is very rough. A constant area of the projected ore body is thus measured edge-on with a fixed depth vertical profile, as required for determination of area concentrations.

If the separation between the source and detector is small relative to their distance from the sample surface,

the line normal to the surface of the sample is an axis of sample symmetry.

So far calibration factors have been empirically determined with sandwich ore samples. More work still has to be done to calculate the sample shape for the conversion of mass concentrations to area concentration units.

11 INSTRUMENTATION FOR THE GOLD ANALYSER

11.1 Instrumental requirements

The main instrumental requirements were the following:

Portability even in difficult locations underground,

Radiation, cryogenic and electrical safety,

Simplicity of operation, and

Fast measurement of trace quantities.

- Portability - The gold analyser is by present day standards, a very complex field instrument that sometimes has to be operated under very difficult conditions. Packaging of the instrument presented a major challenge as ruggedness is essential for underground conditions. It was realized that several kilograms of instrumentation were involved. Since this weight cannot, for prolonged periods, be carried as a single package with an outstretched arm while scanning a stope face and crawling or crouching, it was decided to use a handheld measuring probe connected by cable to a chest pack (or back pack). The chest pack contains all the components that need not be in the probe so that the probe can be as light as possible. The lighter the probe the less it will tire the operator and the less inclined he will be to discontinue measuring or to scan inaccurately. The negatives are appropriate here as underground conditions make the operation strenuous.

- Safety - Aspects of radiation, cryogenic and

electrical intrinsic safety in explosive (methane) atmospheres were given careful attention from the outset of the project and are discussed in chapter 13.

- Operational simplicity - An instrument as complex as this could easily overwhelm an operator if he had to control a large number of the functions under mining conditions. During the development a method of operating the instrument was evolved by which the operator may focus all his attention in scanning the correct strata in the exposed mine face. Operational control for scanning was reduced to a single lever in the probe supporting grip. This lever allowed automatic sequencing of measuring and data storage, and actuated the source shutter and sample illumination light. Automatic storage in the instrument of all the day's data reduces drastically the amount of writing an operator has to do underground, and it eliminates human recording errors.

Control of the measurement during scanning is via a five digit LED display and a 9 LED bar on the front of the probe within the field of vision of the operator for almost any orientation of the probe. During measurement the 5 digit LED display functions as a "scan rate monitor" (displaying percentage of preset background counts) to assist the operator in maintaining a fairly uniform scanning speed parallel to the rock face. On completion of a measurement the measured gold value in calibrated units is shown on the display so that the operator can immediately base his valuation strategy on this value. On storage of the value the number of the measurement (from 0 to 255) is displayed

so that the operator may (occasionally) note down the correspondence between measurement number and the exact location in the mine, or record other comments on the measurement.

The 9 LED bar is a ratemeter display fuctioning as a probe-to-sample distance indicator. Should the distance be outside the range limits, the display flashes and data accumulation is interrupted.

The sample light and LED displays also serve as warning indicators for possible instrument malfuctions.

A great deal of effort by the manufacturer of the prototypes has gone into stabilisation of the electronic circuits so that the instrument will not require recalibration under widely varying, harsh conditions and over extended periods. Controls for (e.g. weekly) calibration checks are, however, accessible in the chest pack. High instrument stability greatly simplifies its operability.

- Fast measurement - Optimum parameters for efficient and high quality signal processing were discussed in previous chapters. The implementation of these parameters in some respects had to be compromised with limited battery capacity available in a portable field instrument.

11.2 Evolution of the instrument

The first experiments in the laboratory were performed with a 3mCi Co-57 source, a lithium drifted germanium detector with 30 litre cryostat and an amplifier plus multichannel analyser.

This developed towards 100mCi Cd-109 excitation, a

hyperpure germanium detector in a 3 litre omnidirectional cryostat which was portable although it weighed 11 kg. Pulsed optical feedback was used in the preamplifier. The amplifier incorporated pileup rejection and the amplified signal was analysed with three single-channel pulse height analysers in a pseudo-two-channel arrangement on the gold $K\beta_1'$ peak and two scalers.

Nuclear instrument modules (NIM) were used in a NIM bin with power supply. This was then housed in a box with self-contained air-conditioner and saturated core voltage regulation. This box, which weighed over 100kg, was then installed down a mine where it was installed near to a stope face. It had to be supplied, from a crosscut 300m away, with 3 KVA of 220 V single phase power from the mine's 550 V three phase network. This instrument is shown in Figure 11.1.

The first portable gold analyser consisted of a 1,5 kg probe with a liquid nitrogen holding time of about two hours and batteries, an analog board and a digital board in a 4 kg chest pack. A central 100mCi Cd-109 source was used and a $2cm^2$ x 7mm deep hyperpure germanium detector with resistive feedback in the preamplifier. The detector high voltage bias supply was housed in the probe. Liquid nitrogen in the probe had to be replenished from a portable dewar every one and a half hours and this caused many problems underground. Data stored in a solid state memory in the chest pack was printed out on surface after the end of each day's work. This instrument is shown in use in Figure 11.2.

The probe of the second prototype portable analyser was more ruggedly packaged and had a liquid nitrogen holding

time of six hours, adequate for one shift's work after tilling on surface. Three sources averaging 40mCi each were used in a peripheral source geometry to permit an improved source shutter design and to allow source replacement by rotation. This geometry resulted in too high a scatter background from the protective cover that was used. In this prototype a multiplier was provided replacing one of two preset numbers thus providing a freer choice of calibration factors.

In the third prototype a central source geometry was once again used as the peripheral source geometry had resulted in an increase in measuring time for measurements of the same precision. The ruggedness of the probe had been further improved, operation had been simplified and the layout of the digital board was improved for production streamlining. In this last prototype version, visibility of the sample and the LED indicators was finally accceptable. This instrument is shown in Figure 11.3.

11.3 Components (block diagram)

Specifications for the third prototype of the portable gold analyser are given in a Chamber of Mines Research Report (LLoyd and Rolle, 1977), and these were presented to ORTEC INC. for implementation (Hill et al., 1978). Only the main components of the instrument are described below.

The instrument consists of a handheld probe assembly permanently connected by a short cable to a chestpack assembly, and an above-ground support module.

The analyser was separated into a probe and a chestpack to reduce the handheld mass to the minimum necessary so that



ig. 11.1 First modular analyzer for in situ analysis



Fig. 11.2 First prototype portable analyzer in use underground



Fig. 11.3 Third prototype portable gold analyzer

the operational effort could be lightened. A pack worn on the back would have restricted crawling through narrow stopes. Complete, simplified operation of the source safety shutter and the functions of data accumulation, display and storage is controlled by a multifunction trigger in the probe handle. Two operational displays and a sample illumination light, multiplexed with warning signals, are strategically positioned on the probe. Protected controls on the chestpack serve only for calibration and 'On/Stand' switching of the instrument. The support module contains a battery charger, a readout module for the stored data, calibration support and a liquid nitrogen filling system.

An electronic block diagram of the analyzer is shown in Figure 11.4.

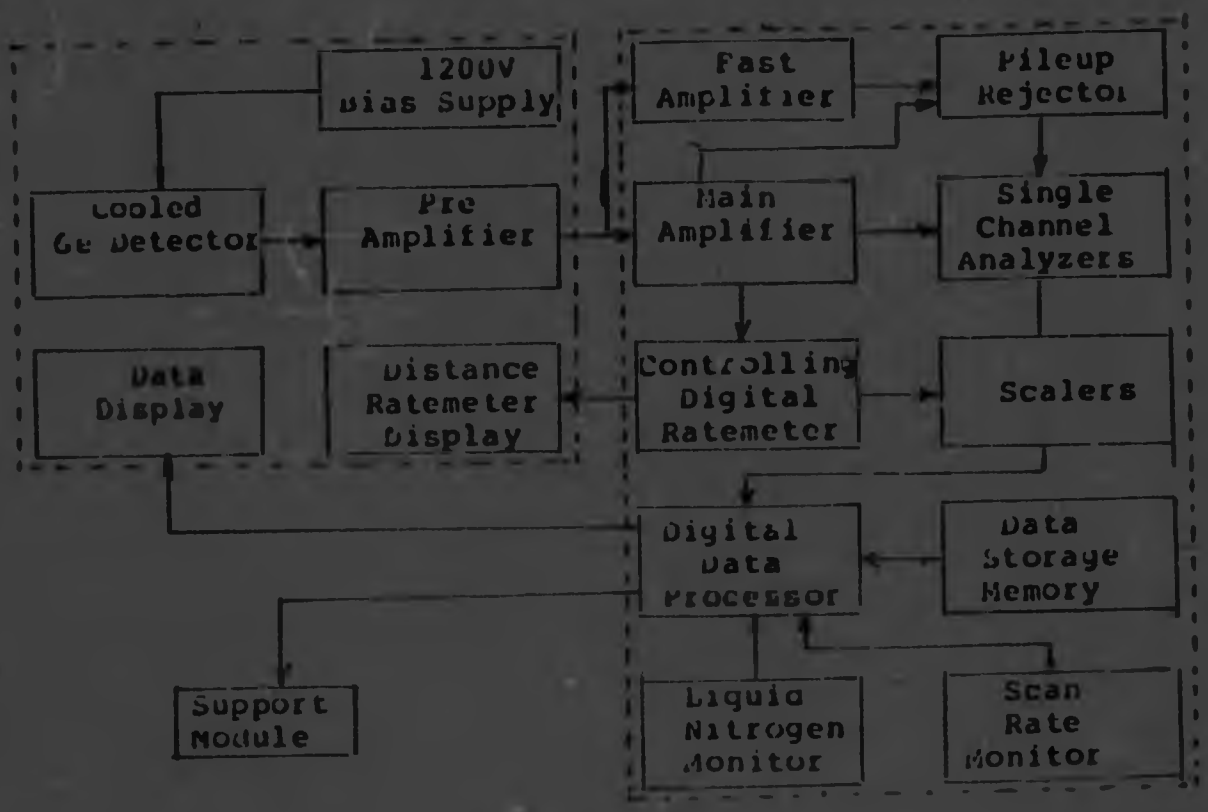


Fig. 11.4 Electronic block diagram of the third prototype portable gold analyzer

A miniature high voltage power supply in the probe provides the bias for the cooled Ge detector diode. The detector and the first stage of the preamplifier are cooled (to -196^{o}C) for high resolution. The preamplifier circuits are trimmed to allow count rates up to 500 kHz. The preamplifier and high voltage power supply are potted and all leads shielded or current limited to assure intrinsic safety.

The main amplifier uses a semi-Gaussian filter with a shaping time constant TC = 0,5us for good energy resolution consistent with the high count rates encountered in the measurement. The main amplifier pulse width w^a = 5us, i.e. 10TC, and the leading edge of the pulse ℓ^a = 1,4us i.e. 2,8TC. A gated baseline restorer is used and the baseline is monitored and the noise threshold automatically adjusted.

A fast amplifier, having a shaping time constant of 20ns, and a peak detector on the main amplifier output operate the pileup rejector. This has a pulse pair resolution time, p, of about 350ns, testing for pileup events greater than 6 keV.

A biased amplifier stage expands the region around 80 Kev to facilitate analysis by six pulse height discriminators. The output from these single channel analyzers to two scalers is gated by the pileup rejector and the distance controlling ratemeter.

The non-extending processing time of the analyzers $\ell^* = 0.25$us concurrent with the trailing edge of the amplifier pulse. The leading edge overlap limit is thus also 0,25us. However the use of the peak detector results in a trailing edge pileup overlap limit equal to ℓ^*, i.e. $\beta - 1,4$us.

The total count rate above 80 KeV is measured by the digitial ratemeter every five milliseconds and displayed at the probe by a linear array of nine light emitting diodes to indicate the probe to sample distance.

The digital data processor converts the scaler contents to units of area gold concentration for display at the probe and for storage in a solid state memory, which can retain the results from 256 measurements. A preset timer monitors the holding time of liquid nitrogen and shuts off the 1200 V bias supply to the detector after a preset time to protect the cooled stage of the preamplifier.

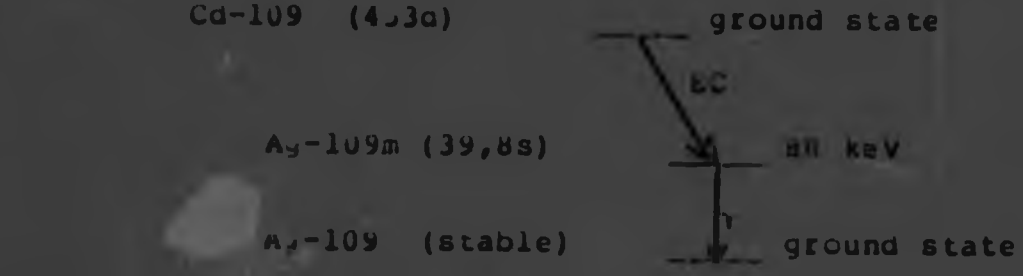
In the development of the portable gold analyzer several

high technology disciplines were brought together to solve a particular problem. A ruggedized hyperpure germanium detector, a small portable cryostat and high performance low power electronics adjusted to optimum parameters make this instrument possible.

high technology disciplines were brought together to solve a particular problem. A ruggedized hyperpure germanium detector, a small portable cryostat and high performance low power electronics adjusted to optimum parameters make this instrument possible.

.2 CADMIUM-109 SOURCE AND COLLIMATOR

Tne decay scneme for 453d Cd-109 is as follows -



Cadmium-109 decays by electron capture to Ag-109m yielding 67,7% 22 keV silver K X-rays. This, in turn, decays with a 39,8s halflife to the ground state of Ag-109 by emission of 88 keV gamma rays. Approximately 96,4% of these are internally converted with a 34.6% yield of silver K X-rays; only the remaining 3,8% of the 88 keV gammas are useful for gold K level excitation.

A small source of about 100mCi (3,7 GBq) of Cd-109 is required in the instrument for gold valuation.

The source is a rather critical component. Its design was optimised so as to make efficient use of costly activity, at the same time reducing the potential radiation hazard and producing a source that can be handled safely underground.

12.1 Production and specific activity of Cd-109

Cadmium-109 is one of about twenty known isotopes of cadmium, eight of which are stable. Table 12.1 lists various

Table 12.1 Isotopes relevant in the production of Cd-109

Isotope	Halflife or nat. Abundance	Reaction	Remarks
^{107}Ag	51,82%	$(\alpha,pn)^{109}Cd$	cyclotron production
		$(\alpha,2n)^{109}In \rightarrow ^{109}$	cyclotron production
		$(n,\gamma)^{108}Ag$	
^{108}Ag	2,4m	$\beta^- \rightarrow ^{108}Cd(n,\gamma)^{109}$	reactor production
		4% $\beta^+ \rightarrow ^{108}Pd$	
^{109}Ag	48,18%	$(d,2n)^{109}Cd$	cyclotron production
		$(p,n)^{109}Cd$	cyclotron production
		$(n,\gamma)^{110m}Ag$	
^{110m}Ag	253d	$\beta^- \rightarrow ^{110}Cd$	radiochem. impurity & reactor production
^{108}Cd	0,88%	$(n,\gamma)^{109}Cd$	reactor production
^{109}Cd	453d	$EC \rightarrow ^{109m}Ag \gamma \rightarrow ^{109}Ag$	
		$(n,\gamma)^{110}Cd$	reduces reactor prod.
^{110}Cd	12,39%		specific activity
^{112}Cd	24,07%	$(n,\gamma)^{113m}Cd$	reactor produced
^{113m}Cd	13,6y		radioisotopic impurity
^{114}Cd	28,86%	$(n,\gamma)^{115m}Cd$	reactor produced
^{115}Cd	44,1d		radioisotopic impurity

Isotopes relevant in the production of Cd-109.

Cadmium-109 can be produced by the (n,γ) reaction of Cd-108, by the (p,n) or (d,2n) reactions of Ag-109, or the (α,pn) reaction or $(\alpha,2n)$ followed by β^+ decay of Ag-107.

Reactor production of radioisotopes is normally cheaper than cyclotron production, but the isotopes cannot, usually,

be produced carrier-free i.e. without other stable isotopes of the same element. A carrier-free activity is desirable to reduce the attenuation of the gamma flux by self-absorption.

Reactor production through thermal neutron irradiation of natural cadmium is very inefficient as Cd-108 is only 0,88% abundant in natural cadmium and has a thermal neutron cross section of only 1,1 barn. Furthermore low activities of 13,6y Cd-113m and 44,1d Cd-115 would be produced as radioisotopic impurities, both emitting photons that would interfere with the spectrum from Cd-109.

The activity produced may be calculated as follows -

$$dN/dt \sim N\sigma\phi \quad (1 - 2^{-t/453d})$$

where N = number of atoms suitable for reaction

σ = cross section for Cd-109 formation

ϕ = particle flux

and the last term in parentheses being the saturation factor; the expression is not exact because subsequent nuclear reaction of Cd-109 and flux attenuation by the sample have been neglected. Substituting Avogadro's number, the natural abundance and atomic mass for N, the specific activity after 453d irradiation (half saturation) in a thermal neutron flux of $10^{14} cm^{-2}.s^{-1}$ is

$$[6,023 \times 10^{23} \times 0,0088/112,4] \times 1,1 \times 10^{-24} \times 10^{14} \times 0,5/3,7 \times 10^{10} \text{ Ci/g}$$

$$= 0,070 \text{ Ci/g} \quad = 2,59 \text{ TBq/kg}$$

$$\approx 8,05 \text{ Mg/m}^3 \text{ Cd} \quad = 0,61 \text{ mCi/mm}^3 \quad = 22,4 \text{ GBq/m}^3$$

The millimetre unit has been used for rationalization to source dimensions.

With highly enriched Cd-106 the specific activity could be increased by the relative abundance 1/0,0088 to 8,2 Ci/g

be produced carrier-free i.e. without other stable isotopes of the same element. A carrier-free activity is desirable to reduce the attenuation of the gamma flux by self-absorption.

Reactor production through thermal neutron irradiation of natural cadmium is very inefficient as Cd-108 is only 0,88% abundant in natural cadmium and has a thermal neutron cross section of only 1,1 barn. Furthermore low activities of 13,6y Cd-113m and 44,1d Cd-115 would be produced as radioisotopic impurities, both emitting photons that would interfere with the spectrum from Cd-109.

The activity produced may be calculated as follows -

$$dN/dt \sim N\sigma\phi \quad (1 - 2^{-t/453d})$$

where N = number of atoms suitable for reaction

σ = cross section for Cd-109 formation

ϕ = particle flux

and the last term in parentheses being the saturation factor; the expression is not exact because subsequent nuclear reaction of Cd-109 and flux attenuation by the sample have been neglected. Substituting Avogadro's number, the natural abundance and atomic mass for N, the specific activity after 453d irradiation (half saturation) in a thermal neutron flux of $10^{14} cm^{-2}.s^{-1}$ is

$$[6,023 \times 10^{23} \times 0,0088/112,4] \times 1,1 \times 10^{-24} \times 10^{14} \times 0,5/3,7 \times 10^{10} \text{ Ci/g}$$

$$= 0,070 \text{ Ci/g} \quad = 2,59 \text{ TBq/kg}$$

$$\approx 8,05 \text{ Ag/m}^3 \text{ Cd} \quad = 0,61 \text{ mCi/mm}^3 \quad = 22,4 \text{ EBq/m}^3$$

The millimetre unit has been used for rationalization to source dimensions.

With highly enriched Cd-108 the specific activity could be increased by the relative abundance 1/0,0088 to 8,2 Ci/g

or 71mCi/mm^3.

Russell (1964) irradiated natural silver foil for a period of four years in a thermal neutron flux of $\sim 2 \times 10^{14} cm^{-2}.s^{-1}$ to produce enriched Cd-108 and Cd-109 by the reactions

$$^{107}Ag\ (n,\gamma)\ ^{108}Ag \xrightarrow[2,4m]{\beta^-}\ ^{108}Cd\ (n,\gamma)\ ^{109}Cd$$

Burnup of the Ag-109 and of Cd-109 produced also stable Cd-110, Cd-111 and Cd-112. The specific activity reached was 1,6 ^{1}/g or 14mCi/mm^3 Cd.

Cadmium-109 sources having a Cd thickness greater than 0,1mm substantially self-absorb 88 keV photons and the above specific activities thus indicate 100mCi source areas of the order of 1cm^2 for reactor produced Cd-109.

The (p,n) and (d,2n) activation functions of Ag-109 have peak values of 0,36 barn for 10 MeV protons and 0,62 barns for 14 MeV deuterons respectively, while the (α,2n+pn) combined activation function peaks at 1 barn for 27 MeV alphas (Wing et al., 1962; Dimitriev et al., 1967). The natural-silver thick-target yields shown in Figure 12.1 were reported by Dimitriev.

The cyclotron at the Council for Scientific and Industrial Research in Pretoria can accelerate 0.5mA of 16 MeV deuterons to produce 2mCi/n with a natural silver target or 4mCi/n with enriched (>99%) Ag-109 (@ R52/g). The 2,2m (86 inch) cyclotron at Oak Ridge National Laboratory accelerates 1,2mA of 22 MeV protons to produce 9mCi/n with a natural Ag-109 target. Thus yields are in agreement with the values shown in Figure 12.1. In some particle accelerators silver beam stops behind thin targets yield low-cost Cd-109.

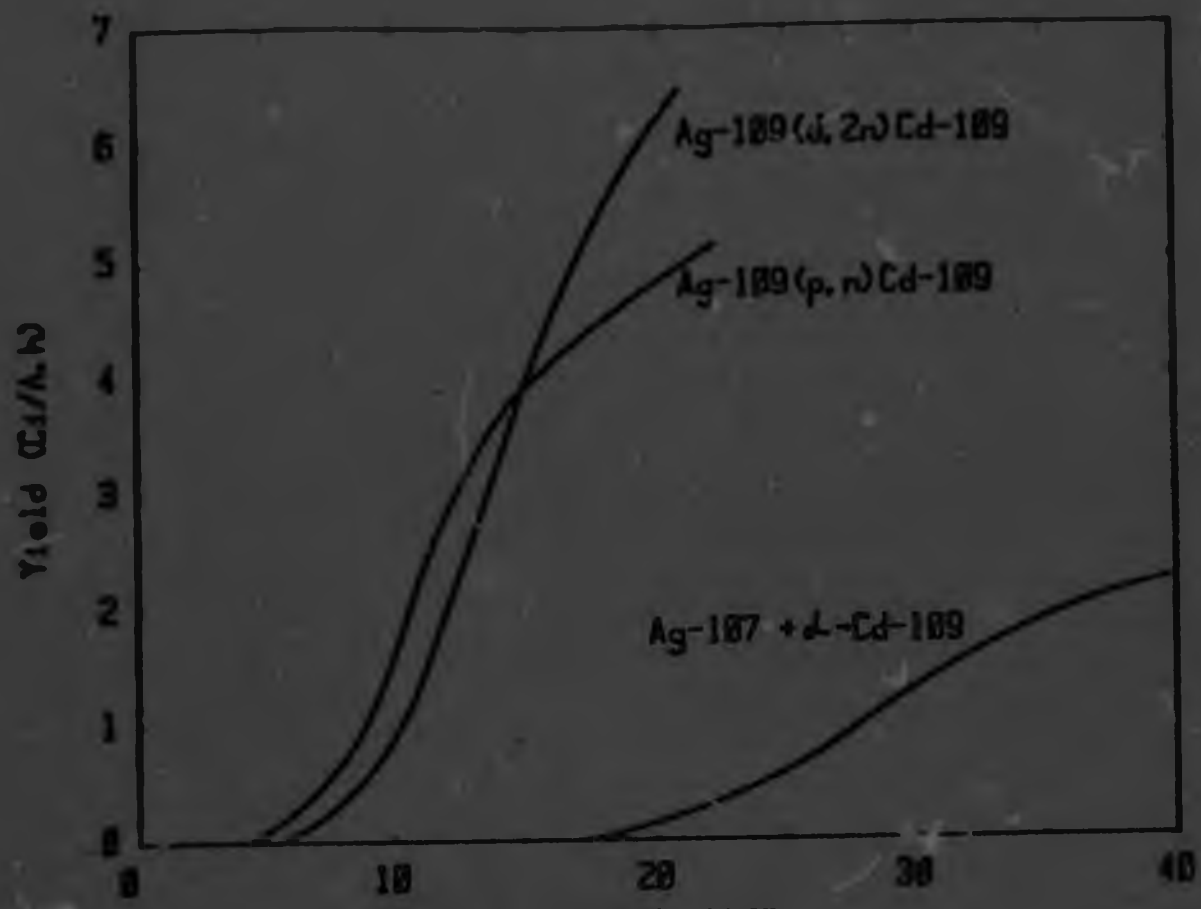


Fig. 12.1 Cyclotron production yield of Cd-109
(Dimitriev et al., 1967)

The specific activity of isotopically pure Cd-109 is

$$\frac{dN/dt}{N} = \frac{\ln 2}{45} \text{ disintegrations per day per atom}$$

$$= [6{,}023\times10^{23}/109] \times \frac{\ln 2}{453\times24\times3600} \times [1/3{,}7\times10^{10}] \text{ Ci/g}$$

$$= 264 \text{ Ci/g}$$

$$= 22{,}9 \text{ Ci/mm}^3$$

In charged particle reactions some stable Cd isotopes are also produced. Trace amounts of cadmium originally present in a silver target and introduced during radiochemical separation may also reduce the specific activity slightly. Consequently the specific activity of the freshly separated, carrier-free product does not normally exceed half the theoretical value and decreases as the Cd-109 decays.

The high specific activity of carrier-free Cd-109 has made possible 100mCi sources of less than 1mm² area without appreciable self-absorption losses of the 88 keV photons.

The Cd-109 may be radiochemically separated from irradiated silver targets. Russell (1964) used AgCl precipitation followed by chloroform/ pyridine solvent-extraction and Dowex 50-8X cation exchange. For carrier-free production, very high quality separation is desirable. Strelow (1978), after electroplating of the silver onto copper, separated the Cd in a nitric acid/ hydrobromic acid solution on an AG1-X8 anion resin.

4.4.2 Source and collimator design

The effect on gold measuring time of the photon scattering angle, from source to sample to detector, was discussed in section 4.3 and a central-source detector arrangement was found to be optimum. For this arrangement, shadowing of the detector demands that the source with its collimator be as small as practical. The minimum size of the source and collimator was limited by the available source manufacturing technology. With materials such as tungsten a shielding thickness of the order of 1mm was indicated and there would be little reduction in shadowing for sources smaller than 1mm diameter.

In the early stages of development difficulties were experienced by the C.S.I.R. in electroplating a nominal 100mCi activity of Cd-109 onto an area of about 1mm², but these problems were solved as the impurity levels in the Cd-109 plating solution were decreased. The integrity of the plated layer was improved and inactivation of the plated

surface by overplating with inactive cadmium or another metal, was considered for additional protection from possible exposure to corrosive atmospheres underground. Another metal would be preferable for overplating so as not to lower the specific activity for future recycling of partially decayed sources.

The low melting point of cadmium (321°C) presents a problem during the encapsulation of small sources by heat sealing methods such as welding.

At the start of the source development it appeared reasonable to use the radiation collimator with a suitable window for encapsulation of the electroplated activity, thereby eliminating additional encapsulating material which would increase the collimator diameter.

A molybdenum source window was silver-soldered into a tungsten collimator, the plated activity inserted and closed from the back with a tungsten screw which was cold-sealed with an inorganic thread sealant. Metal O-ring seals were also considered because in an earlier source, where the activity had been sealed from the front with an epoxied molybdenum window, the epoxy seal had undergone radiation damage and subsequently the source had leaked. The outside diameter (O.D.) of the tungsten collimator was 3mm, thus shadowing only 3.5% of a 200mm^2 detector.

Although it seems that all the source performance standards (ANSI, 1968) required for portable instruments could be met by the above integral source-collimator design, the reliability of the window seal and vibration and temperature classifications of the source (should the

instrument be left in a fire) were questioned by two commercial source manufacturers. A 2,5mm O.D. x 3mm long welded stainless steel capsule, meeting ANSI N5.10-1968 classification C33232,was thus developed as this type of design had been proven in the industry with existing source manufacturing technology.

Tungsten-inert-gas welding is used with the aid of a carbon block heat sink to prevent migration of the plated activity from the front of the source.

A 5,5mm O.D. tungsten alloy collimator was designed for the source capsule, shadowing 12% of the detector.

In Figure 12.2 the source-detector arrangement used in the third prototype of the portable gold analyser is shown. The window and shield thickness derivations are given in the following sections.

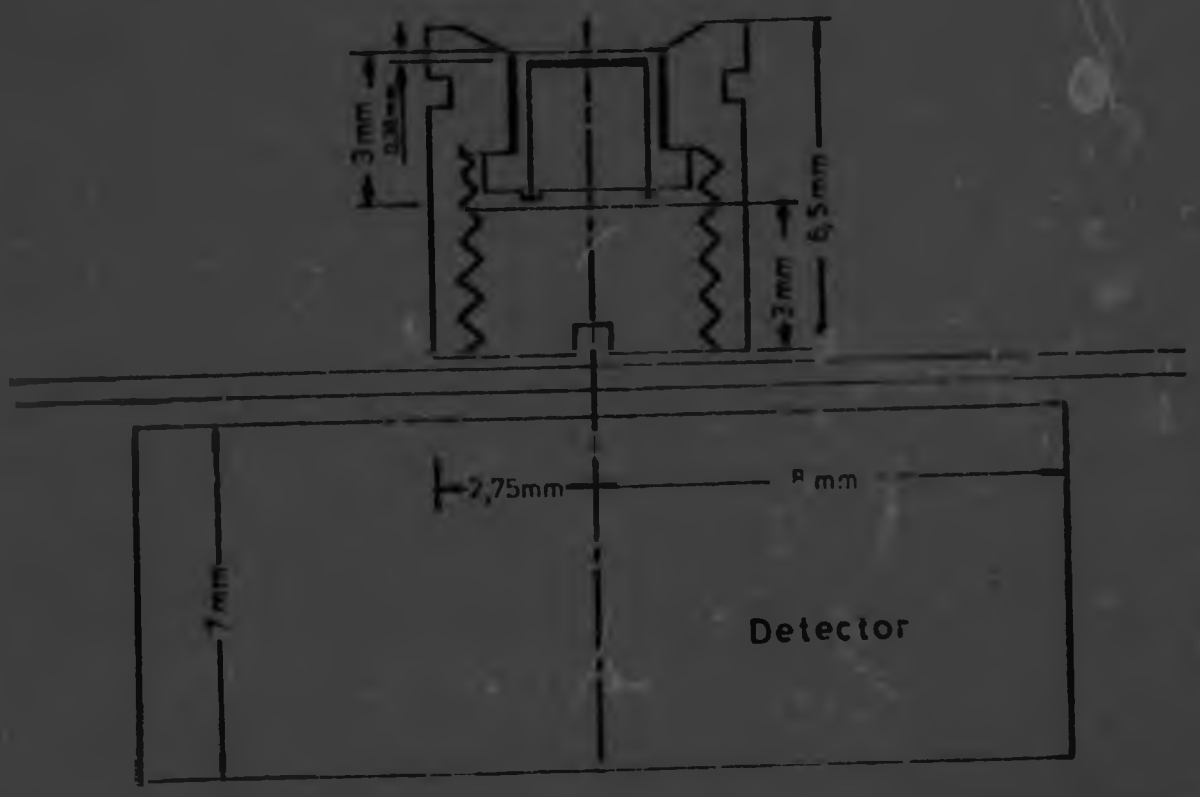


Fig. 12.2 Source detector arrangement in the third prototype gold analyzer

12.2.1 Source window

The window of the source was designed, in combination with the detector window, to filter out most of the unwanted low energy (22 keV) radiation with minimum attenuation of the useful high energy (88 keV) radiation.

The most suitable elements for filtration are those having a high mass absorption ratio for 22 keV and 80 keV photons. Elements Z = 22 to 43 (Ti to Tc) have mass absorption ratios between 40 and 47 while outside this range of atomic numbers the ratios fall sharply except for elements heavier than lead. There is little difference within this range of elements, so that iron with mass absorption coefficients of 25,0cm^2/g at 20 keV and 0,55cm^2/g at 80 keV is a convenient metal to use.

A thickness of d centimeters of stainless steel of density 7,86g/cm^3 reduces the ratio of 20 to 80 keV radiation intensity by the factor $e^{-7,86(25,0-0,55)d}=e^{-192d}$, where d is in centimeters. The intensity ratio of 22 keV to 88 keV radiation emitted by Cd-109 is 96,4/3,6 = 27. A ratio of the order of 0,01 is desirable at the detector so that the increase in total count rate from the low energy radiation may be insignificant. This requires a ratio reduction by about 2700 which is attained by a stainless steel filter of (ℓn2700)/192cm = 0,4mm thickness.

In the interest of reducing possible radiation exposure it would have been preferable to position most of this combined thickness at the origin of the radiation path, i.e. at the source window and to use the minimum thickness required for mechanical strength at the detector window.

The minimum detector window thickness allowed by the instrument manufacturer for an integral stainless steel-endcap of 41mm diameter was, however, 0,38mm. Consequently a thickness of 0,16mm stainless steel was allowed for the source window, in addition to the 0,38mm, to reduce the ratio in the open measuring field from 27 to 1,25, at which ratio the 22 keV radiation contributes less than 20% to the exposure in the external radiation field (see chapter 13).

The window thicknesses of 0,38mm and 0,16mm stainless steel attenuate the useful 80 keV radiation from the source to 85%x93%=79% at the detector. A 2,4mm thick protective polycarbonate cover ($\mu_{16}=16^{-1}$) attenuates this still further, a. 94% to a rather poor 94% of 79%, i.e.74%. Any self-absorption in the plated activity attenuates the useful radiation still further; it is, therefore, important that all the Cd-109 be positioned against the source window within the shield's collimation angle.

The detector window causes the largest attenuation in useful radiation. A reduction in the presently employed thickness of 0,38mm stainless steel would increase the 85% transmission factor proportionately, without adversely affecting the detected spectrum.

12.2.2 Collimator shield

The purpose of the collimator shield is to reduce the direct radiation from the source to the detector to a level low enough not to cause interference in the spectrum from a sample. A forward collimation angle of 120^{o} provides protection for the operator behind and to the side of the

probe.

The material used for the collimator needs to have a high linear absorption coefficient for photons of energies that might interfere in the spectrum; this applies not only to the 88 keV source radiation, but in particular to the X-rays generated in the shield, to which the shield is fairly transparent. A high linear absorption coefficient reduces the necessary size of the collimator thus shadowing less of the detector.

Several high density metals were considered for this application. Their absorption properties are listed in Table 12.2. Of these Ir, Pt and Au have Kβ X-rays in the

Table 12.2 Absorption properties of shielding metals (Berry 1962, Davisson 1968)

ELEMENT	DENSITY	MASS ABS. COEFF.		LINEAR ABS. COEFF.	
	g/cm^3	$\mu_{88}\ cm^2/g$	$\mu_{K\alpha},\ cm^2/g$	$\mu_{88}\rho cm^{-1}$	$\mu_{K\alpha},\rho cm^{-1}$
Ta	16.6	6,0	3,5	100	58
W	19,3	6,2	3,4	120	66
Re	21,0	6,4	3,3	134	69
Os	22,6	6,6	3,2	150	72
Ir	22,5	6,8	3,0	153	68
Pt	21,4	7,0	2,9	150	62
Au	19,3	7,2	2,7	139	52
Pb	11,4	7,8	2,5	89	29
U	19,1	3,7		70	

energy region between the Pb $K\alpha_1$ and $K\beta_1$ lines and are thus to be avoided for gold determination. Metalworking of Os and Re is rather difficult, while the relatively low density of Pb and Ta gives these metals a correspondingly lower linear coefficient. Shielding by uranium is less because it does not offer K-level absorption of the 88 keV photons. Tungsten, or a heavy tungsten alloy which is more amenable to metalworking, is thus the shielding metal of choice.

The minimum amount of shielding may be calculated by stipulating that the constant intensity from the source directly to the detector should constitute only about one or two percent of the intensity from the sample at the limiting probe-to-sample distance.

The total count rate from a massive sample at a limit distance of 0,5cm from a 125mCi Cd-109 source and $200mm^2$ detector was determined to be 37,5 kHz.

The source radiation to be shielded may be considered as comprised of two components. The primary component is the 88 keV photons (of 3,6% abundance) i.e. $125x0,036x3,7x10^7=1,67x10^8$ photons/second emitted into 4π steradians. Since the mean range of 88 keV photons in tungsten is only $1/\mu_{88}\ \rho \sim 0,1mm$, a secondary component of tungsten K X-rays is produced in the inner layer of the tungsten shield. The fraction of 88 keV photo-electric absorption, leading to W K-level excitation in a thick W target, relative to the total absorption (i.e. inclusive of incoherent scattering and L level excitation) is about 0,81 but only 0,94 of the excited W atoms produce K X-rays. With a $2\theta=120^o$, i.e. $\int_0^{\theta} 2\pi \sin\phi d\phi = 2\pi(\cos 0 - \cos\theta) = 3,14sr$, forward

collimation angle of the shield, the shield intercepts $(4\pi-3,14)/4\pi=0,75$ of the primary radiation producing a secondary component of $1,67\times10^{8}\times0,81\times0,94\times0,75 \approx 0,95\times10^{8}$ W K X-rays per second emitted into 4πsr.

A detector of 8mm radius positioned 7mm behind a point source subtends a half angle of $\theta=\arctan(8/7)$ and a solid angle of $2\pi(\cos0-\cos\theta)=2,15$sr of the source. Thus a fraction $2,15/4\pi=0,17$ of the primary and secondary source components are directed at the detector. Equating the two components of the source radiation passing through the tungsten shield of thickness d, to 1s (or 2s) of the intensity of the radiation from the sample, we have -

$$1,67\times10^{8}\times0,17e^{-\mu_{x}d}+0,95\times10^{8}\times0,17\times e^{-\mu_{x}d}= 0,01\times37500$$

giving $d \approx 1,6$mm (1,5mm for 2s)

The source backing thus ought to be 1,6mm thick while the oblique direction sideways through the shield requires only a $1,6 \times \arctan(8/7)=1,2$mm wall thickness. With heavy tungsten alloys these shielding thicknesses need to be increased by the ratio of the density of pure tungsten ($19,3g/cm^{3}$) to the density of the alloy.

A wall thickness of 2mm and a backing thickness of 3mm in a W alloy of $18,2g/cm^{3}$, formed by powder metallurgy, were provided by the instrument manufacturer. The increase in thicknesses from the minimum was arbitrarily provided to allow for undercuts in the shield wall for a source retaining collar and for secure molding into a polycarbonate cover, and for a slot in the W alloy screw in the shield backing.

The overall diameter of 5,5mm of this collimator with a

welded stainless steel source capsule results in a shadow area of 23,[illegible]mm^2 i.e. 12% of a 200mm^2 detector. With a smaller plated area of the Cd-109 activity and an integral source encapsulating shield this could be reduced to about 4 percent.

The relatively small improvements discussed in this chapter could all lead to a reduction in the amount of Cd-109 activity required to measure gold at optimum speed, and the radiation dose rate, to which an operator might be exposed, would be similarly decreased. However, it has essentially been found necessary to increase the Cd-109 activity in order to provide a safe means of securing the source while permitting its ready replacement.

13 SAFETY ASPECTS

The gold analyser presents three potential hazards, particularly since it is a portable instrument which is to be used under arduous conditions underground. These potential hazards arise from the use of liquid nitrogen as a coolant, the use of electronic circuits in atmospheres which may contain flammable or explosive gases such as methane, and the use of a radiation source.

13.1 Liquid nitrogen

High resolution germanium detectors operate at 77° - 90°K and usually are cooled with liquid nitrogen.

As an altenative coolant a solid-liquid propane system which could be completely contained (Boynton, 1974), was considered for this application. The latent heat of melting (80 J/g at 91°K) is, however, lower than that of boiling liquid nitrogen (199 J/g at 77°K) so ... weight and volume considerations favoured the latter. Lightweight (6 kg) mechanical refrigerators (Hogan, 1968; Carrol, 1971) operating on Sterling or Solvay cryogenic cycles were also investigated but their power requirements rendered them unsuitable for this portable application.

The potential hazards to the operator from liquid nitrogen are skin 'burns' from accidental contact with extremely cold surfaces or liquid and from the 174-fold volume expansion at the phase change which could cause

pressure problems in c ed systems.

Small droplets of liquid nitrogen when spilled onto the skin usually roll off and do not cause 'burns' unless they wet the skin.

To minimize the contact hazard, a spillproof dewar, which could be pointed in any direction, was specified. A design based on a commercially available, non-pressurized dewar was suggested; this had two vent pipes, at least one of which could always vent from above the liquid surface to the opposite outside without spillage, with minor restrictions on the orientation of the dewar. The instrument manufacturer simplified this to a single vent cum fill pipe terminating in the centre of a cylindrical dewar. In this design the dewar can be filled only to half the volume of the cylinder but it removes all restrictions on orientation of the dewar.

For handling of liquid nitrogen it is safer if the liquid need not be pressurized during transfer and use. Lightweight, quick-connect couplings for refilling of liquid nitrogen are prone to leakage due to cooling from ambient tempe. tures to below 80^{o}K, and pressurization would aggravate this problem. Icing-up of the coupling can hardly be prevented when the weight of the probe has to be reduced to a minimum, but this inconvenience was found to be small for filling periods of less than an hour.

The diameter of the ve t pipe was a critical parameter. For spillage during operation it ought to be small whereas for refilling a larger diameter is preferable, especially if the liquid has to run down the pipe with a counterflow of

displaced air and evaporated liquid. If two pipes to the centre of the cylinder were used the filling could be accomplished with smaller diameters than is needed for a single pipe. A single pipe, however, simplifies construction of the cryostat and a divider in the pipe was therefore suggested, which should allow some reduction in diameter as it separates opposing flows; with this design it has been possible to fill a warm probe, having a 3mm inside diameter fill tube, from a clip-on funnel within ten minutes.

For the first prototype portable analyser a liquid nitrogen holding time of one hour was specified, and the instrument manufacturer produced a probe with a holding time of nearly two hours. The refill system, which had to be carried underground, often failed as it could not stand up to normal underground treatment. For the second and third prototypes the liquid nitrogen holding time of the probe was increased to six hours, so eliminating the need to refill the probe underground.

If the probe of the fill system were pressurized with intermittent pressure release then there would always be the possibility that the pressure relief mechanism could ice up or fail otherwise and that vessels could rupture from pressure buildup. With an ambient pressure system the continuous boiling of the liquid nitrogen ensures that vents are continuously kept open so that ice cannot block the vent completely. Care must, however, still be exercised to keep water or ice out of the system during filling.

The small amount of liquid nitrogen required for operation thus need only be transfered above ground, and

handling there has been simplified so as to reduce potential hazards to a minimum. During filling of the large storage container it will be necessary to observe the simple precautions normally taken when handling potentially hazardous liquids. Underground the liquid is contained at ambient pressure in a spillproof dewar which presents no potential hazard unless the vent is blocked deliberately.

13.2 Intrinsic safety for fiery mines

The carbonaceous content of ores in some gold mines gives rise to methane (firedamp) which can present a potential explosion hazard. For these fiery mines instruments must either be encased in explosion-proof boxes, or they must be intrinsically safe, i.e. during operation or malfunctioning the energy in any spark that may be generated by the instrument must be less than that required for ignition of any methane-air mixture.

The armouring required for explosion-proof enclosures is incompatible with a lightweight, portable instrument. The remaining solution, intrinsic safety, had not been implemented on a related type of instrument before and presented a number of problems that had to be resolved in the design as discussed below.

The high-voltage bias supply (1200 V) for the detector was located in the probe and not in the chest pack so that energy storage in cables to the detector could be kept to a minimum; all circuits were resistively current limited and fuse protected at the nickel-cadmium batteries so that even short circuits could not produce energetic sparks; the incandescent sample light was specially enclosed to protect

it from external breakage. The possibility for tampering with the instrument was limited.

Aluminium and titanium were strong contenders for the probe vessel. However, when these metals are struck on iron oxides, widely present in a mine, the exothermic reaction can produce sparks and these metals were, therefore, avoided as structural materials. Cadmium also could not be used e.g. on plated screws. The fiery mine problem and corrosion problems underground made stainless steel the structural metal of choice.

After several consultations during the design stage the third prototype portable analyzer was submitted to the Explosives Hazards Division of the South African Bureau of Standards where it was tested and found to comply with the standard for intrinsically safe electrical apparatus (SABS, 1977). Approval was obtained from the Government Mining Engineer to use this prototype underground in Group 1 atmospheres, i.e. in the presence of firedamp.

13.3 Radiation safety

Approximately 4,6 GBq (125mCi) of Cd-109 in the gold analyser allow an acceptable measurement rate for ore valuation of narrow reefs. The potential radiation and contamination hazards from such a source thus had to be analysed.

Operator safety was carefully considered in the instrumental requirements from the initiation of the design. This demanded that the activity should be used efficiently and as safely as possible. The following features contributed towards these objectives:

The source was designed to filter most of the unwanted 22 keV silver K X-rays with only a small reduction in the useful 88 keV radiation. A proven stainless steel encapsulation was used, and the source and collimator were securely and protectively mounted in the probe front cover to prevent damage to or loss of the source. A source-sample-detector geometry was developed which allowed a wide collimation angle for maximum use of the source, the close geometry enhancing the measurement of narrow reef bands. The detector size was made as large as resolution considerations permitted; the electronics were optimised to attain the highest practical rate of gold determination particularly at marginal gold values.

The nature of the measurement, i.e. backscatter scanning of extended rough rock faces, is such that it is impossible to contain the radiation within the system as can be done with a small sample which can be introduced into a system. Reef scanning *in situ* requires good visibility around the probe head and as portable a probe as possible. The possibility of reducing the radiation by shielding was thus limited. The source is completely shielded to the rear and a close fitting tungsten shutter contains most of the source radiation whenever the operational trigger is released. A shutter lock was provided to prevent accidental opening. A light shining (at the sample) in the same direction as the source serves as a radiation warning; this light is switched on as soon as the shutter is opened.

Elaborate shutter systems had been contemplated, but it was realized that with this type of measurement a fail-safe

design is well-nigh impossible and could only give a false sense of security. A small potential radiation hazard should be considered present under all operating conditions. It can, however, easily be ascertained that the shutter is not damaged and is functioning correctly and whenever this is done the operator can rest assured that he receives no significant radiation dose when the shutter is closed. When not in operation, the probe can be clipped onto the chest pack where a lead cap over the source and shutter allows complete reliance on more than adequate shielding. Radiation warning lables are prominently displayed on the probe to discourage misuse or tampering.

Under normal operation the highest radiation dose rate would be received by the hand supporting the probe. In the first portable prototype the probe handle was near the front of the probe and the hand was shielded by a tantalum foil. In the second and third prototypes the handle was positioned under the centre of mass of the probe further back where the radiation intensity is less. The problem of accurately measuring dose rates close to low energy sources (<100 keV) is not simple and requires specialized equipment which was not available for this project. The radiation dose received by the hand can, however, be calculated from the blank backscatter spectrum shown in Figure 4.1 and the 50 kHz count rate received by the detector under normal operation.

The absorbed dose rate may be calculated from

$$\int_{>0}^{E_{max}} \text{flux}(\text{photons}/n.mm^2) \times E(\text{Joules}) \times \frac{\mu}{\rho}(mm^2/kg)\, dE \text{ Gy/h}$$

if $\frac{\mu}{\rho}$ is the energy transfer coefficient for air (Davisson,

1968 p841), division by 0,877 will adjust the values to the absorption response of human tissue. The total photon flux of 50 kHz falls on 176mm^2 of unshadowed area of the detector, i.e. 1,02x10^6 photons/h.mm^2. The flux of photons of energy between E and E + ΔE may be calculated from the spectrum on Figure 4.1 -

$$1{,}02\times10^6 \; I_E \Delta E \; / \; \sum^{88} I_E \Delta E \quad \text{photons/h.mm}^2$$

Approximate numerical integration over all energies gave an absorbed dose of 40μGy/h (4mrem/h).

For radiation calculations, at a nominal probe to sample distance of 40mm, the source may be considered as imaged 50mm behind the effective centre of mass of the sample 10mm deep in the rock, i.e. 100mm in front of the detector. The absorbed dose rate of 40μGy/h at 100mm may be converted to any position behind the shielded source by the inverse square distance relationship.

The fingers on the probe handle are positioned approximately 125mm behind the shielded source, and at that distance the dose rate is 40(100/225)^2 = 7,9μGy/h. The dose limit (IAEA, 1967) for the hand of individual members of the public that need not be registered as radiation workers, is 75 milliGray per year (7,5rem/year). Under the most unlikely situation where an operator were to pull the probe trigger continuously for 40 hours per week, 52 weeks per year, the dose absorbed by his operating hand would be one fifth of the absorbed dose limit permissible for the public; if he ware registered as a radiation worker the permissible limit would be still ten times higher.

The eyes cannot, normally, be closer than 300mm from the virtual position of the source in the rock opposite the probe, and at that distance the absorbed dose rate is 4,5 μGy/h. Since the permissible dose limit for the eye is five times lower than that for the hand, regular exposure of the most sensitive organ relevant in this application also does not give rise for the need to register the operator as a radiation worker.

For direct exposure to the 4,6 GBq (filtered, i.e.x0,038) Cd-109 source with the shutter open, the flux at 1m is

$0,038 \times 4,6 \times 10^{9} \times 3600 / 4\pi = 5 \times 10^{9}$ 88 kev photons/h.m^2

giving an absorbed dose rate of -

5×10^{10}(photons/h.m^2) x $88 \times 1,6 \times 10^{-16}$(J) x $2,66 \times 10^{-3}$(m^2/kg)

= 1,87 μGy/h (0,18mrem/h) at 1m

This rate has an inverse square distance relationship, for example, at 100mm from the source the absorbed dose rate is 187μGy/h.

It may be seen that continuous direct exposure close to the source may result in the permissible weekly absorbed dose being reached over a small part of the body within several hours. Operators of the instrument thus will be trained so that accidental direct exposure may be kept to a minimum. Notwithstanding the unlikelyhood of reaching the permissible absorbed dose for non-radiation workers, it is envisaged that operators will be registered as radiation workers and that routine personnel monitoring will be implemented.

From the above mentioned considerations it should be clear that all possible potential safety hazards have been adequately taken care of and are so small that they need not be of concern for general application of the gold analyser in the harsh mining environment.

14 RESULTS OF THE FLUORESCENCE METHOD

To test the feasibility of the method and to test instrumentation, a series of measurements had to be carried out underground. The first modular instrument was installed in a stope at Leslie Gold Mine Ltd.. The first prototype portable analyzer was tried on a number of panels at Harievale Gold Mine Ltd. and in an experimental stope at Blyvooruitzicht Gold Mine Ltd. Testing at this site continued with the second and third prototype analyzers.

14.1 Measurements at Leslie Gold Mine Ltd.

14.1.1 Equipment

The analyser consisted of an electronic package connected to a portable measuring probe by a 13m cable.

The package comprised a modular three-channel pulse height analyser with pile-up rejector and constant voltage power supplies, mounted in a temperature-controlled box. The box dimensions were approximately 0,6x0,6x1,2m and weighed about 100 kg.

The measuring probe consisted of a 100mCi Cd-109 radioisotope point source in a tungsten cup of outside diameter 3mm mounted concentrically 3mm in front of a 100mm^2 hyperpure Ge detector. The detector was cooled by liquid nitrogen held in a portable two-litre omnidirectional cryostat. An analog ratemeter functioned as an effective distance meter. The probe was tripod mounted and weighed

approximately 11 kg when full of liquid nitrogen.

14.1.2 Test site

The tests were carried out in the western area of the mine in stope 11A 28 Too on the two east panels adjacent to end-tipper track No.4.

Compared with samples from other parts of the mine, the values of chip samples from the western area, as revealed by repeat sampling of previous sampling channels, indicate a much larger scatter. Even though the ratio of projected sampled area to projected mined area of the reef in the western area was more than ten times greater than that for the rest of the mine, evaluation of the average grade of individual stope faces in the western area was more difficult than elsewhere in the mine.

In the test panels a single reef-band was located easily at the contact between the light-coloured quartzite hanging wall and the dark shale footwall. The thickness of the reef-band varied from a few centimetres to virtually zero. The surface of the face was particularly rough across the contact where the measurements were made. Steps of a few centimetres often occurred at the contact.

The stoping width ranged from 350mm to 1m, the dip was approximately at an angle of 20°, and the temperature 29°C dry-bulb.

14.1.3 Experimental

The electronic package and mains supply were installed in the end-tipper track for four weeks. The probe was filled daily with liquid nitrogen on surface.

At the beginning of each shift tests were made in the track for the presence of methane; as a further precaution a jet of compressed air was directed over the electronic package. The temperature controller was then switched on and the electronic calibration of the instrument was checked.

A continuous row of rectangles, 150mm wide and 80mm high (from 55mm above the contact down to 25mm into the shale) was marked along the face by a sampling official. Measurements were made centrally on both halves of each rectangle. The rectangles were afterwards chip sampled.

Coarse adjustments of the tripod for positioning the probe centrally in front of each half rectangle was rather difficult in the stope, and usually required more time than that needed for the actual counting. Fine adjustment to a precalibrated 40mm effective probe-sample distance could, however, be made within seconds.

At convenient points, where a high gold value was found by the measurements referred to above, a few extra measurements were made to explore the spatial distribution of the gold in the region in which it was concentrated.

The distance resolution for the calibrated measuring geometry used was sufficient to show that vertical distribution of gold was no more than 50mm. Abrupt changes in concentration were observed over about 20mm in the direction normal to the face. This evolved from repeat XRF measurement after chip sampling.

14.1.4 Details of the fluorescence measurements

In the tests the probe was adjusted before each measurement to give a total count rate equal to that obtained when the

probe was 40mm from a smooth rock surface. It was calculated that at this distance the sample of solid rock from which more than 90% of the measured intensity was received was equivalent to a bowl-shaped mass 10cm in diameter and 2,5cm deep.

The instrument was initially calibrated by means of powdered nomogeneous samples. The calibration was later adjusted to the inhomogeneous, layered structure of the reef. It was later found that this adjustment had not been quite accurate, and that there had been some residual bias. A more precise calibration factor for a layered structure still had to be determined.

It was realized that the thickness of the gold-bearing layer influences the calibration factor to some extent. In these tests the thickness of the visible reef was consistently less than 50mm. It was estimated that any variation in thickness between 0 and 50mm could only have resulted in a shift in the calibration factor of less than about 7%.

The exposed rock face was measured at fixed positions for two counting periods of 100 seconds each. The counts analysed in each channel were displayed on the elecronic package. The gold concent expressed in terms of either g/t or cm.g/t could then be calculated directly from the readings.

The random counting error amounted to an almost constant absolute standard deviation of 17g/t or 140cm.g/t gold in each pair of analyses. Because of this statistical error, negative values for the gold content were sometimes obtained

at low concentr ions (<25g/t or 200cm.g/t).

The coefficient of variation,, CV, i.e. the relative statistical error, was inversely proportional to the gold concentration; the total random error in the fluorescence sampling and analysis of individual values below 1000cm.g/t was thus predominantly the linear 140cm.g/t standard deviation resulting from counting statistics.

14.1.5 Details of chip sampling and analysis

Chip smamples at the mine had a nominal standard height of 80mm and a nominal depth of 20mm into the face. A nominal width of 150mm was chipped in the tests to permit comparison with flourescence measurements made at two adjacent points.

At the test site it was difficult to cut samples of the required size because of the transition from quartzite in the hangingwall to shale in the footwall. The chipping depth of individual samples was observed to vary from 5mm to 60mm over the height of the sample, while the mean height varied from 60 to 100mm and the mean width from 120 to 220mm. In other words the ratio of sample mass to projected area of the gold-bearing part of the sample varied significantly, which does affect the evaluation when sampling a thin layered deposit. It would be extremely difficult to overcome variations of this kind in this particulaar area and the precision of the results obtained would be significantly affected for this reason.

The time taken to chip a sample was approximately the same as the actual counting time (excluding set-up time) in the fluorescence measurement of the same sample. The chip samples were taken to the assaying department where they

were individually crushed, ground to -150μm and well mixed. Duplicate fire assays for gold on weighed portions of the homogeneous sample agreed to within about 10cm.g/t.

14.1.6 Comparison of XRF and chip sample values

In Figure 14.1 fire assay values of several contiguous groups of individual chip samples are plotted; directly above these the corresponding fluorescence values are shown. It will be observed that there is, generally, good correlation between the upper and lower patterns. The means of sample groups are given in Table 14.1, and the correlation coefficients between XRF and chip values in Table 14.3, and the probability that the coefficients could have resulted from purely random fluctuation is evaluated using a transformation due to R.A.Fisher (Davies 1956). Group means and their standard deviations are shown in Figure 14.2.

Table 14.1 Comparison of means of XRF and chip samples

Sample group	XRF Mean	Chip Mean	N
A	9,7	10,4	11
B	56	56	19
C	77	93	10
D	38	38	23
E	57	69	27
F	120	103	19
G	45	17,7	29
H	38	32	16
A to H	62,9 (σ=60)*	57,7 (σ=72,7)	136
A to F and H**	67,9 (σ=64,9)	68,3 (σ=77,0)	107

* σ = standard deviation of mean

** Group G eliminated because the results were suspect

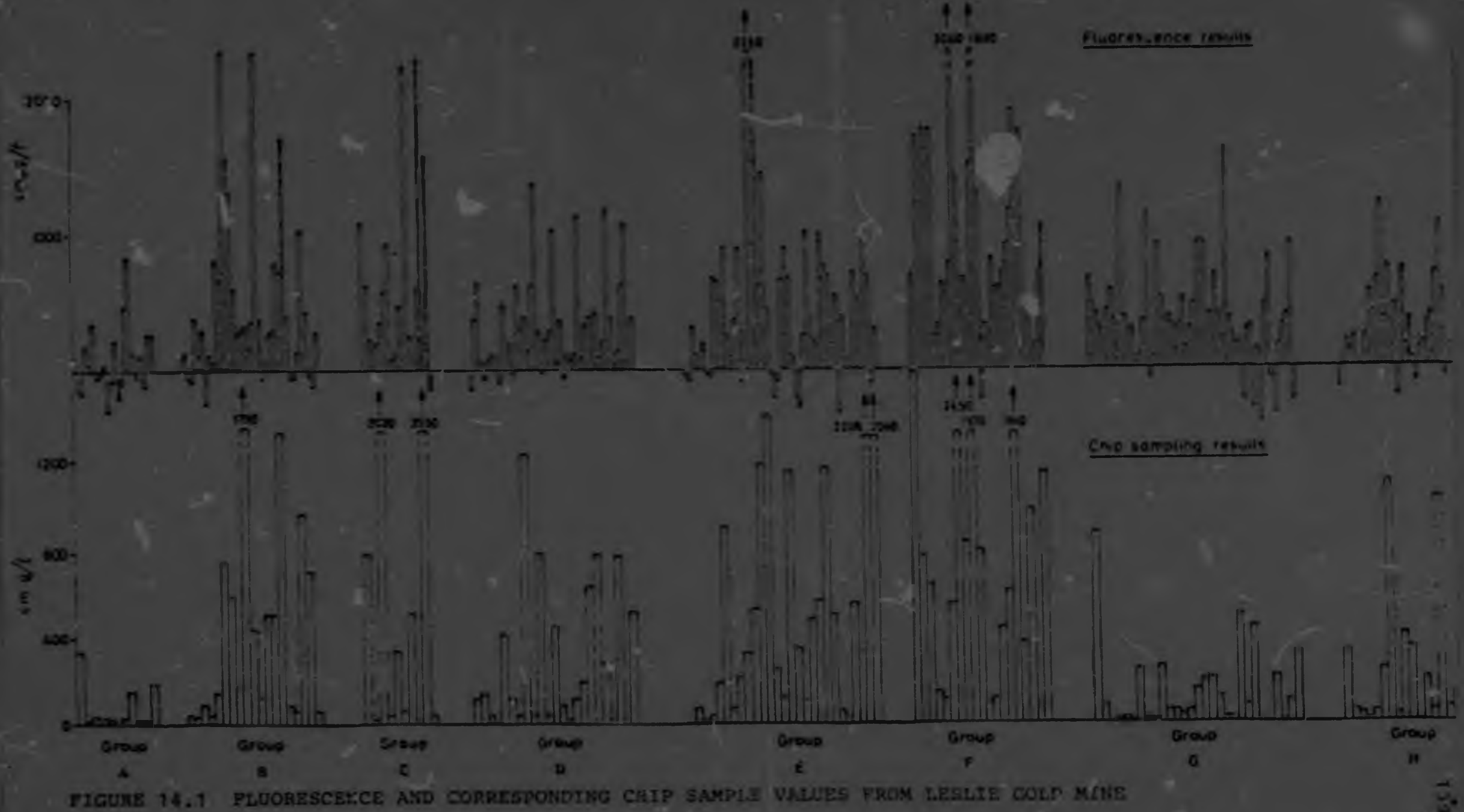


FIGURE 14.1 FLUORESCENCE AND CORRESPONDING CHIP SAMPLE VALUES FROM LESLIE GOLD MINE

Table 14.1 Correlation between XRF and chip values

Comparison	N	r	Fisher transf. $z=0,5\ln(\frac{1+r}{1-r})$	$1/\sqrt{(N-3)}$	Null Probability
Individual samples	136	0,442	0,47	0,086	10^{-6}
Groups A to H	8	0,911	1,35	0,44	0,002
Groups A - F and H*	7	0,95	1,83	0,5	0,001

* Group G eliminated because results were suspect

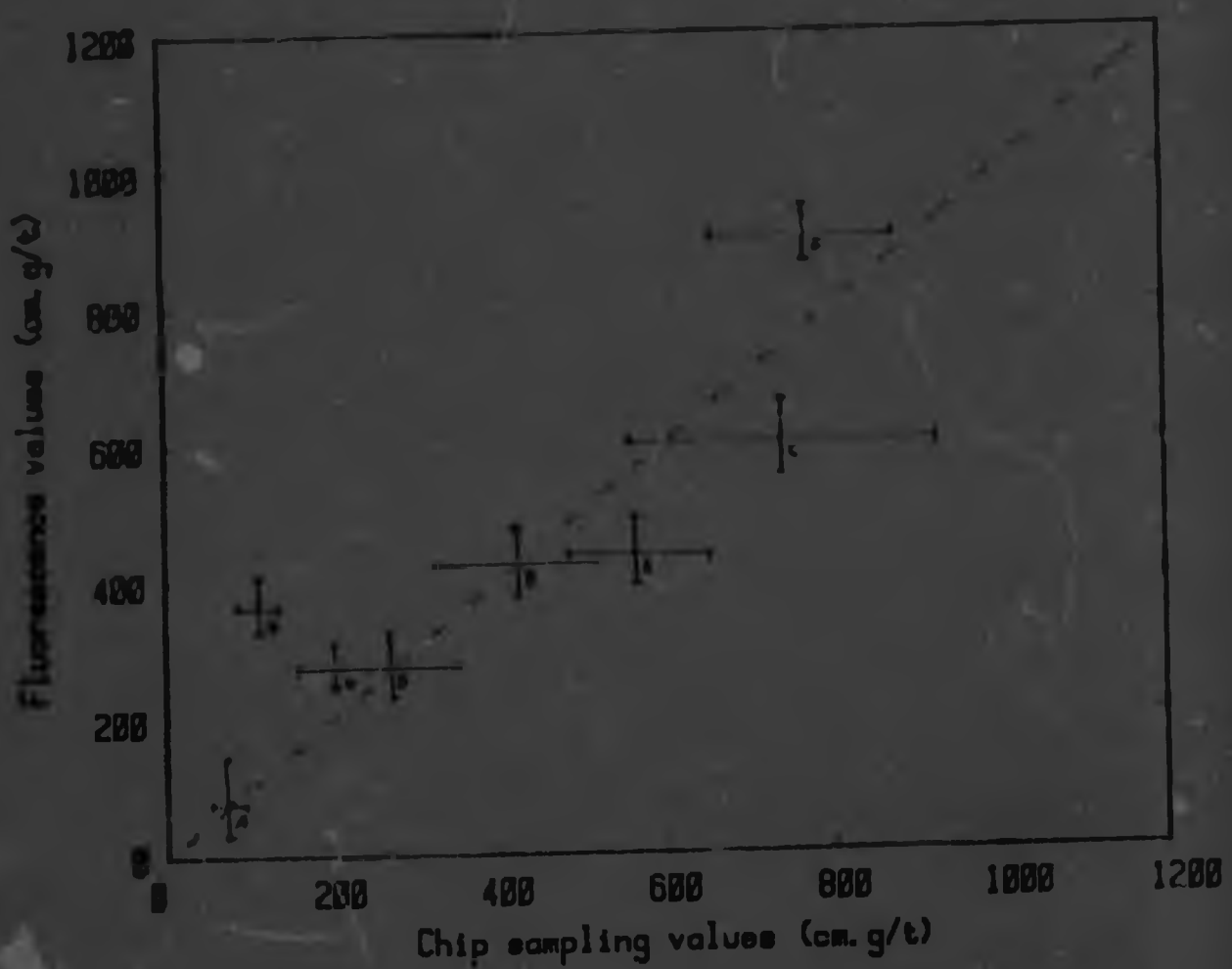


Fig. 14.2 Group means of fluorescence and chip values

This statistical analysis shows that the means of the results obtained from chip sampling and assaying agree very well with those obtained by the flourescence method. This holds true for corresponding results obtained from individual measurements as well as those from groups of contiguous samples.

Once the close linear relationship between the XRF and the chip values had been shown, estimates of the variation in the underlying gold distribution and of the variation in the chip sampling method could be made, since the variation in the XRF method was reasonably well known and small because of the large number of repeat measurements done.

The coefficient of variation, i.e. relative standard deviation of measured values is made up of the coefficient of variation of measuring, CV_m, and that of the underlying gold distribution, CV_g, summed in quadrature:

$$CV^2 = CV_m^2 + CV_g^2$$

The XRF measurements have a $CV^2 = (60/62,9)^2 = 0,91$ (excluding group G, $CV^2 = (64,9/67,9)^2 = 0,91$). The standard deviation of the XRF measurements, known from Poisson statistics, is approximately 17g/t, which gives $CV_m^2 = (17/62,9)^2 = 0,07$ (= 0,06 excluding group G).

Thus $CV_g = \sqrt{0,84} = 0,92$ (=0,92 excluding group G). It can be reasonably assumed that for over 100 corresponding measurements the underlying CV_g must have been very similar for both the fluorescence and chip values. The measured chip values have $CV^2 = (72,7/57,7)^2 = 1,59$ (=1,28 excluding group G); subtracting the CV_g^2 found above leaves for the chip sampling plus assaying $CV_m = \sqrt{0,75} = 0,87$ (=0,66 excluding

group G).

The derivation of the value of the CV_m for chip sampling and assaying is insensitive to errors in the estimation of the CV_m of the fluorescence measurement. It does, however, rely on the assumption of a similar value for CV_g which becomes less accurate when fewer than about 100 samples are compared.

These calculations show that the variation in the fluorescence method in these tests was much less than the variation in the chip sampling method for equal chipping and measuring times.

The above comparison may also be interpreted as indicating that for a specific measuring precision the fluorescence measurement was approximately ten times faster than the taking of chip samples.

14.1.7 Discussion

The results from the site at Leslie Gold Mines Ltd. had shown that at that site it was feasible to perform the *in situ* determination of gold on a stope face by means of a gamma-ray fluorescence analyser. It was also found that, whereas a continuous sample along the face yields the true average value of the face, samples taken over short distances every few metres may not give a true reflection of the value.

Whether the feasibility could be demonstrated at any other site was not certain. It was thought that in going to wider reefs or rock with better chipping characteristics the chip sampling precision could possibly improve to a greater extent than the precision in the XRF measurements. The

observed ten-fold speed advantage of the XRF measurement, when adjusting the measurement time to obtain the same precision as in chip sampling, would the be somewhat diminished but even for very wide reefs of much lower local concentration it was thought that there should still remain some advantage.

While it had been shown at Leslie that the fluorescence method of measurement was feasible, it had not yet been shown that it was practical.

In the tests the overall measuring speed, including positioning of the probe, was far slower than the actual measuring speed. To make the method practical and thus attain the abovementioned speed advantage over chip sampling, a far lighter and more robust instrument than was used in these tests had to be developed. It was realised that the electronic package needed to be easily portable but the probe, in particular, had to be convenient for continuous, rapid hand scanning of the face. At that stage the development entailed largely an adaption and integration of technology then available and did not appear to present any fundamental difficulties.

The equipment used in these tests was for various reasons operated considerably below its maximum measuring speed. The experience gained in these tests led to several simple modifications in the design of subsequent instruments which resulted in about an order of magnitude in increase in measuring speed.

At that stage little was known as to what the optimum measuring speed should be. It was realized, however, that

the measuring speed relates the measurement time of an effective amount of rock to the measurement precision, and that these parameters can be manipulated at will to suit the precision requirement.

The tests showed that with the right instrument the overall measuring speed could be at least increased to ten times the chipping speed under most situations.

In these tests the instrument was measuring in fixed positions. It is possible to measure a large number of discrete samples in this way to obtain a precise average. The sampling statistics of many discrete samples measured to high precision are, however, poorer than those of a large number of practically independent small samples such as would result from the continuous examination of a face by flourescence scanning for the same total measuring time. Scanning of a face to obtain an average value, when the gold is very heterogeneously distributed, is likely to yield a far better estimate of the true value of the face than chip sampling at a few fixed positions. This is so in spite of the fact that the total volume of rock "sampled" may be less in the case of fluorescence measurement by scanning than in the case of chip sampling. It may be noted that scanning may actually take more time than chip sampling, but it is contended that the value of a chosen sampling strategy cannot be judged on the time taken for sampling any more than it can be judged on the weight of sample taken. The only criterion is whether the results of sampling enable better mining decisions to be taken, so as to increase the overall profitability of mining. Whether scanning would in

fact permit an improved sampling strategy to be developed, still had to be tested, and indications were that this looked very promising.

Another important advantage of the fluoresence method was experienced, namely, that spot or area values are immediately available and that this could be of great assistance in locating and tracing invisible gold bands, thus making possible improved sampling strategies.

It was concluded that the first underground tests of the gamma-ray fluorescence technique had proved the feasibility of the technique for ore valuation at the present ore pay limit in a location where sampling was by no means easy, and that improved equipment was required to conduct further tests.

14.2 First-prototype results from Marievale Gold Mine

The fluorescence measurements experiment at Marievale gold mine was designed to determine the reproducibility of measurements when all the sources of error were taken into account. The relative magnitudes of the different types of error were investigated to confirm that there were no unacceptably large errors.

On block No.25, thirty contiguous samples were marked off and scanned 28 times over a period of a month. The results are given in Table 14.3. The mean value of all the measurements was 359 cm.g/t, but the "zero" value of the instrument drifted continuously and was therefore measured frequently. Interpolation of these "sero" mesurements for the 28 scans gave a mean sero offset of 148cm.g/t so that the average gold value was 211cm.g/t. The 30x28 measurements

TABLE 14.] FLUORESCENCE MEASUREMENTS WITH FIRST PORTABLE PROTOTYPE ON 30 STOPE FACE SAMPLES AT MARIEVALE. Units on g/t.

Sample No.

Scan No.

	1	2	3	4	5	6	7	8	9	10	11	12	13	14	15	16	17	18	19	20	21	22	23	24	25	26	27	28	$\bar{x}_i$	$S(x_i)$
1	340	270	490	20	-760	430	520	530	510	490	270	470	510	-170	400	260	470	270	120	220	330	330	410	700	-40	230	280	700	343	257
2	310		620	850	1360	560	760	150	140	520	1010	-140		0	1380	1000	560	960	730	530	410	130	700	450	660	900	1140	490	1080	672	442
3		60	600	520	-240	770	440	-120	190	360	-30	100	590	310	-530	-50	-100	510	820	1270	730	-10	-50	340	-60	470	330	740	760	394	394
4	-260	-70	400	340	-190	1020	-250		30	250	140	670	710	190	-140	770	250	-190	480	540	860	770	670	200		10	710	360	1540	910	374	451
5	100	-420	590		0	910	750	230	-70	1200	-520	110	550	140	510	810	140	910	1070	450	400	580	120	-210	730	800	850	1170	600	444	459
6	120	-270	820	910	370	600	800	-30	-740	-70	550	450	740		10	450	-140	520	-10	360	420	670	800	510	-170	480	430	110	1180	870	437	456
7	740	100	450	400	540	740	-210	130	950	150	480	490	210	240	570	740	250	190	1100	120	730	360	580	370	500	1470	120	1010	448	377
8	490	870	500	1070	-110	660	-750	-230	490	-10	890	560	-10	1040	100	110	670	150	610	1180	730	-110	470		70	860	620	360	690	524	444
9	-710		0	50	-700	100	720	-190	470	1290		100	890		20	880	110	840	550	1700	400	220	-60	480	-90	180	710	830	800	610	460	272	296
10	-170	750	500	400		80	110	100		90		150	740	-40	170	1060	-410	730	840	770		10	-20	530	-560	800	790	770	210	650	790	653	296
11	-550	-170	730	1010		70	-420	-80	-140	540	840	-410	-720		80	470	820	950	720	-110	-140	660	940		20	810		610	210	750	850	810	173	323
12	470	170	310	540	870	890	160	-590	910	-90		-10	170	150	-70		80	-70	950	700	620	-410		80	330		-10	800	-480		1070	-800	515	484
13																														
14	-200	730	-470	260		80		80	810	160	-150	-470	910	840	190	940	-60	500	510	-60		40	890	450	730	800	810		-0	940	750	380	820	327
15	-70	150	720	740	220	610	190	-570	140	750	110	1080	730	750		-10	610	610	770		-10	490	560	100	830	520	-180	1190	980	1090		419	491
16	-10	700		70	610	870	540	-170	470	140	680	700	-300	240	930	260	940	1140		710	260	410	560	570	560		50	410	210	490	670	485	369
17		220	790	500	1000	790		-0	930	960	950	450	950	1020	110	280	470	870	810	110	-310	770	1000	850	140	1170	1260	950	520	470	543	315
18	-110		20	980	-70	960	640	610	-20	490	110	1090	-290	520	760	100	560	950	840	940	910	700	130	520	-400	670	1230	150	840		457	445
19	150	-60	950	-80		790	-30	-110	-970	970	980	740	430	410	790	620	280	870	640	470	100	620	920	810	940	980	940	1080	1340		417	400
20	-70	720	-70	300	510	300	-740	-270	950		30	210	460	500	1410	-270	740		-70	-670	940	440	620	800	870	-100	150	450	1000	1270		392	524
21	-40	-150	690	-240		40	470	1200		90	170	620	660	910	190	710	200		740	-280	670	200	-200	-130		40	810	100	890		90	670	900		251	418
22	-410	770	630	-760	490		-40		60	720	-980	170	790	-100		40	-270	790	450	510	770	550	490		-60	390	120		60	240		70	1070	980		244	418
23	-410		160	870	760	960	910	160	-10	170	710	220	560	-410	600		90		90	700	870	520	740		-20	820	140		-40	200	180	210	540		256	412
24	140	110	200	670	510	100	-570	-570	710		70	160	500	-100	190	560	210	570	700	460	150	230		-80	-170	460		-70	720	660		-40		139	329
25	260	240	-720	230	-310	420	240		-70	610	440	110	470	770	800	670	920		40	670		-50	480	990	210	1240		150		80	1820	170	960		264	471
26		38	500	130	-770	500	770		-70		0	540	-180	-720	420	530	880		40	910	140	380	670	410	-200	-280	-200	-250		-50	180	360	470		138	354
27	210	190	-280	150	200		80		30	950	-140		-30	190	600		-40	720	850	870	270	470	400	630	440	-280		50	250	920	540		370	350		410	370
28	170	460	170		-40	950	910	-280		270	2300	230		240	740	280	-430	920	560		-60	550	880	590	-490	970	280		-60	810	540	950		337	481
29	170	710	-410	1040		-30	290		-40	-10	650	750	790	510	-190	740		950	410	740		0	-470	1300		700	310	590	420		90	-190	650	270		312	471
30	870	470		80	150		30	-60		0	-740	470	670	100	740	950	-240	910	-100	690		-20	670	750	160	740	740	810	450	450	950	700		359	403
$\bar{x}$																													$\bar{x}$	$S(\bar{x}_i)$
$\bar{x}_i$	97	265	712	749	771	792	104	-12	825	847	818	774	840	865	674	713	830	745	810	484	407	838	817	754	874	482	645	654	359	150
$S(x_i)$	268	346	732	676	454	924	421	741	846	768	1870		779	729	790	238	741	949	794	380	924	471	978	745	736	392	975	894	739	394

Interpolated blank values

	-40	140	110	110	-71	-74	-85	-95	-146	-180	-177	252	755	252	810	706	700	100	95	645	760	240	190	210	230	80	39	380	149	

were analysed to obtain an indication of the distribution of gold at the sampling site, of the overall geometrical effect and of the instrument calibration stability over a period of a month. Four types of standard deviations were calculated: S_c the theoretical counting standard deviation, S_g the overall geometrical standard deviation for an individual measurement, S_d the instrumental drift standard deviation for successive measurements, and S_{Au} the inherent gold standard deviation in the group of thirty samples. These are set out in Table 14.3 where the subscripts i and j for a measured value $x_{i,j}$ refer to the sample number and successive measurement number respectively, i.e. to the i^{th} row and j^{th} column in Table 14.3.

Every individual measurement is subject to a counting error, S_c, and a geometrical error, S_g, analogous to assaying and sampling errors in chip sampling. When the same sample is scanned repeatedly over many days the observed standard deviation includes the instrumental drift S_d from scan to scan, as in equations 14.1 and 14.4 in Table 14.4. The short-term (0,5 hour) drift for a scan of thirty samples was assumed to be insignificant. The observed standard deviation of many samples in a scan thus includes only the gold distribution, S_{Au}, as in equations 14.2 and 14.3. The theoretical counting standard deviation for individual measurement, S_c, is determined by the background count preset in the instrument, and is given in equation 14.5, from which S_g, S_d and S_{Au} may be calculated, with the results given in equations 14.6 to 14.8.

These values show that the geometrical error was

Table 14.4
Calculation of the variances in the determination of gold concentrations at Marlevale

$$\overline{s^2(x_i)} = s_c^2 + s_g^2 + s_d^2 = (409 \text{ cm g/t})^2 \quad 14.1$$

$$s^2(\bar{x}_i) = (s_c^2 + s_g^2)/28 + s_{Au}^2 = (113 \text{ cm g/t})^2 \quad 14.2$$

$$\overline{s^2(x_j)} = s_c^2 + s_g^2 + s_{Au}^2 = (397 \text{ cm g/t})^2 \quad 14.3$$

$$s^2(\bar{x}_j) = (s_c^2 + s_g^2)/30 + s_d^2 = (150 \text{ cm g/t})^2 \quad 14.4$$

$$s_c = 10\sqrt{1\,000 \times 4/3} = 365 \text{ cm g/t} \quad 14.5.$$

$$\therefore s_g = 129 \text{ cm g/t} \quad 14.6$$

$$s_d = 132 \text{ cm g/t} \quad 14.7$$

$$\text{and } s_{Au} = 88 \text{ cm g/t} \quad 14.8$$

considerably smaller than the counting error and thus had only a small effect on the measurement error. The combined errors $s_d^2 + s_g^2$ can be expected to decrease as the number of fixed-time measurements in an average increases, or as the measurement time increases, as shown in Figure 14.3. Drift for successive scans in the first prototype dominated the measurement error for measurement times exceeding three minutes, as can be seen from equation 14.4. The drift s_d = 132 cm.g/t for successive scans was of the same order of magnitude as the overall gold value (211 cm.g/t) at this site, making it difficult to get reproducible scan averages. For routine valuation, instrument drift should be less than 5% of the current pay-limit value of the ore (approximately 500cm.g/t), without requiring daily adjustment of the instrument. Some of the large drifts observed with the first portable prototype could have been the result of the

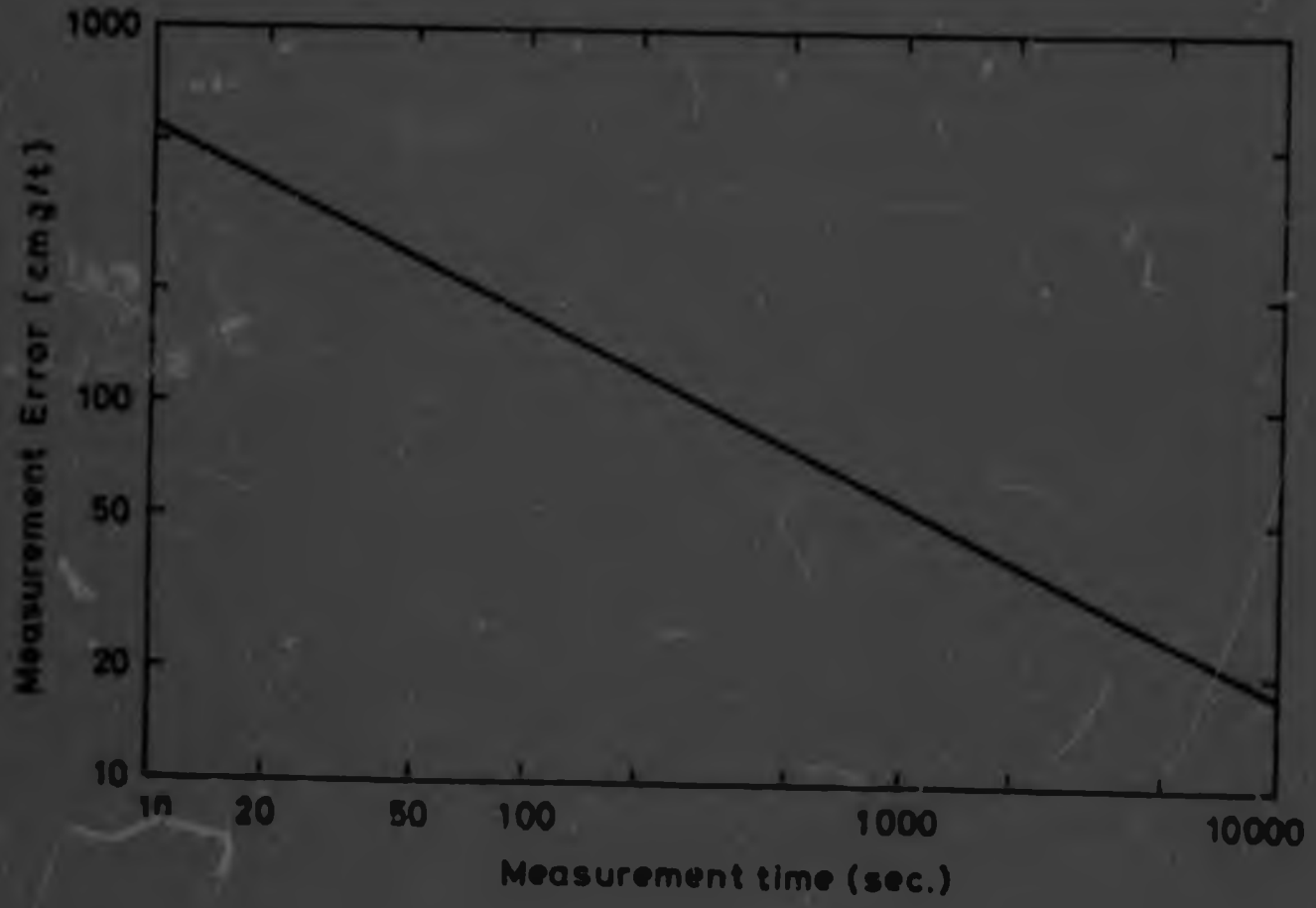


Figure 4.3 Prototype 1 Measurement Error $(S_c^2 \cdot S_g^2)^{1/2}$

instrument "ZERO" fault. A five-fold improvement in stability was sought in the design of the second prototype.

14.2.1 Minimum length of stope face for quantitative estimation of the gold content at Marievale Gold Mine

The most important valuation decisions are required when ore values are marginal. In the following it is assumed that the pay limit is 500cm.g/t and that a valuation precision of 50cm.g/t (10% of the pay-limit) may be considered a satisfactory requirement for quantitative estimation. At this site, a coefficient-of-variation for the gold of $CV_{Au} = S_{Au}/mean = 88/211 = 0,42$ was found for 15cm wide x 2,5cm deep samples. Assuming a constant CV_{Au} this would indicate a gold variation of $S_{Au} = 0,42 \times 500 = 210$cm.g/t at the pay-limit for 15cm wide samples and a variation of $S_{Au} = 50$cm.g/t for $(210/50)^2 \times 15cm = 2,6m$ of stope face.

It would, however, not be practical to estimate the gold content of the ore with a negligibly small error, as this would be too time consuming. In scanning trials underground, no difficulty was experienced in tracing the reef at scanning rates of up to about three metres per minute, while maintaining the probe between 2,5 and 6,5cm from the face. The geometrical error S_g may thus be assumed to be independent of rate and to depend only on the total measurement time as shown in Figure 14.3. Adding a measurement error $(S_c^2 + S_g^2)^{0,5}$ to S_{Au} increases, by a factor equal to the variance ratio, $(S_c^2 + S_g^2 + S_{Au}^2)/S_{Au}^2$, the minimum face length required to reach a precision of 50cm.g/t in the estimate of the gold value. The results of

such a calculation are shown in Figure 14.4. From this figure a stope face length of about 10m measured in about half an hour appears a practical minimum length for quantitative estimation of marginal grades. "Quantitative", in this context, means a valuation precision of 50cm.g/t, and if less precision is desired, the length of face required for the estimation of the gold content would be reduced accordingly. For instance, a precision of the order of 100cm.g/t could be achieved in about 2,5m and 6min scan time, and a precision of 25cm.g/t in about 40m and 100min scan time.

14.3 Results obtained with the first prototype at Blyvooruitzicht Gold Mine

Two experiments were conducted at Blyvooruitzicht with the first portable prototype. One experiment was designed to determine the extent to which fluorescence sampling of the face could yield an estimate of the bulk content of the gold in the reef. The other experiment was designed to confirm, by correlation of the results with those of chip-sampling, that the gold analyser could be used to measure quantitatively. The results of measurements are given in Table 14.5.

Of the 64 batches (4m face x 0,5m on blast) of blocks 1E to 8E mined in the experimental stope, 41 batch faces were scanned with the fluorescence analyser to a precision of about 75cm.g/t (1 standard deviation). The averages of the values measured with the fluorescence analyser were compared with the bulk batch values for reef to the east, (see Figure 14.2), and for reef to the west of the face, and the

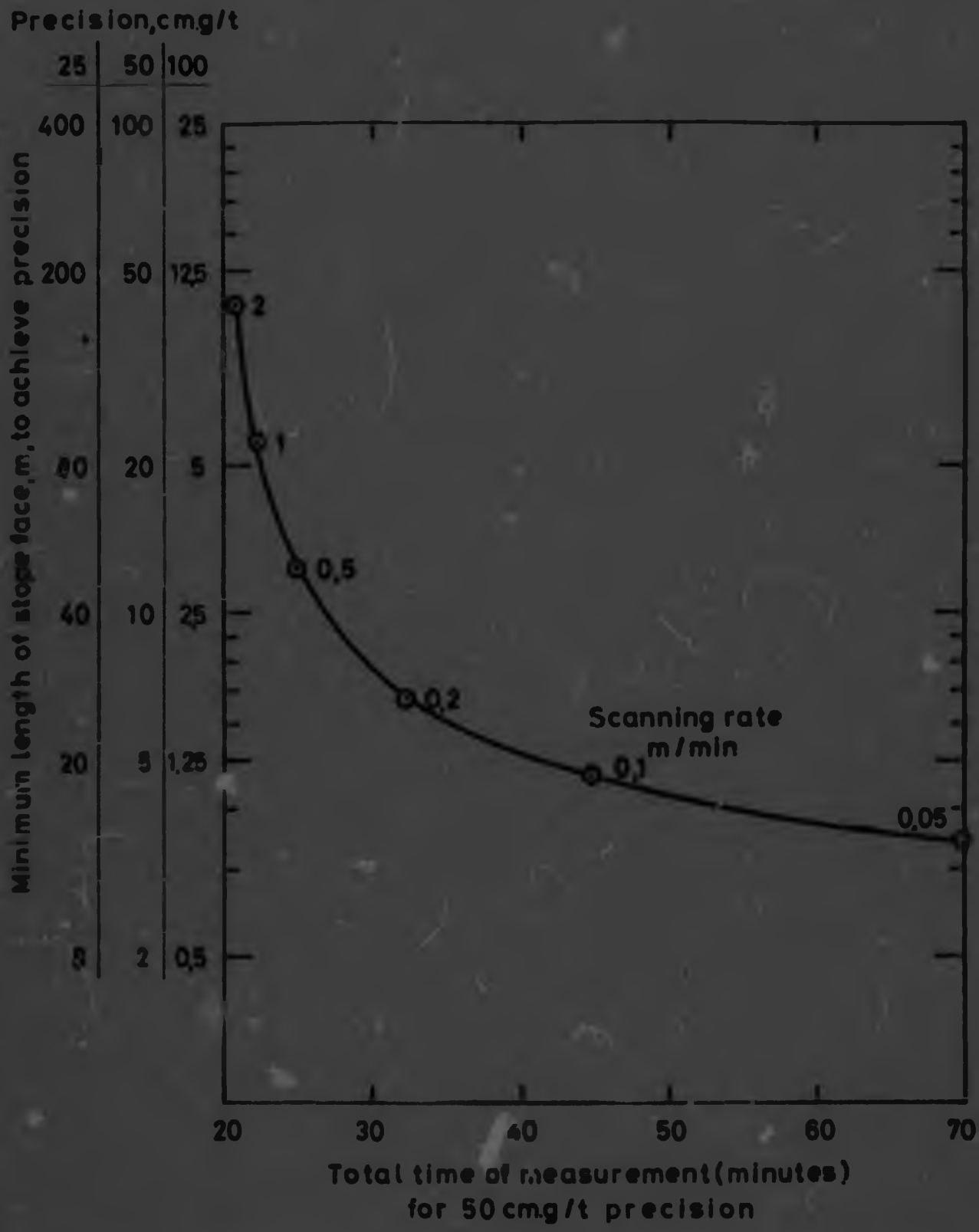


Figure 14.4 Length of face to be scanned at Marievale using Prototype 1, to achieve the given precision in the given time

TABLE 14.5

BATCH MEASUREMENTS AT BLYVOORUITZICHT

Units cm g/t

3a Bulk batch values.

Block No.	Batch No.							
	1	2	3	4	5	6	7	8
1W	2064	1638	1403	1486	727	651		667
1E	1338	1274	1634	1233	1082	1604	1726	1621
2E	545	1328	1762	1438	728	953	1431	2865
3E	1654	1865	1764	1618	2130	1381	1517	2847
4E	2265	2407	2318	1695	1138	1087	1103	1132
5E	851	895	1101	1200	1307	1618	1453	2417
6E	1318	1647	1566	1520	1312	1321	1421	1303
7E	950	1275	1450	1152	2016	1891	1910	1699
8E	1095	1584	2225					

3b Face values by fluorescence measurement

Block No.	Batch No.							
	1	2	3	4	5	6	7	8
1W								
1E	735	1105	885	1135	1040		1165	1000
2E	1260	690	765	1720	1080			
3E	1253				1850	2330	2670	
4E	2370	2920	2740		1080	1291	1680	
5E	1180	1820	1710	1490	2210		1660	2340
6E	2395	2820	1590	1520				1350
7E	1365		1720		1230		2170	1530
8E	730		2860					

3c Face values by chip sampling.

Block No.	Batch No.	
	1	5
1W	576	938
1E	1142	1515
2E	1956	893
3E	2053	1981
4E	1956	1197
5E	979	1384
6E	2142	1683
7E	1368	1624
8E	1717	

correlattion coefficents found (r = 0,54 and r = 1,48 with 40 degrees of freedom) had a probability of about 0,1% of coming from random values. This very high level of significance of the correlation coefficient supports the hypothesis that the fluorescence method can be used for quantitative measurement of the gold content of the ore. The fairly low value of the correlation coefficient shows merely that the gold content varied considerably within a batch while the fluorescence sample (4m face x 2,5cm deep) represents only 5% of the batch. High variability at this site is shown by the values in Figure 14.6, and the semivariogram in Figure 14.7, of 128 consecutive batches of ore. A striking periodicity of the values every 18 batches, or 9m, is apparent from the variogram. Instrument drift as well as insufficient operator expertise in tracing unmarked reef could also have introduced variation into the measurements.

The face of every fourth batch of the 64 batches was chip-sampled contiguously. The average for the 4m faces, when compared with the bulk batch values for the ore to the east and to the west of the face, gave correlation coefficients (r = 0,47 and 0,70 with 14 degrees of freedom) having probabilities between 7% and 0,1% of coming from random values. This is not significantly different from the result obtained with the fluorescence analyser.

The results of chip-sample and fluorescence measurements on six faces (15cm wide) were compared. The measurements are given in Table 14.6. For six faces the correlation of results of fluorescence and chip-sample measurements for

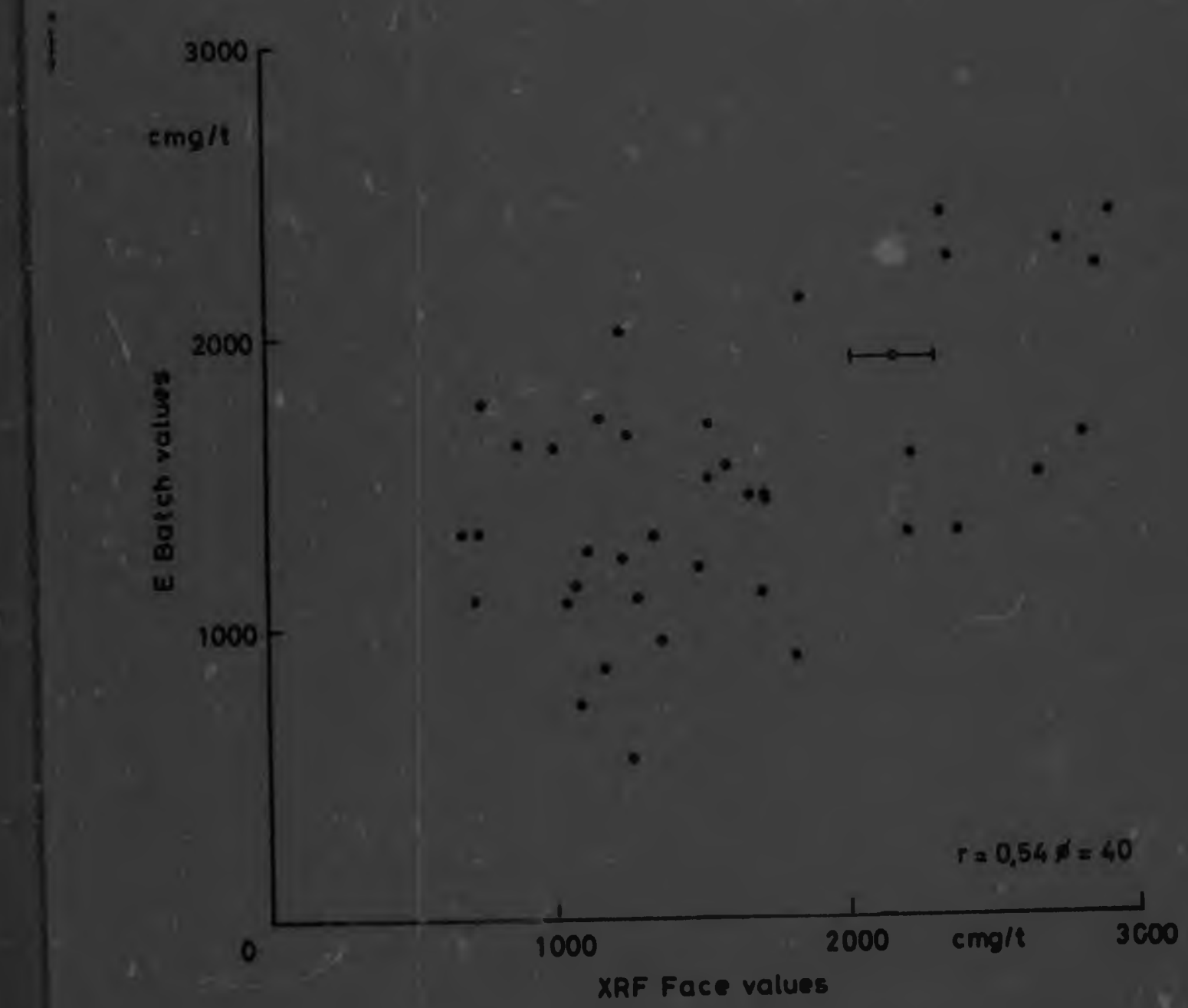


Figure 45 Comparison of batch and X-ray fluorescence estimates at Blyvooruitzicht. Error bar shows standard deviation of fluorescence estimate. Error of batch estimate unknown

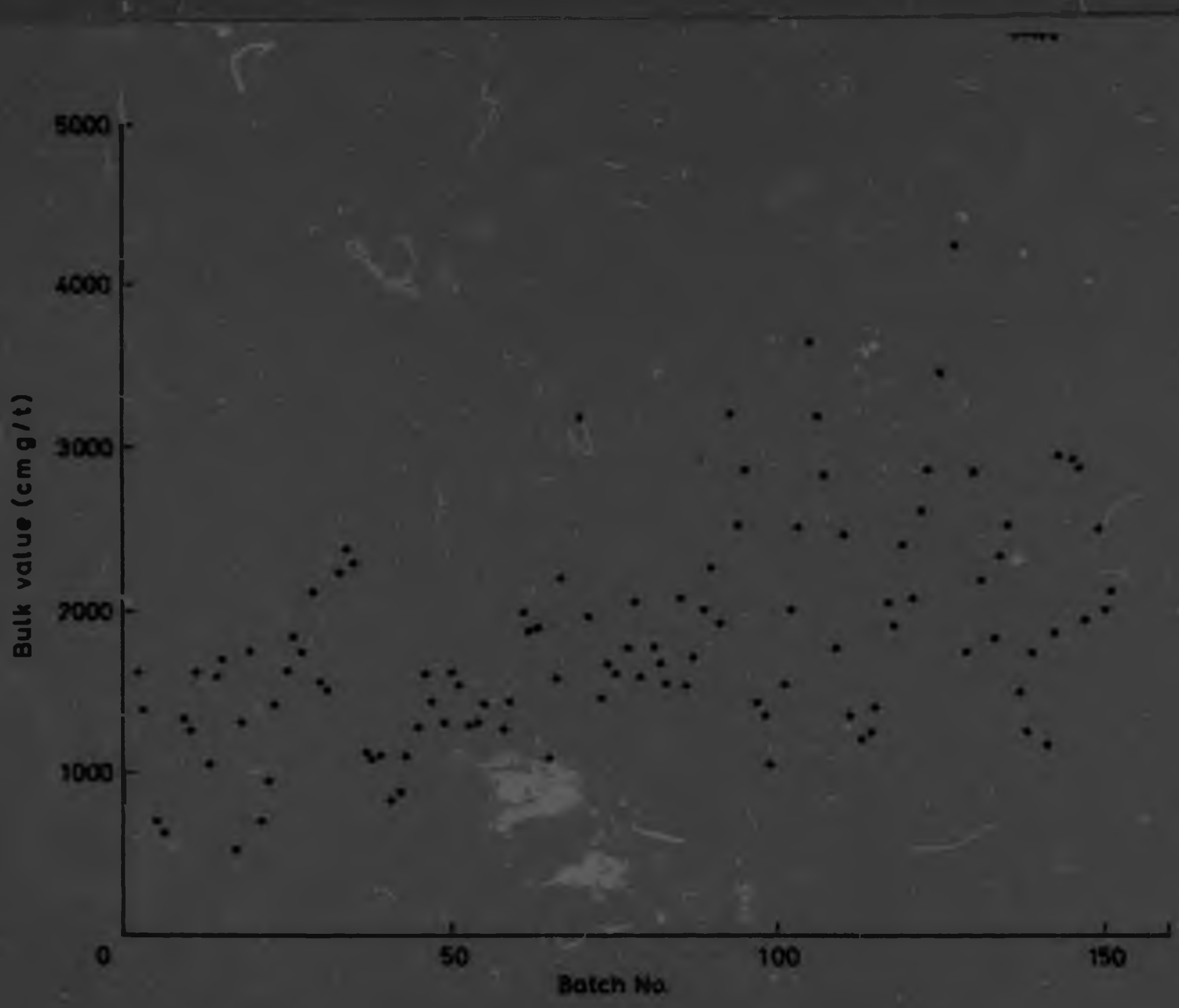


Figure 17.6 Bulk values of 152 batches at Blyvooruitzicht, in consecutive batch number

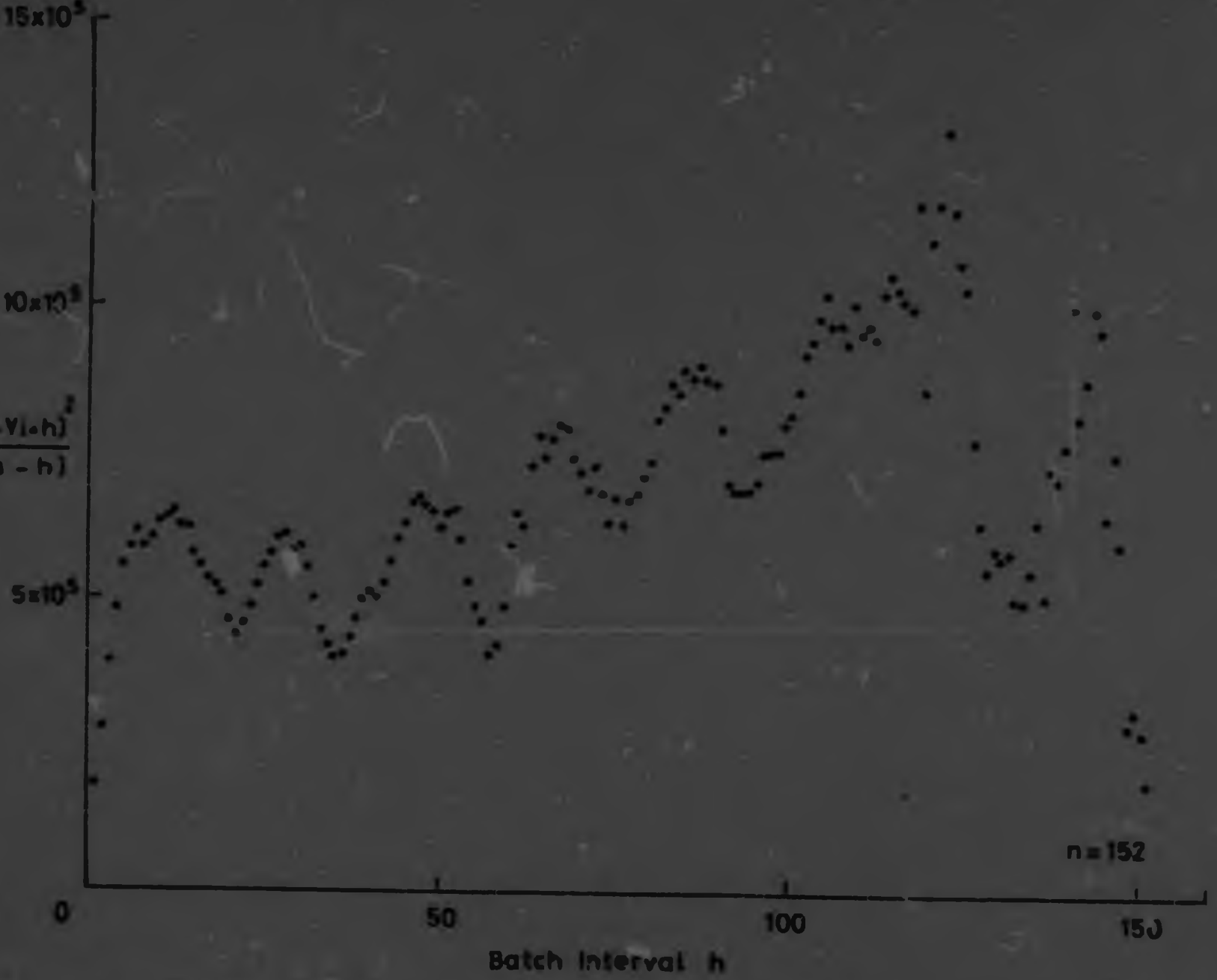


Figure 4.3 Variogram of 152 consecutive batch values at Blyvooruitzicht

TABLE 14.6. Prototype 1 fluorescence-(XRF) and chip values and their correlation coefficients at Blyvooruitzicht.

SAMPLE NO.	BLOCK AND BATCH NO.											
	3EB5		4EB5		4E NORTH		5EB1		6E SOUTH		7EB1	
	XRF	CHIP	XRF	CHIP	XRF	CHIP	XRF	CHIP	XRF	CHIP	XRF	CHIP
1					3170	2368	2220	1741			780	1343
2					270	747	1830	1709			1340	1322
3					1820	932	370	952			1180	560
4					1580	1561	1280	1578			770	840
5					1640	1355	1130	1195			590	378
					2720	1212	1300	1726			260	619
					2250	858	810	1340			940	663
					4210	1432	890	719			2540	766
					2900	2956	920	619			1030	1210
10					4470	4535	230	671	2020	1946	1450	1726
					5010	5139	640	722	2280	2561	1550	1322
					8210	6756	250	261	930	1083	2180	1873
			890	932	5400	3048	210	484	1100	1524	520	1248
			920	1120	3000	2093	960	604	1590	2277	2520	1707
15			590	1138	2500	2298	2110	766	2350	2277	1580	2228
			1010	876	6340	2093	1110	1909	1090	2764	2100	932
			1260	1304	3010	2919	2790	2020	990	971	1890	3397
	1150	1414	1500	2313	2970	2020	1240	1276	1530	2350	5940	3778
	1190	3905	1030	784	1680	812	170	1008	940	1083	4760	1781
20	2320	1928	210	766	-330	1389	180	1120	880	368	3150	1909
	1890	2515	-130	290	1280	1260	910	1340	6440	3727	5050	2846
	-30	952	710	217	1170	1649	210	376	1210	1442	3460	3268
	150	803	990	319	1610	2444	750	772	2010	4700	3050	1285
	1060	1047	2120	1909	3210	3690	850	1285			1380	1175
25	1210	1083	2000	1871	1250	1138	540	334			1100	1027
	1780	2094	1270	2313	100	988	240	254			2000	1597
	1030	1474	390	766	1590	914	530	174			2320	1744
	1000	1570	670	803	990	1138	770	432				
					3850	1800	350	503				
30					2560	1782						
					1190	1386						
	r=0,49		r=0,71		r=0,76		r=0,73		r=0,60		r=0,70	

Overall r = 0,73

individual samples gave correlation coefficients (r = 0,5 to 0,8 with 10 and 30 degrees of freedom) having probabilities 4% to <0,01% of arising from random values, with an overall coefficient for the 123 samples (r = 0,73 and 127 degrees of freedom) having a probability <<0,01% of arising from random values. This very high level of significance of the correlation coefficient leaves little doubt regarding the validity of the fluorescence method for quantitative measurement.

In the batch comparisons the correlation coefficients were fairly low because only 5% of a very variable gold distribution was sampled. In the comparison of results obtained by the fluorescence analyser and chip-sampling methods the coefficients were fairly low partly because counting and geometrical errors were permitted to be relatively large and partly because the shapes and sizes of the samples used in the two methods were different.

14.3.1 Results using the second prototype at Blyvooruitzicht Gold Mine

An attempt was made to determine the correlation between batch and chip values using the second prototype portable analyser. However, too few batch faces could be measured to permit a meaningful statistical evaluation to be made of the correlation between fluorescence and batch results.

On four faces of block 14E, corresponding individual fluorescence measurements and chip-samples were taken; the results are given in Table 14.7. The four correlation coefficients (r = 0,71; 0,73; 0,54; 0,69) calculated for the sets of data given in Table 14.7 all have a probability

TABLE 14.7 Proto 2 Fluorescence and chip values(cmg/t)

SAMPLE NO.

BLOCK AND BATCH NO.

	14E SOUTH		14EB5		14E NORTH		15EB1	
	XRF	CHIP	XRF	CHIP	XRF	CHIP	XRF	CHIP
1	560	159	-1770	1891	2580	2460	540	971
2	1300	513	1660	1781	1910	1248	490	1625
3	2140	1414	5720	4425	300	1138	430	729
4	3680	2368	3000	2552	600	971	770	393
5	1280	268	580	971	1950	1065	640	699
6	(6750)	638	510	437	2700	2130	-410	722
7	1930	1763	440	459	6650	4094	510	1324
8	810	451	720	246	5140	4370	-90	546
9	3470	2001	1480	2745	1580	3617	2170	568
10	1540	1506	2350	2460	2360	6150	1290	840
11	790	714	1600	1561	750	1340	1610	3029
12	1760	404	3140	1450	990	480	620	5205
13	4960	3522	1710	2736	-140	876	1180	3286
14	1620	1873	3810	4691	-230	144	11980	8391
15	3080	4186	1780	3837	-180	42	3960	3231
16	3490	2020	1820	2580	360	126	360	72
17	290	368	4060	5178	(70	8354)	90	57
18	1380	1506	12[illegible]	2700	-360	342	4870	2020
19	4800	1487	-430	320	710	614	-280	130
20	2520	1065	500	503	2340	9620	160	790
21			760	568	2810	1909	2400	1450
22			250	1120	1520	8703	1770	1377
23			1180	2773	1620	3745	3290	8622
24			1170	3415	9770	20233	4230	4406
25			520	2111	(10760)	3801	780	1726
26							750	2607
27					5900	2938	1640	2306
28					1730	2625	2000	1083
29							1540	876
30					1390	952	1310	971
31							1430	1047
32					2260	1561	2620	1597
33							2310	1212

Correlation coefficient:

r=0,71 r=0,73 r=0,64 r=0,69

TABLE 14.7 Proto 2 Fluorescence and chip values(cmg/t)

SAMPLE NO.

	BLOCK AND BATCH NC							
	14E SOUTH		14EB5		14E NORTH		15EB1	
	XRF	CHIP	XRF	CHIP	XRF	CHIP	XRF	CHIP
1	560	159	-1770	1891	2580	2460	540	971
2	1300	513	1660	1781	1910	1248	490	1625
3	2140	1414	5720	4425	300	1138	430	729
4	3680	2368	3000	2552	600	971	770	393
5	1280	268	580	971	1950	1065	640	699
6	(6750)	638	510	437	2700	2130	-410	722
7	1930	1763	440	459	6650	4094	510	1324
8	810	451	720	246	5140	4370	-90	543
9	3470	2001	1480	2745	1580	3617	2170	568
10	1540	1506	2350	2460	2360	6150	1290	840
11	790	714	1600	1561	750	1340	1610	3029
12	1760	404	3140	1450	990	480	620	5205
13	4960	3522	1710	2736	-140	876	1180	3286
14	1620	1873	3810	4691	-230	144	11980	8391
15	3080	4186	1780	3837	-180	42	3960	3231
16	3490	2020	1820	2680	360	126	360	72
17	290	368	4060	5178	(70	8354)	90	57
18	1380	1506	1250	2700	-360	342	4870	2020
19	4800	1487	-430	320	710	614	-280	130
20	2520	1065	500	503	2340	9620	160	790
21			760	568	2810	1909	2400	1450
22			250	1120	1520	8703	1770	1377
23			1180	2773	1620	3745	3290	8622
24			1170	3415	9770	20233	4230	4406
25			520	2111	(10760)	3801	790	1726
26							750	2607
27					5900	2938	1640	2306
28					1730	2625	2000	1083
29							1540	876
30					1390	952	1310	971
31							1430	1047
32					2260	1561	2620	1597
33							2310	1212

Correlation coefficie it:

r=0,71 r=0,73 r=0,64 r=0,69

below 1,1% of arising from random values and thu significance of the correlation of the combined data is still far higher. This finding adds further suppor to the hypothes s that th fllуorescence method c n be used quantitatively.

In addition, an experimer was conducted to determine the reproducibility of measurements using the second prototype, and to test for the effects of possible differences in technique between one operator and another. The experiment was undertaken on the north face of block No.11 in the experimental stope. Nineteen samples 15cm wide by 10cm high were marked off on a narrow reef and were measured 14 times in succession by two operators. The values obtained are shown in Table 14.8.

The instrument had been calibrated to give, for individual measurements (aproximately 40s) a counting standard-deviation, s_c, of 425cm.g/t. Both operators obtained identical within-sample measurement variances of $(s_c^2 + s_g^2) = (445\text{cm.g/t})^2$. The value of the geometrical standard-deviation, s_g, of 132cm.g/t was not unexpected in view of the uneven nature of the rock face scanned. Both operators were thus capable of performing measurements within counting statistics. The means (of 14 measurements) of the 19 samples had a highly significant correllation for the two operators ($r = 0,97$; 18 degrees of freedom) with a probability of less than 0,01% of coming f om random values. The high correlation coefficent shows the good reproducibility of the method at an average ore value of 939cm.g/t, that is, at about twice the pay limit. The 8%

TABLE14.8 Prototype 2 fluorescence measurements on 19 samples of Blyvooruitzicht. Units cm g/t.

OPERATOR A.

Sample No	Measurement No. 1	2	3	4	5	6	7	8	9	10
1	1420	1130	230	2170	950	1000	1600	1150	1180	-160
2	450	270	30	770	500	700	820	150	220	360
3	1000	830	60	270	870	150	1090	220	890	1020
4	-100	-280	300	1130	-440	1140	500	130	340	450
5	460	520	710	300	-420	570	600	-490	540	-590
6	-420	470	320	-160	200	-320	-40	110	-220	630
7	-360	-110	460	-660	580	-640	-480	-20	700	250
8	970	970	40	650	140	950	110	780	210	630
9	960	900	800	1130	-220	1020	390	430	840	1000
10	1260	1320	1230	540	1000	1070	940	1130	1540	1830
11	3390	3020	3430	2880	2730	2500	3018	3820	2530	2630
12	2710	2650	2400	2140	2130	22[illegible]	1920	1380	2000	1850
13	1810	390	1270	1310	1880	181[illegible]	1810	1080	540	1020
14	2770	1630	1050	1550	1440	1700	190	1360	1770	1820
15	860	660	1090	820	1490	1210	950	1190	730	1110
16	1910	1330	2390	1630	1270	870	2000	1440	1950	1730
17	1680	1060	1910	630	1010	710	240	430	2310	360
18	270	800	870	1410	558	820	1380	1140	860	390
19	-90	130	660	410	830	340	490	680	290	540

OPERATOR B.

	Measurement No. 11	12	13	14	15	16	17	18
1	1228	770	1240	1300	1150	1390	920	540
2	1330	1470	780	30	320	-430	720	250
3	690	540	960	1040	730	420	720	780
4	850	730	-70	160	1260	360	250	860
5	60	660	820	590	720	-630	-300	1300
6	810	310	310	390	30	-330	-630	-230
7	110	-90	-20	-60	550	-220	-210	570
8	-170	60	950	360	310	-110	500	610
9	1040	200	440	480	-300	270	500	-220
10	1830	1030	920	1300	1150	1040	860	970
11	3910	1270	3180	2660	3900	3160	2880	3460
12	2350	2340	1320	1350	2450	2730	2660	2380
13	1450	810	960	1400	740	590	1680	1230
14	1900	1590	1560	720	1370	960	780	1320
15	1640	1210	1100	1180	1520	680	1240	1180
16	1620	1450	1420	7050	1590	1360	1720	2250
17	1630	1130	540	820	1210	1780	1140	70
18	750	1410	720	1280	950	780	1350	1040
19	1050	850	720	280	-560	710	610	-360

TABLE 14.8(Continued)

OPERATOR B. (Continued)

Sample No.	Measurement No.									
	19	20	21	22	23	24	25	26	27	28
1	1360	1360	590	300	850	700	1010	1010	1500	440
2	780	1030	1180	810	240	410	-110	230	250	0
3	610	780	1080	-560	760	510	540	250	310	1630
4	220	1620	60	640	720	1100	520	240	320	500
5	30	530	470	-700	1010	610	810	210	470	50
6	-180	310	-170	40	130	-640	-590	80	-290	280
7	470	-1160	220	-300	-490	-460	-410	-220	130	-400
8	590	460	210	630	500	570	-420	780	960	-120
9	1180	610	200	-220	490	1000	480	30	490	-60
10	800	1180	820	350	1290	1220	-120	720	980	640
11	2620	4290	2550	3620	2840	2310	3190	3500	3280	2330
12	2320	1500	2360	2100	1950	2620	1580	1950	1490	2360
13	1590	480	1930	1040	1640	510	1390	470	910	830
14	2030	1110	830	1760	1100	1440	860	1120	2120	1210
15	1090	1730	940	1840	1250	1290	1850	760	1650	530
16	1940	1610	1260	2590	1640	1450	1560	1480	1620	1770
17	1620	740	610	1410	1280	1120	1210	1350	1500	1820
18	460	1630	1270	1000	1250	1270	910	200	820	1230
19	350	570	-20	-130	-200	330	130	260	-220	-90

	A		B		A and B	
	i=1 to 14		i=15 to 28		i=1 to 28	
	$\bar{x}_i$	S_{x_i}	$\bar{x}_i$	S_{x_i}	$\bar{x}_i$	S_{x_i}
1	1086	559	937	385	1011	477
2	563	446	406	450	484	447
3	688	368	611	481	650	422
4	344	493	619	451	482	484
5	309	475	327	589	318	525
6	170	364	-156	319	7	375
7	-24	424	-138	481	-81	448
8	475	411	391	381	433	391
9	672	392	318	448	495	451
10	1149	308	850	377	999	370
11	3140	556	3138	589	3139	562
12	2059	455	2175	424	2117	435
13	1253	481	1074	502	1163	491
14	1504	593	1286	426	1395	518
15	1089	273	1254	428	1171	362
16	1647	391	1703	354	1675	367
17	1033	632	1204	473	1119	554
18	904	373	1010	373	957	370
19	513	310	99	386	306	403
Means	977	437	900	438	939	445
$S_{\bar{x}_i}$	746		812		774	

difference between the total average values found by the two operators falls within acceptable statistical limits and does not indicate a real bias between these two operators.

14.3.2 Minimum length of stope face at Blyvooruitzicht Mine for quantitative estimation of the gold value

Following the same line of thought as in section 14.2.1, an estimate of the minimum length of stope face required for quantitative valuation may be obtained from the gold distribution S_{Au} found at this site. The variation in sample means was found to be :

$$S^2(x_1) = (S_c^2 + S_q^2)/28 + S_{Au}^2 = (773cm.g/t)^2$$
$$= (445)^2/28 + S_{Au}^2$$

giving S_{Au} = 768cm.g/t at a mean gold value of 939cm.g/t and $CV_{Au} = S_{Au}/mean = 768/939 = 0,82$

Therefore at marginal grades of 500cm.g/t, the value of S_{Au} for 15cm wide x 2,5cm deep samples would be 409cm.g/t, and a valuation precision of S_{Au} = 50cm.g/t would require a measurement of $(409/50)^2$ x 15cm = 10m stope face.

The addition of the measurement error (of the second prototype) $(S_c^2 + S_q^2)^{0,5}$ leads to the minimum stope face length and measurement times shown in Figure 14.9, from which it appears that for the more variable gold distribution at Blyvooruitzicht a stope face length of the order of 330m measured in about 1,5 hours seems to be a practical minimum length of marginal grade for quantitative estimation of gold values.

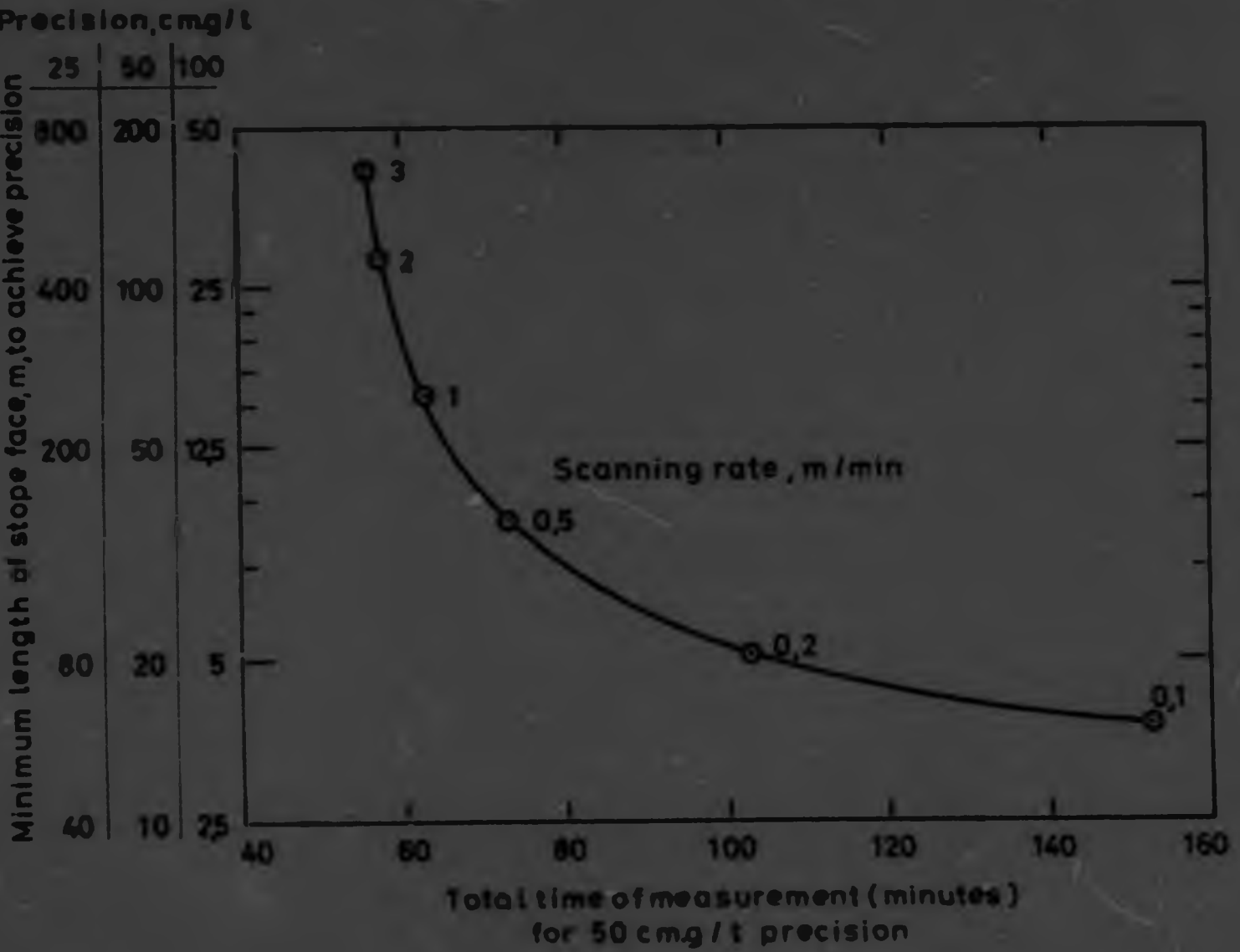


Figure 11.8 Length of face to be scanned at Blyvooruitzicht using Prototype 2, to achieve the given precision in the given time.

15 CONCLUSIONS

The need for improvements in the precision of ore valuation in the gold mining industry has been recognized widely. It has been realized that the conventional method of evaluation by chip sampling and fire assay would allow only a significant improvement in the precision if many more sampling teams were employed, and this would greatly escalate ore valuation costs. Methods of *in situ* instrumental ore evaluation, amenable to scanning greater amounts of exposed rock face, were thus sought.

A number of potential instrumental methods had undergone provisional investigation and of these the gamma ray fluorescence method seemed the most promising. The problems of measuring trace concentrations in situ presented a great challenge. At the outset it was not certain whether gamma ray fluorescence spectrometry could be developed into an economical method of evaluation, but it seemed that with optimization of all the measurement parameters, this goal should be within reach of the available technology.

Many aspects of the method were investigated from fundamental principles to allow quantitative assessment both of the parameters and of the interrelation of the parameters, so that the method as a whole could be optimized for the evaluation of Witwatersrand gold ores to serve as an ore valuation tool and to assist in the identification of geological strata. Quantitative formulation of measurement

parameters made possible the calculation of the maximum improvements available for certain parameters and the trade-off with others. For example, a single-channel pulse-height analyser scheme was optimised so that measurement times therewith would be only a few percent longer than the best possible times with a multichannel scheme, which would have placed greater demands on battery power.

Parallel with the derivation of optimum measurement parameters went the development of laboratory-type instrume[illegible] followed by the development of portable instruments in collaboration with ORTEC INC., the field testing of instruments and continual appraisal of the method.

Some of the instrumental parameters implemented in the third prototype analyzer still fall short of the calculated optimum values because the manufacturer, for some of the sub-units, preferred to rely on familiar or proven technology. For example, a monostable-based timing system to define the amplifier pulse peak position, for the purpose of pileup rejection, was developed by the author, but the instrument manufacturer preferred to use a more familiar amplitude peak detector for which the trailing edge pileup parameter β cannot be optimised to the same degree, and relevant <u>in situ</u> measuring times with the latter system are thus slightly longer. As the gold analyser is going into commercial production some of the sub-units, for which significant improvement is possible, are being redesigned.

The many fluorescence measurement values obtained to date at experimental underground sites with the prototype

instruments, were in all instances found to have a highly significant correlation with those obtained from the same locations by chip or bulk sampling and fire assay.

At the completion of this thesis three units of the third prototype version of the portable gold analyser are being deployed in normal working stopes to derive optimum measurement procedures for ore valuation. Gamma ray fluorescence results from more than 1000 man hours of operation have shown high reproducibility and predictable valuation precision (Davies et al., 1979). True to expectation, at a number of locations it has been possible to show with the fluorescence instrument that mining was following the wrong horizon.

The possibility of simultaneous measurement of uranium and gold with an instrument of this type, and the need in several mines for combined ore valuation of these metals has generated a demand for the addition to the instrument of an analysing channel for uranium. This may mean the rapid evolution of a second generation of commercial instruments, which may be brought closer to the optima which have been identified in this thesis.

REFERENCES

ANSI STANDARD N5.10. 'Classification of Sealed Radioactive Sources'. American National Standards Institute, 1430 Broadway, New York, NY 10018, 1968.

Berry, P.F. 'Shielding Constants; Gamma-Ray Attenuation Coefficients'. Nucleonics Data Sheet No.42, 19:6, 62, 1961.

Boynton, G.R. 'Canister Cryogenic System for Cooling Germanium Semiconductor Detectors in Borehole and Marine Probes'. Nucl. Instrum. Meth., 123, 599-603, 1975.

Burkhalter, P.G. and Marr III, H.E. 'Detection Limit for Gold by Radioisotopic X-Ray Analysis'. Int. J. Appl. Rad. Isotopes, 21, 395-403, 1970.

Carroll, J.E. 'Cryospectroscopy coming of Age in the Analytical Laboratory'. Am. Lab., Aug. 1971.

Chelius, D.R. 'Broken ore Sampling of Stopes'. Rand Mines Ltd., Johannesburg 1973.

Clementi, E., 'Ab Initio Computations in Atoms and Molecules'. IBM Journal, 2-19, Jan. 1965.

Coetzee, C.B. (editor). 'Mineral Resources of the Republic of South Africa'. 5th ed. Handbook 7, 1976.

Compton, A.H. (title not available) Phys. Rev. 21, 483,1923.

Currie, L.A. 'Limits for Qualitative Detection and Quanitative Determination: Application to Radiochemistry'. Anal. Chem. 40, 586-593, 1968.

Davies, O.L. 'Statistical Methods in Research and Production'. 3rd ed., p193, Oliver and Boyd, 1958.

Davies, T.A., LLoyd, P.J.D. and Rolle, R. 'A Portable

Analyser for Measuring Gold Values in Stopes'. Report in preparation, 1979.

Davisson, C.M. 'Interaction of gamma radiation with matter'. Ed. K.Siegbann: ' Alpna-, Beta- and Gamma-ray Spectrometry'. 1968.

Dimitriev, P.P., Konstantinov, I.O. and Krasnov, N.N. 'Excitation Functions of the Reactions Ag-109(p,n); Ag-109(d,2n); Ag-107(d,2n+pn), and Yield of Cd-109'. UDC 539.17.12: 539.172.817.Tanslated from Atomnaya Energiya 22:4, 310-312, Apr. 1967.

Dragun, O., Brabec, V., Rysavy, M., Plch, J., Zderadicka, J. 'Internal Conversion of High- Multipolarity Transitions in Ag-109 and In-113'. Z. Phys. A, 279, 107, 1976.

Eisenberger, P.W. and Reed, W.A. 'Gamma-Ray Compton Scattering: Experimental Compton Profiles for He, N_2, Ar and Kr'. Phys. Rev. A, 5: 6, 1972.

Lederer, M.C., Hollander, J.M. and Perlman, I. 'Table of Isotopes'. 6th ed., John wiley & Sons, Inc. New York,1967.

Groenewald, T. 'Quantitative Determination of Gold by Solvent Extraction and Atomic Absorption Spectrometry'. Anal. Chem., 41: 1012-1015, 1969.

Gwozdz, R., Kunzendorf, H. and Rose-Hansen, J. 'A Compilation of X-ray Interaction Data for X-ray Fluorescence Analysis of Geological Samples'. RISO report No. 297, 1973.

Hallbauer, D.K. Research Review, Chamber of Mines of South Africa, Johannesburg, 1973.

Hallbauer, D.K. 'Private communication, 1977.

Hawkins, D.M., Private communication, 1975.

Hinde, A. 'Application of Infrared Techniques to "On-Reef" Gold Detection'. Research Report 44/71, Chamber of Mines of South Africa, Johannesburg, Aug. 1971.

Hill, R.F. and Garber, W. 'Portable X-ray Analyzer for In Situ Gold Qualification'. IEEE Trans. Nucl. Sci., NS-25, No.1, Feb. 1978.

Hogan, W.H. 'A new Respectability for Cryogenic Refrigerators'. Microwave J., Dec. 1968.

IAEA 'Basic Safety Standards for Radiation Protection'. Safety Series No 9., ed. International Atomic Energy Agency, Vienna, 1967.

Johnson, G.G.Jr and White E.W. 'X-Ray Emission Wavelengths and Key Tables for Non-Diffractive Analysis'. ASTM DATA SERIES DS 46, 1970

Johnston P.S. 'Pay Limits'. J. Inst. Mine Surv. S.Afr., 30, June 1973.

Klein, O. and Nishina Y. (title not available) Z.Physik 52(1929)853.

Krige, D.G. 'A review of the impact of statistics on mine valuation in the gold mining industry'. J. S.Afr. Inst. Min. Metall., Johannesburg, March 1964.

Lederer, M.C., Hollander J.M. and Perlman I. 'Table of Isotopes'. 6th edition, John Wiley & Sons, Inc., New York, 1967.

Lloyd, P.J.D. and Mrost M., Private communication, 1969.

Lloyd, P.J.D. and Rolle R. 'The Testing to Specification of the First and Second Prototypes of the Portable Gold Analyser, and the Specification for the Third Prototype'. Research report No.45/77, Chamber of Mines of South

Africa, Johannesburg, Sept.1977.

Rolle, R. 'Determining Heavy Element Concentrations in Ores'. Chamber of Mines Services (Pty) Ltd., S.Afr. Pat.No. 74/1707, March 1974.

Rolle, R. 'Determining Element Concentrations in Samples'. U.S. Pat. No.4,045,676, Aug.30,1977.

Russell, H.T. 'Reactor production of Cd-109: Isotopic composition of the Cd-109 and its use as an X-ray source'. ORNL-TM 305, pp1-7, 1964.

S.A.B.S. 'Standard Specification for Intrinsically Safe Electrical Apparatus and Circuits for the use in Prescribed Explosive Atmospheres'. SABS 549-1977, South African Bureau of Standards, Private Bag X191, Pretoria 0001.

Storrar, C.D. South African Mine Valuation. Chamber of Mines of South Africa, Johannesburg, 1977.

Strelow, F.W.E. 'Improved Separation of Cd-109 from Silver Cyclotron Targets by Anion-Exchange Chromatography in Nitric Acid - Hydrobromic Acid Mixtures'. Anal. Chim. Acta, 97, 31-91, 1978.

Uken, E.A., Watterson, J.I.W., Knight, A. and Steele, T.W. 'The Application of Neutron Activation Analysis to Sorting Witwatersrand Gold Bearing Ore'. J. S.Afr. Inst. Min. Metall., 67:3, 99, 1966,

Wall, S.G. and Chow, A. 'The Determination of Losses in the Fire Assay of Gold'. Part I. 'Cupellation and Parting Losses'. Anal. Chim. Acta, 69, 439-450, 1974, and

Part II. 'Losses in the Complete Assay and Application of Optimal Procedures'. Anal. Chim.

Acta, 70, 425-438, 1974.

Wing, J. and Huizenga, J.R. (title not available) Phys. Rev., 128, 281, 1962

Woldseth, R. 'X-Ray Energy Spectrometry'. Kevex Corp., Burlingame, California, 1973.

Author Rolle R
Name of thesis Gamma Ray Fluorescence for In Situ evaluation of ore in Witwatersrand Gold Mines 1979

PUBLISHER:
University of the Witwatersrand, Johannesburg
©2013

LEGAL NOTICES:

Copyright Notice: All materials on the University of the Witwatersrand, Johannesburg Library website are protected by South African copyright law and may not be distributed, transmitted, displayed, or otherwise published in any format, without the prior written permission of the copyright owner.

Disclaimer and Terms of Use: Provided that you maintain all copyright and other notices contained therein, you may download material (one machine readable copy and one print copy per page) for your personal and/or educational non-commercial use only.

The University of the Witwatersrand, Johannesburg, is not responsible for any errors or omissions and excludes any and all liability for any errors in or omissions from the information on the Library website.